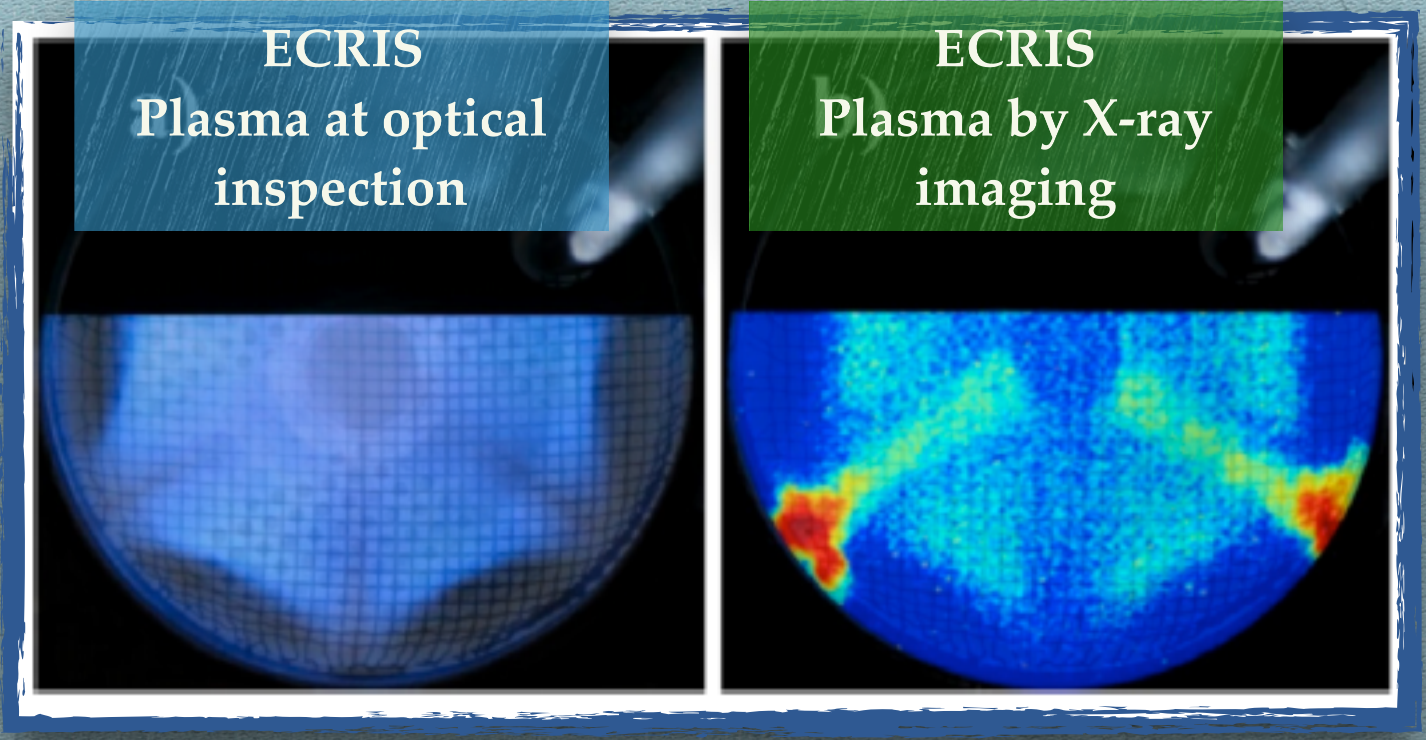

IPAB2016

March 14-15, 2016
Laboratori Nazionali di Legnaro

David Mascali,
Istituto Nazionale di Fisica Nucleare,
Laboratori Nazionali del Sud - Catania

Perspectives about the production of multiply-charged ions at high intensities:

Innovative schemes of microwave-to-plasma matching

The B-min configuration

multiply charged ions production

***Solenoids** for*
Axial confinement

***Hexapole** for*
radial confinement

Extraction
system

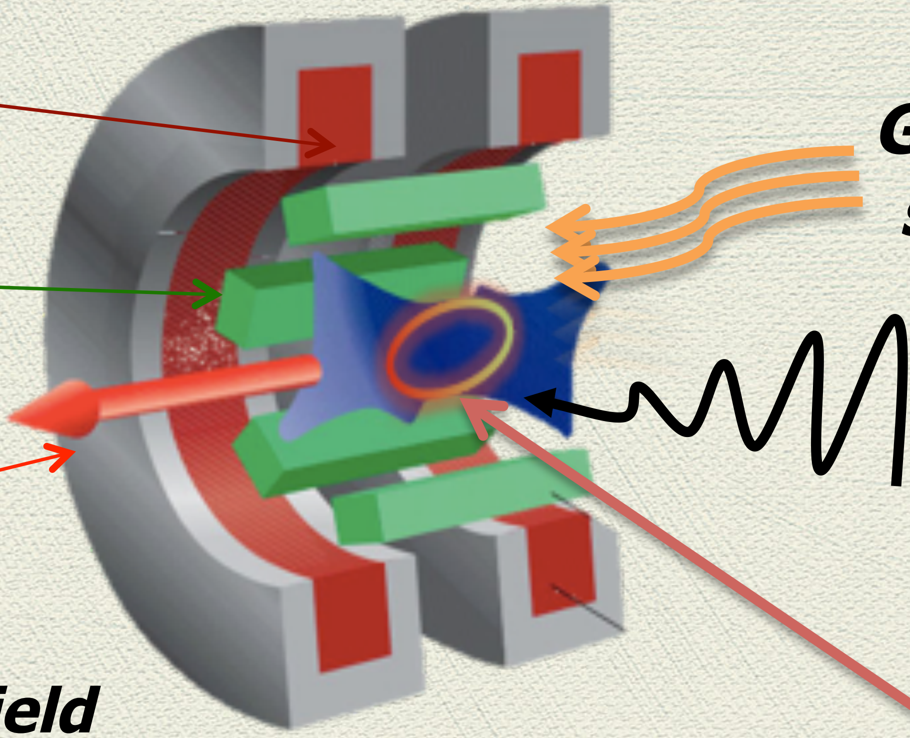

Gas injection
system

Incident microwaves
*few **kW** at **tens GHz***

ECR Surface
$B_{ECR} = \omega_{RF} m_e / e$

"B_minimum" Magnetic Field
structure

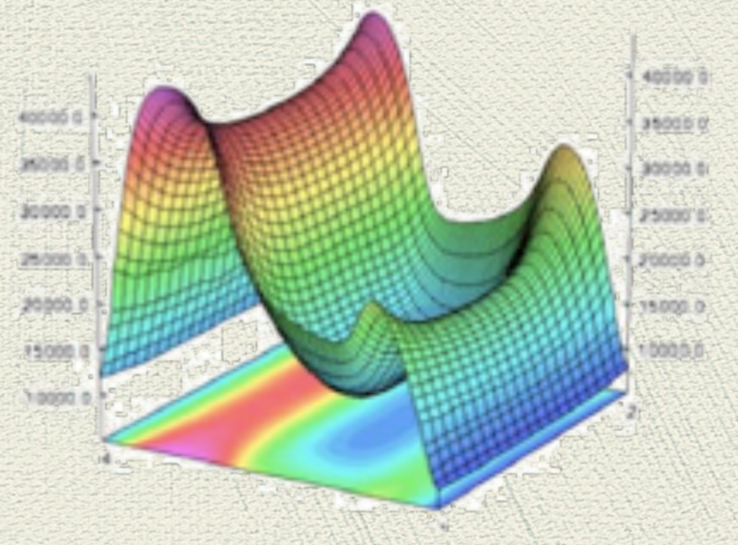

ECR Plasma
$n_e \sim 10^{12}$ cm^{-3}
$T_e \sim$ tens keV
$\tau_{ion} \sim$ ms

ECRIS: classification in terms of "generations"

1st generation:
f=6-14 GHz, P=0.5 kW, I<mA, q=6-12 for Ar

2nd generation:
f=14-18 GHz, P=1-2 kW, I=1-2 mA, q=8-16 for Ar

3rd generation:
f=24-28 GHz, P=5-10 kW, I=20-40 mA, q=14-18 for Ar

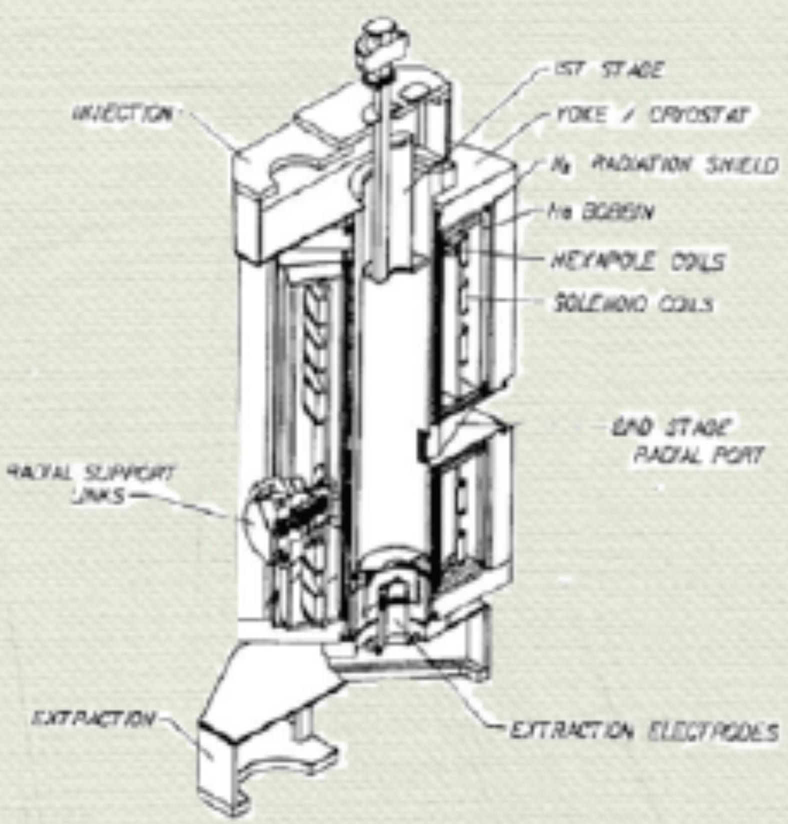

SERSE, INFN-LNS

SC-ECRIS, MSU-NSCL

CAESAR, INFN-LNS

VENUS, LNBL-USA

Overcoming the current limits of ECRIS

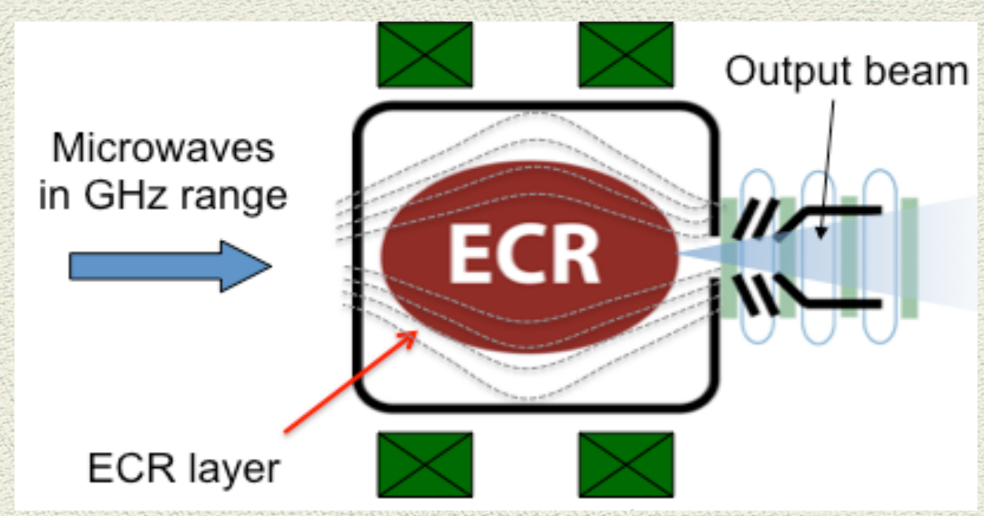

$$\boxed{\omega_p^2 < \omega^2} \rightarrow \boxed{n_e < \frac{\epsilon_0 m_e}{e^2}\omega^2 = n_{cutoff}}$$

Beam characteristics

$$\boxed{\langle q \rangle \propto n_e}$$

$$\boxed{I \propto n_e}$$

ECRIS STD MODEL

$$\boxed{n_e \propto \omega_{RF}^2}$$ → ***INTRINSIC Density limitation***

1. **High Frequency Generators to increase the plasma density**;
2. **High Magnetic Fields to make longer the ions confining time**;

Brute force cannot be anymore used because of technological reasons (magnets, hot electrons generations, plasma overheating, cooling, …)

Alternative heating schemes → **Development of advanced diagnostics tools to make a step forward in understanding heating and confinement mechanism**

A new approach

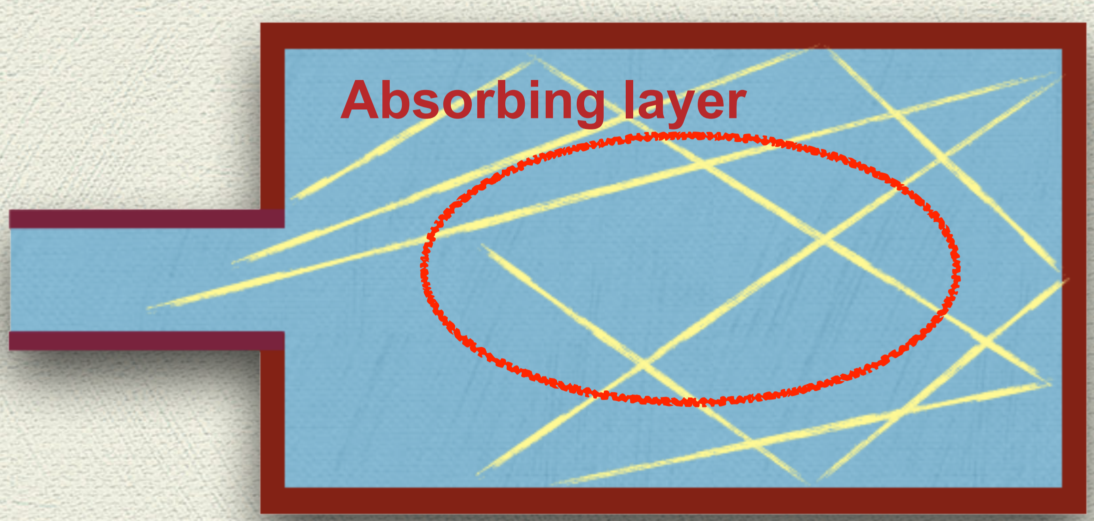

Classical scheme of microwave launching in a ECRIS

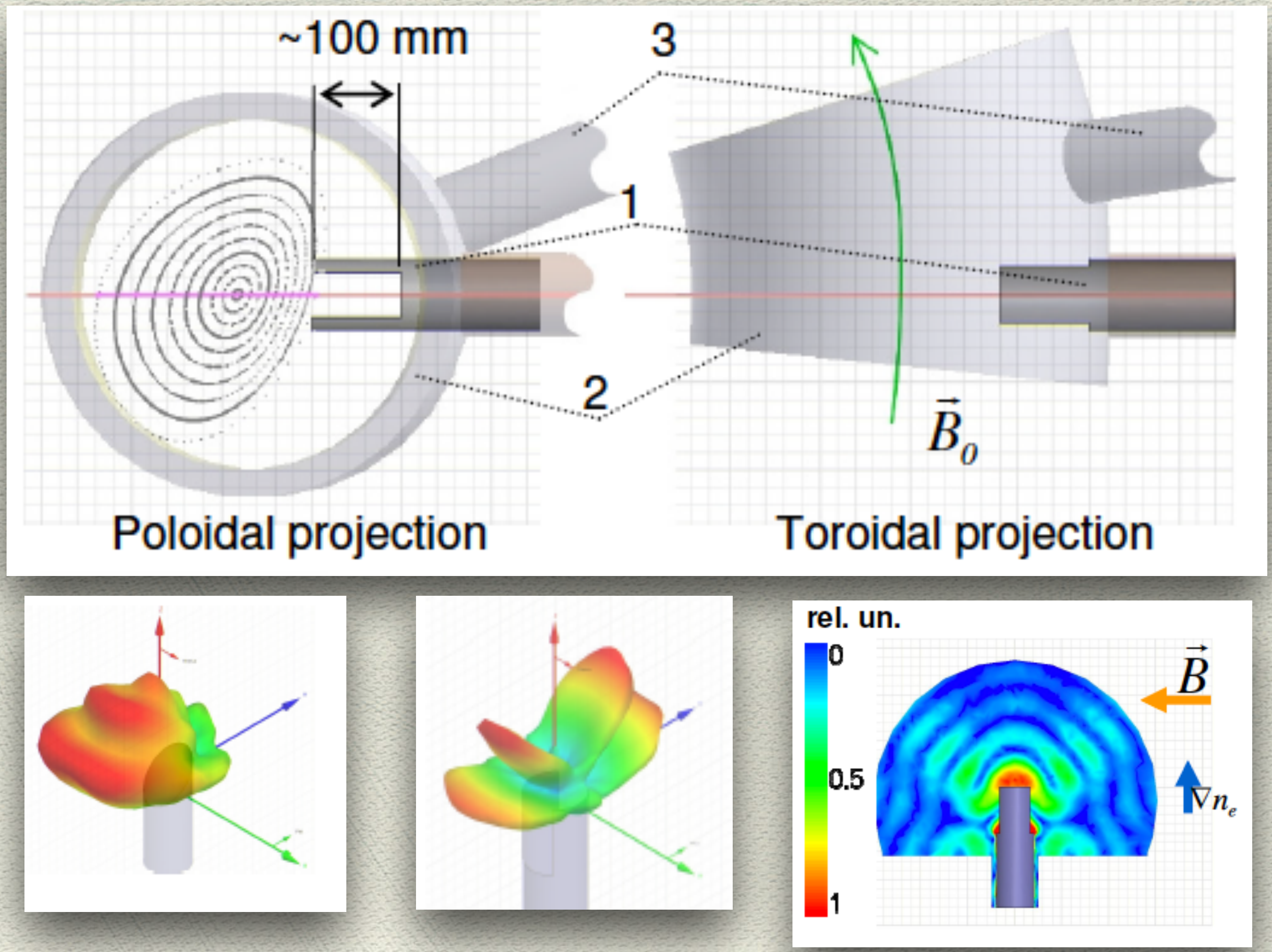

Optimized scheme (single-pass absorption) of microwave launching in the WEGA stellarator at MPI - Greifswald

Switching to a MICROWAVE ABSORPTION ORIENTED DESIGN of ECRIS

Overcoming the current limits of ECRIS

- We are now able to see what happens into the plasma and to model through numerical simulations how it could be happen differently (and in a better way)

- Microwave absorption oriented design is needed: Power deposition into the plasma must be performed in a highly controlled way

Single pass absorption

Some ideas

- STILL IN ECR-heating paradigm: are cylindrical shapes of the plasma chamber still mandatory ?

- OVERCOMING ECR-heating paradigm: on-purpose design of microwave launchers for inner plasma modal conversion

Some questions....

- Does exist an "ECRIS fine structure" with respect to magnetic field and RF frequency tuning?

D. Mascali et al., Rev. Sci. Instrum. 2014

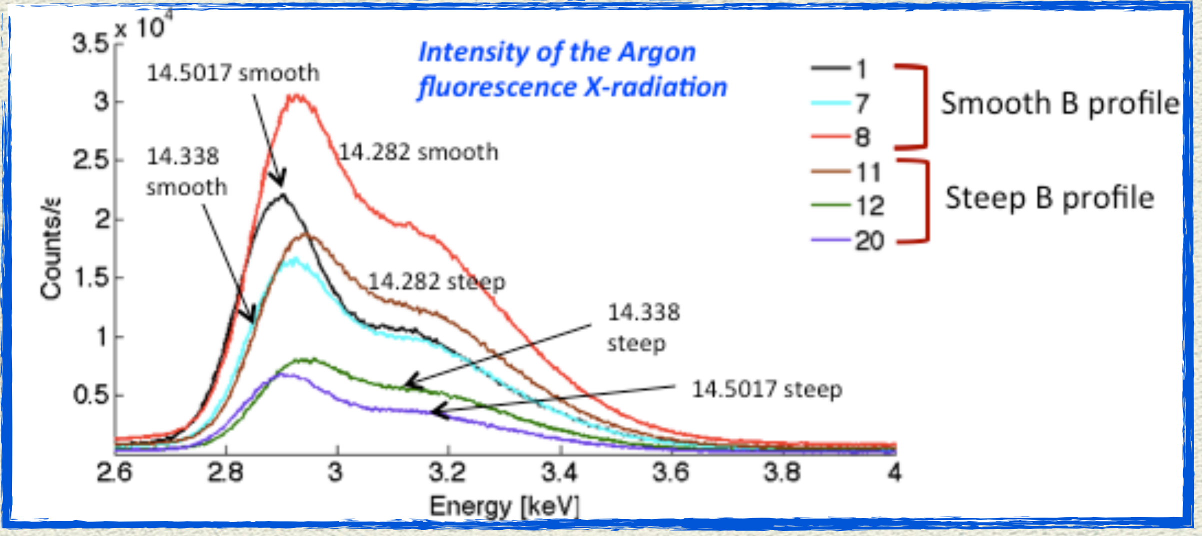

O. Tarvainen et al. Plasma Sour. Sci. Tech. 2014

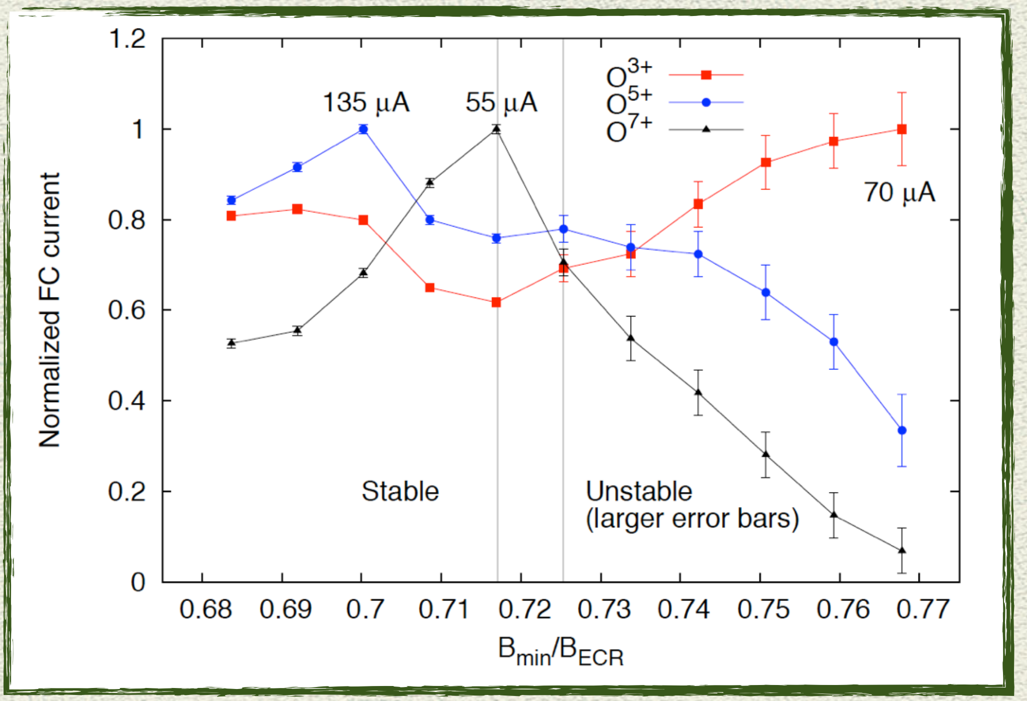

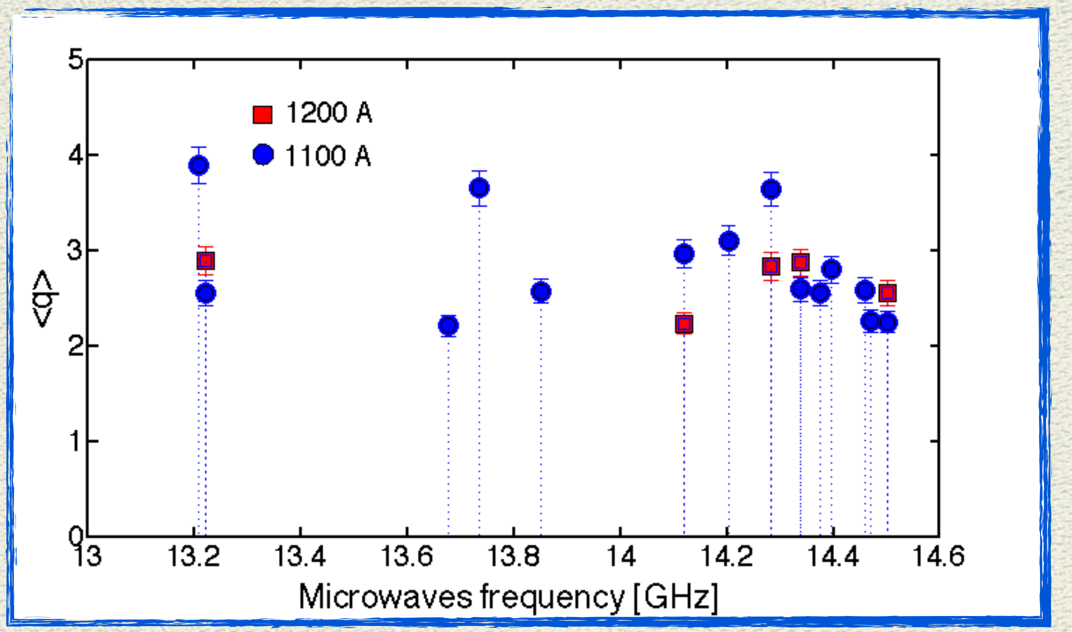

Evidences of plasma instabilities when tuning B

Evidences of strong fluctuations with the RF frequency correlated to X-ray emission

Some questions....

- Does exist an INTERPLAY between the plasma structure and the beam shape, brightness, emittance?

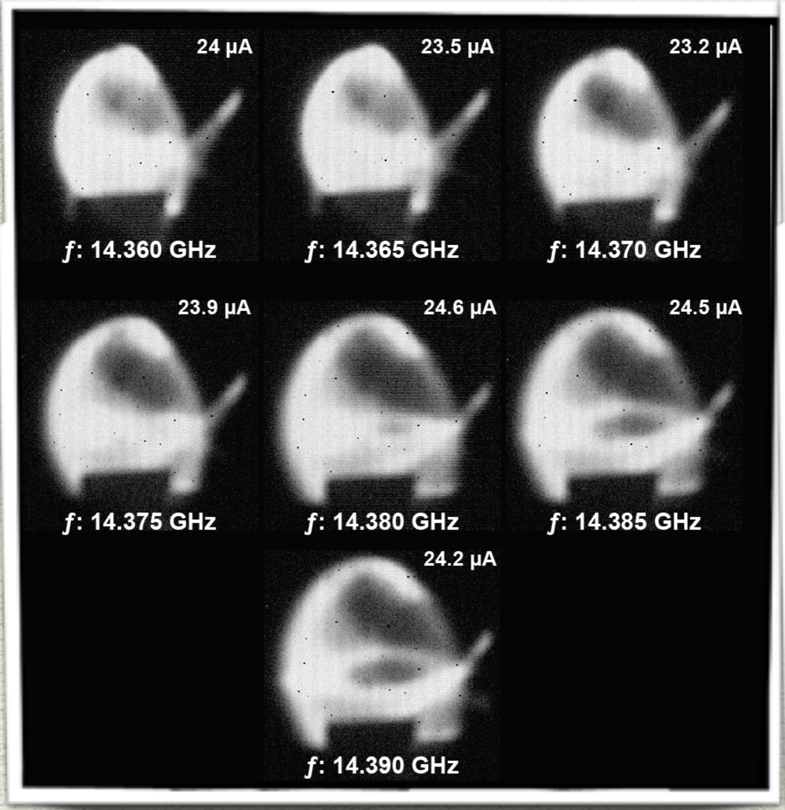

D. Nicolosi et al. ICIS-15, New York City

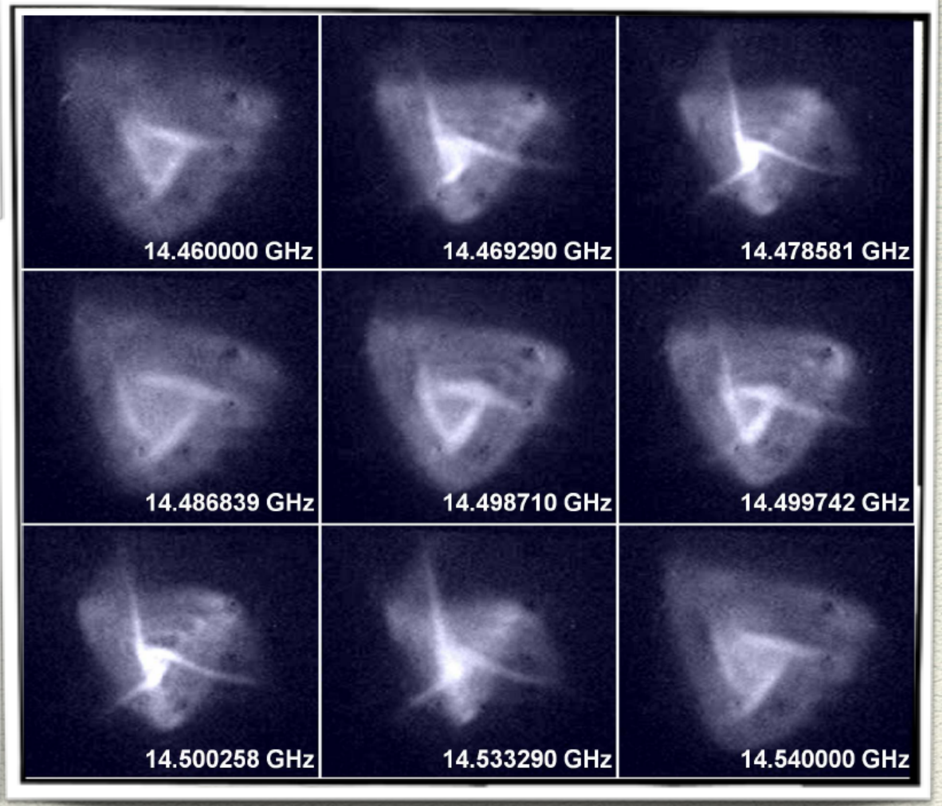

L. Celona et al., Rev. Sci. Instrum. 2008

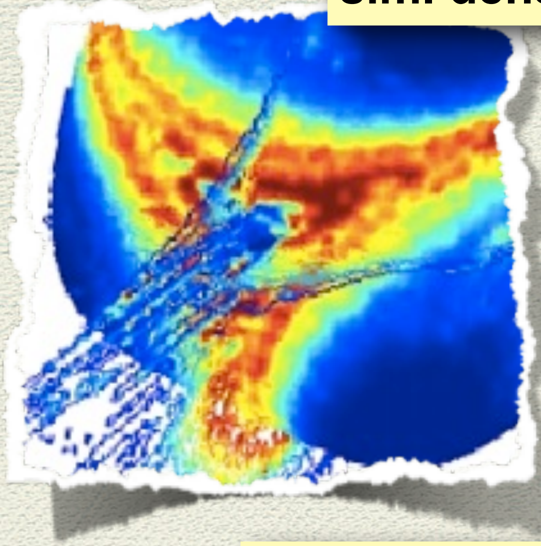

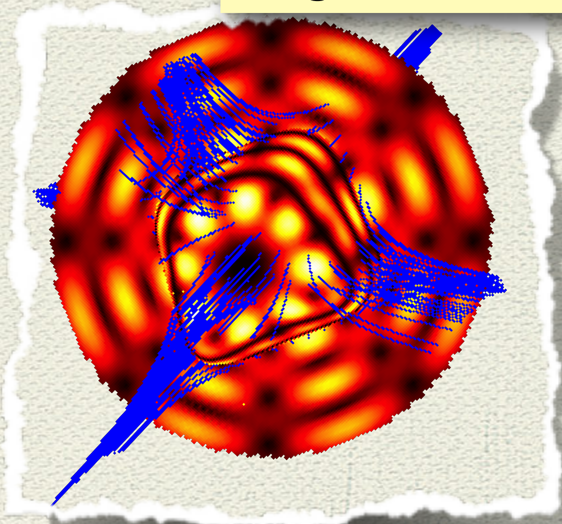

- Does the plasma distribute uniformly?
- Are electrons of different energy domains merged each other or not?

Non-intrusive plasma diagnostics methods

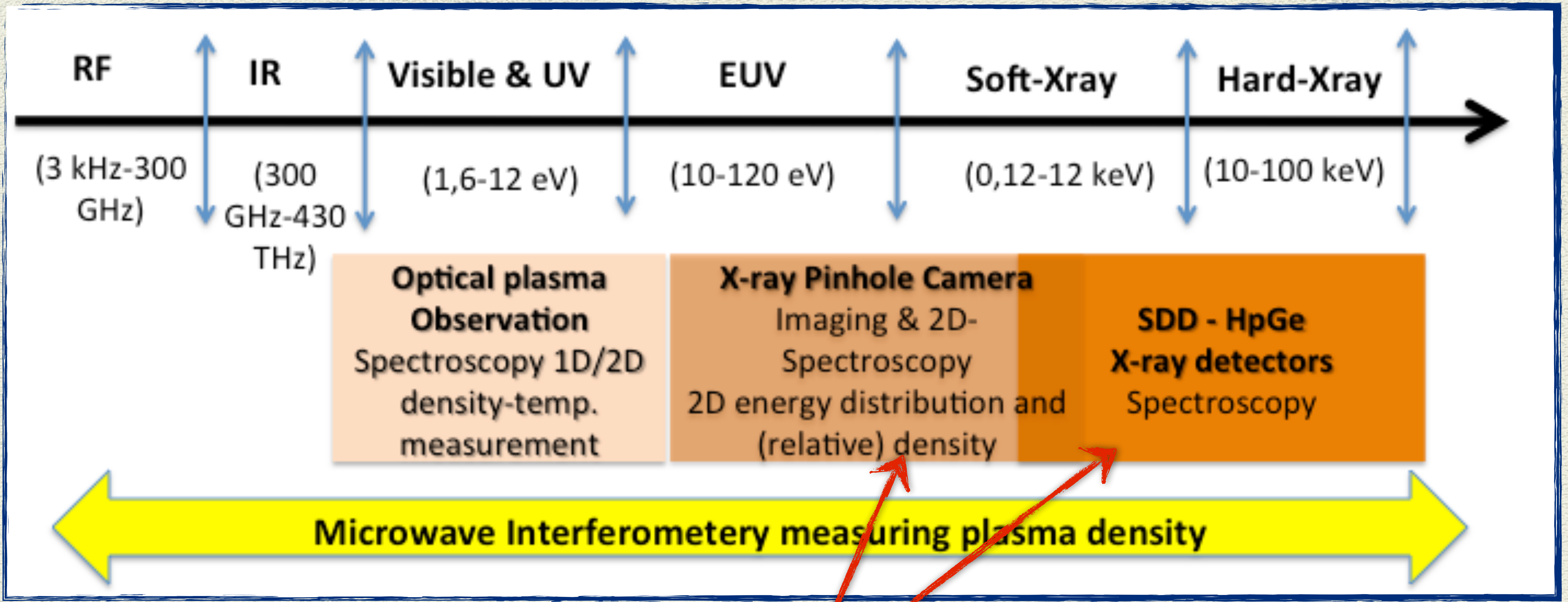

Measuring the plasma density in different energy regimes: density, temperature and plasma structure evaluation under different operative parameters

Experimental setup for simultaneous measurement of density, temperature and CSD

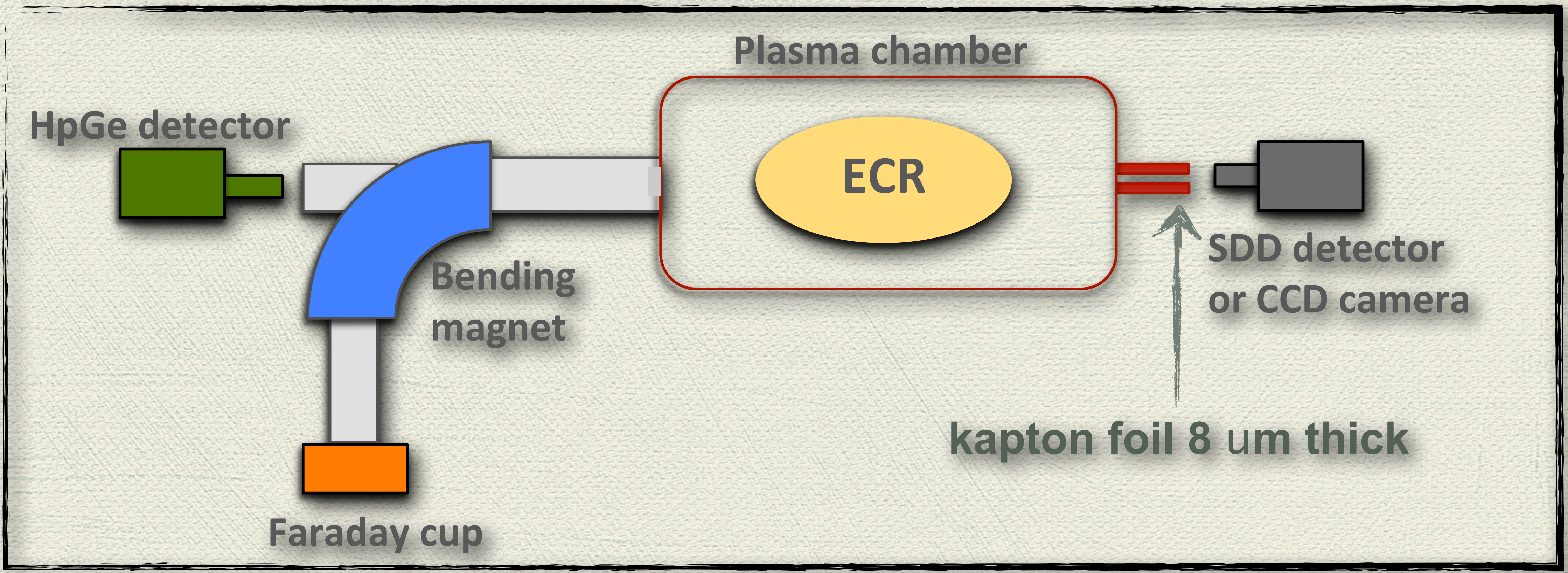

- Three detectors were used for a broad characterization of the EEDF:
  - HpGe for "hot electrons" E>30 keV
  - SDD for "warm electrons" 2<E<30 keV
  - CCD camera for imaging and 2D resolved spectroscopy 1<E<10kEV

SDD – Setup

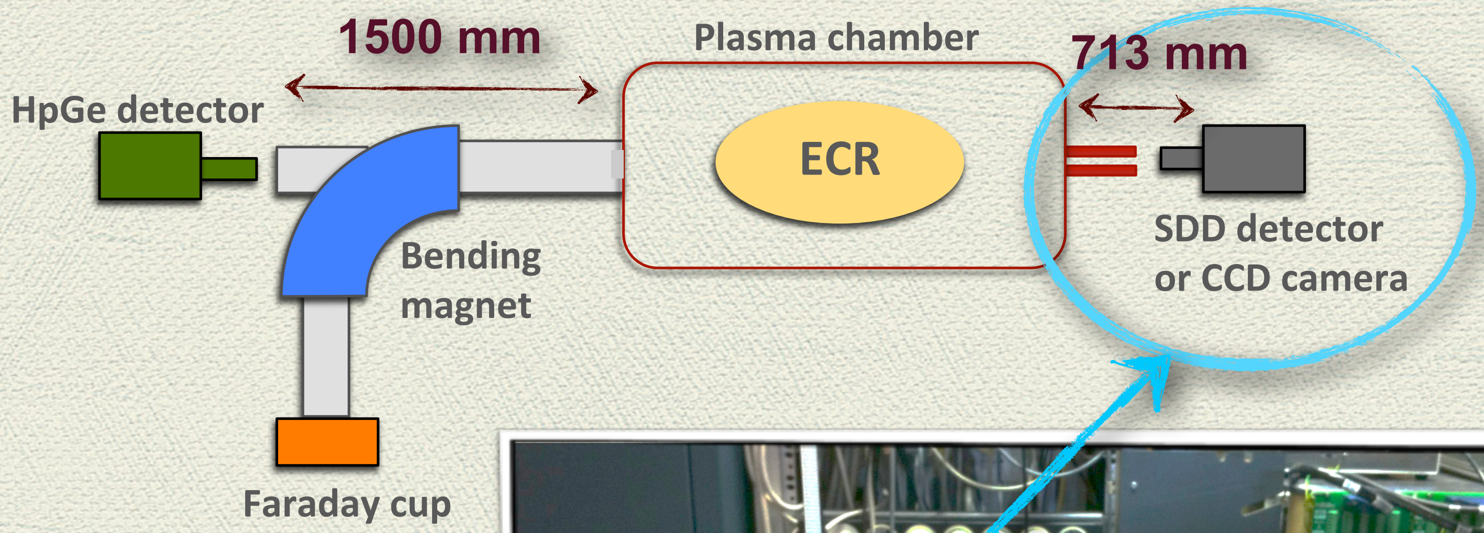

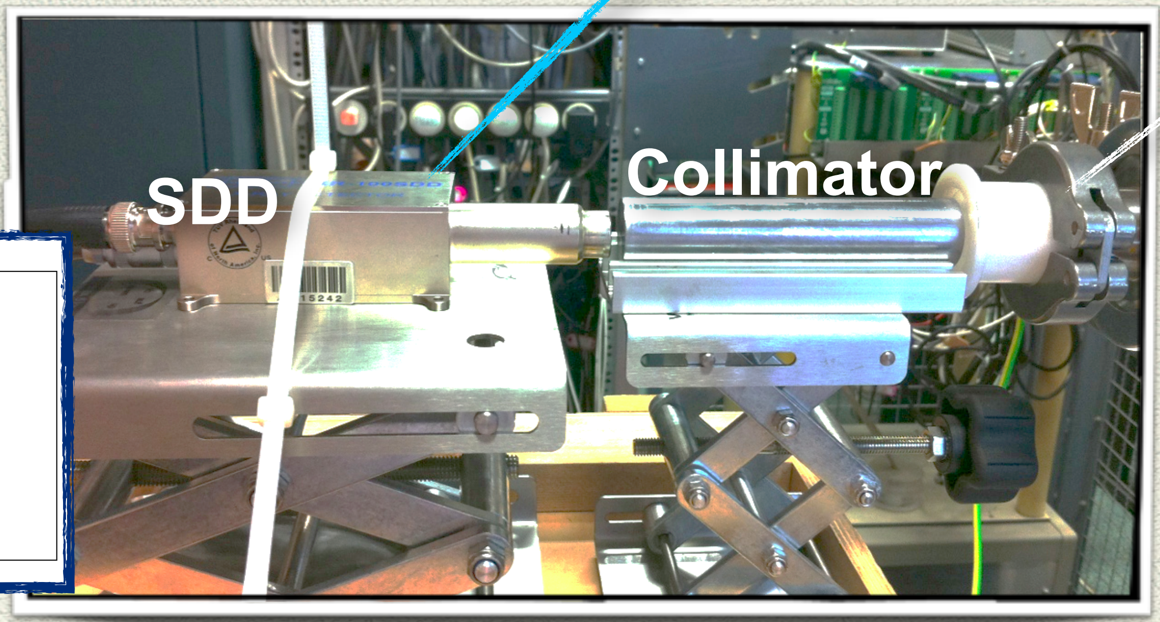

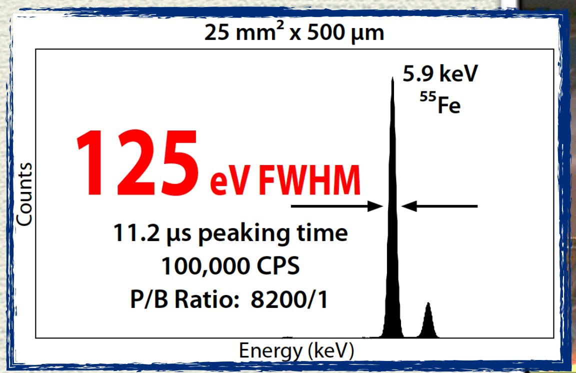

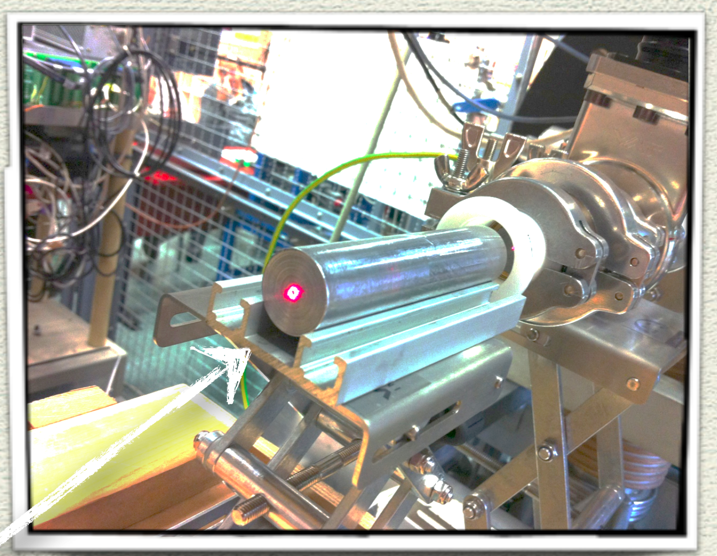

Collimator alignement

Bulk lead 155 mm long drilled collimator for near axis inspection

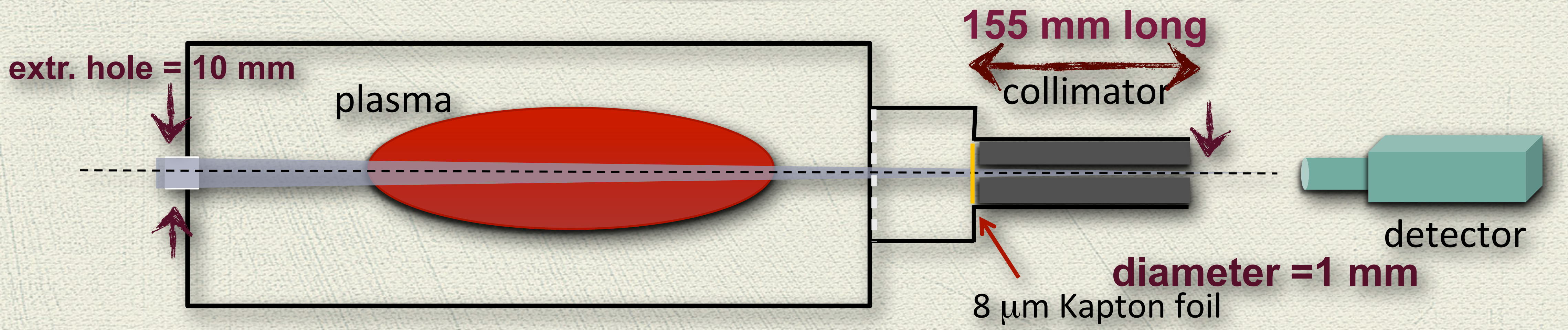

"LONG" collimator

(SDD) F.T.E. study

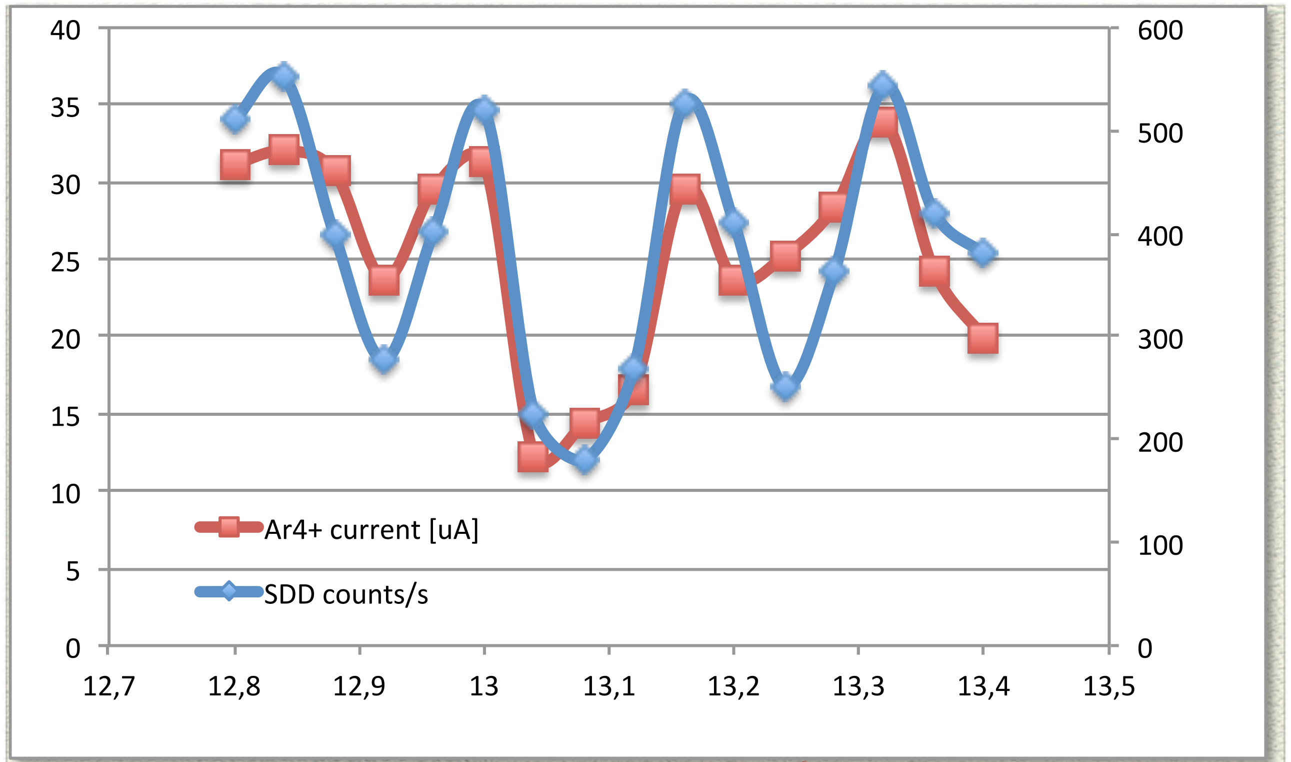

- Very Strong correlation (!!!) between Ar4+ current, X-ray flux and modal density
- Same number of "peaks", but with upshifted frequency (plasma effect).

Strong correlation among:

(i) Ar4+ current,

(ii) SDD counts/sec. and

(iii) e.m. modal density distribution

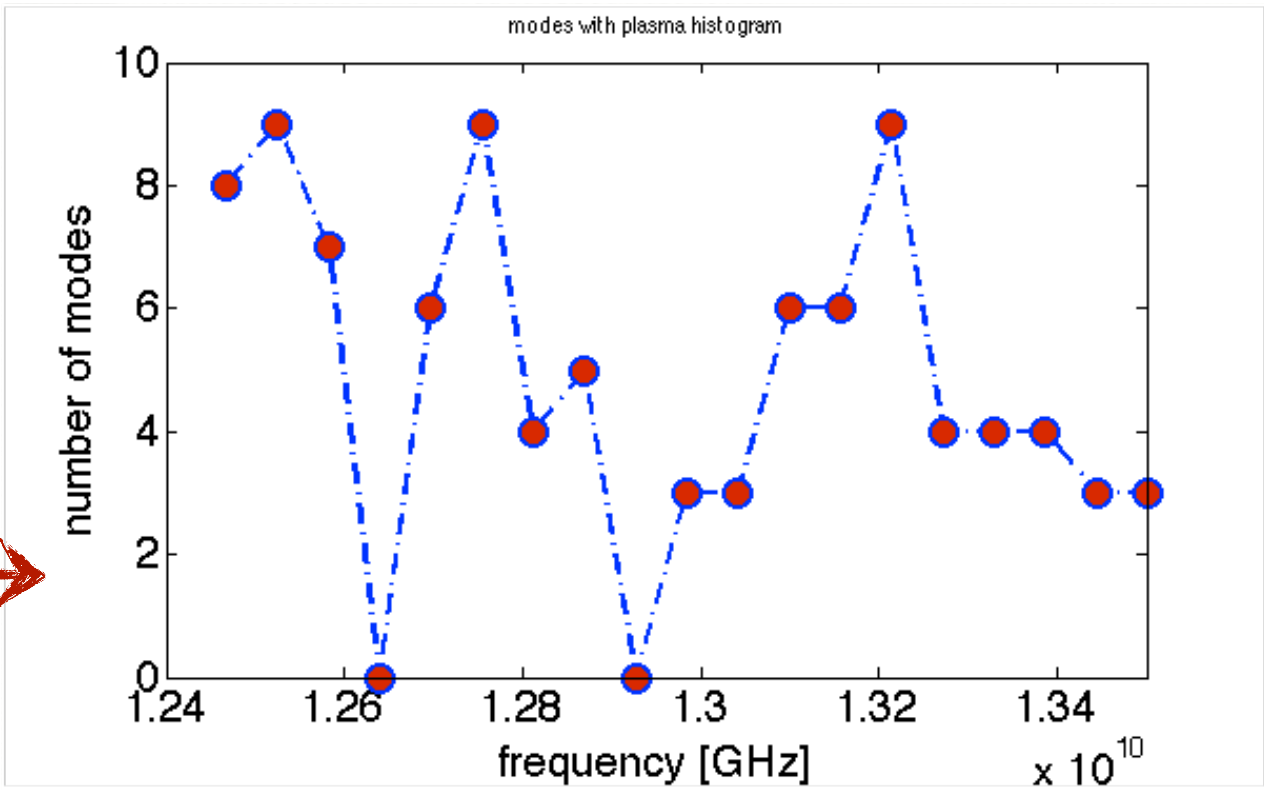

SDD/HpGe - Data Analysis

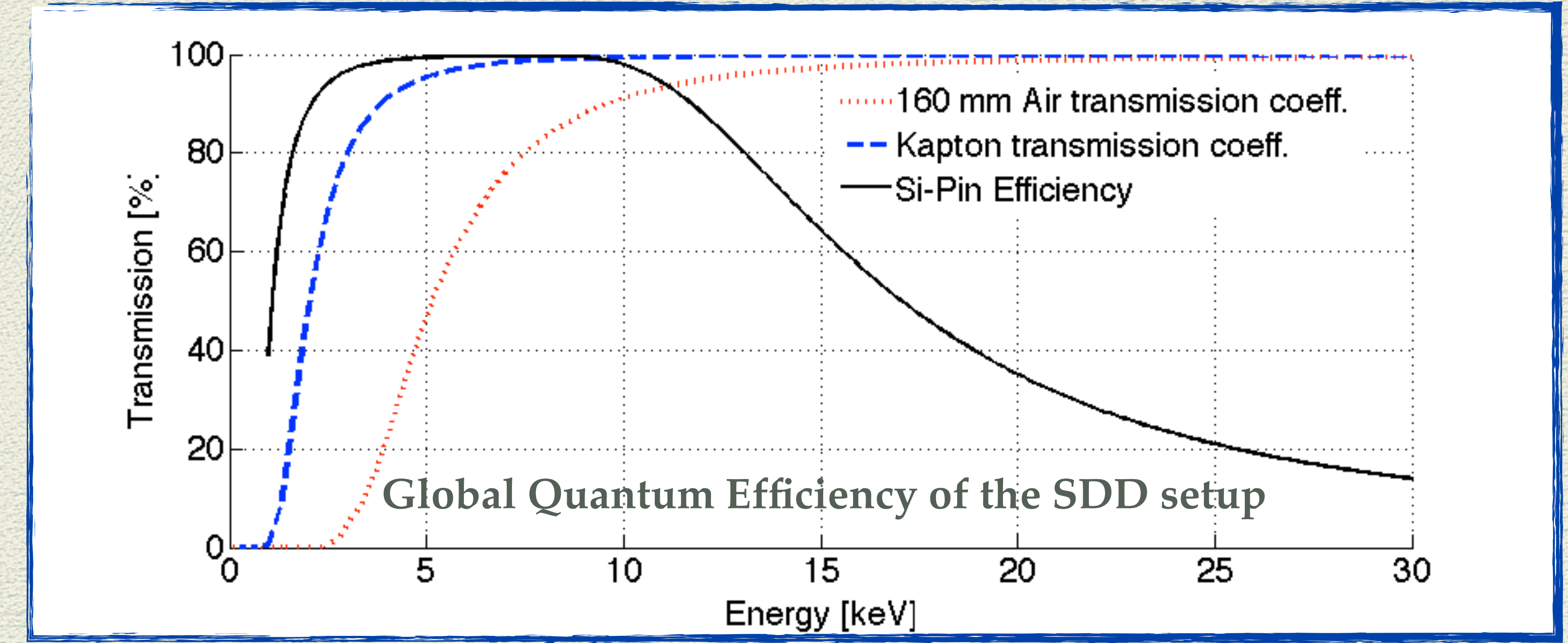

Global Quantum Efficiency of the SDD setup

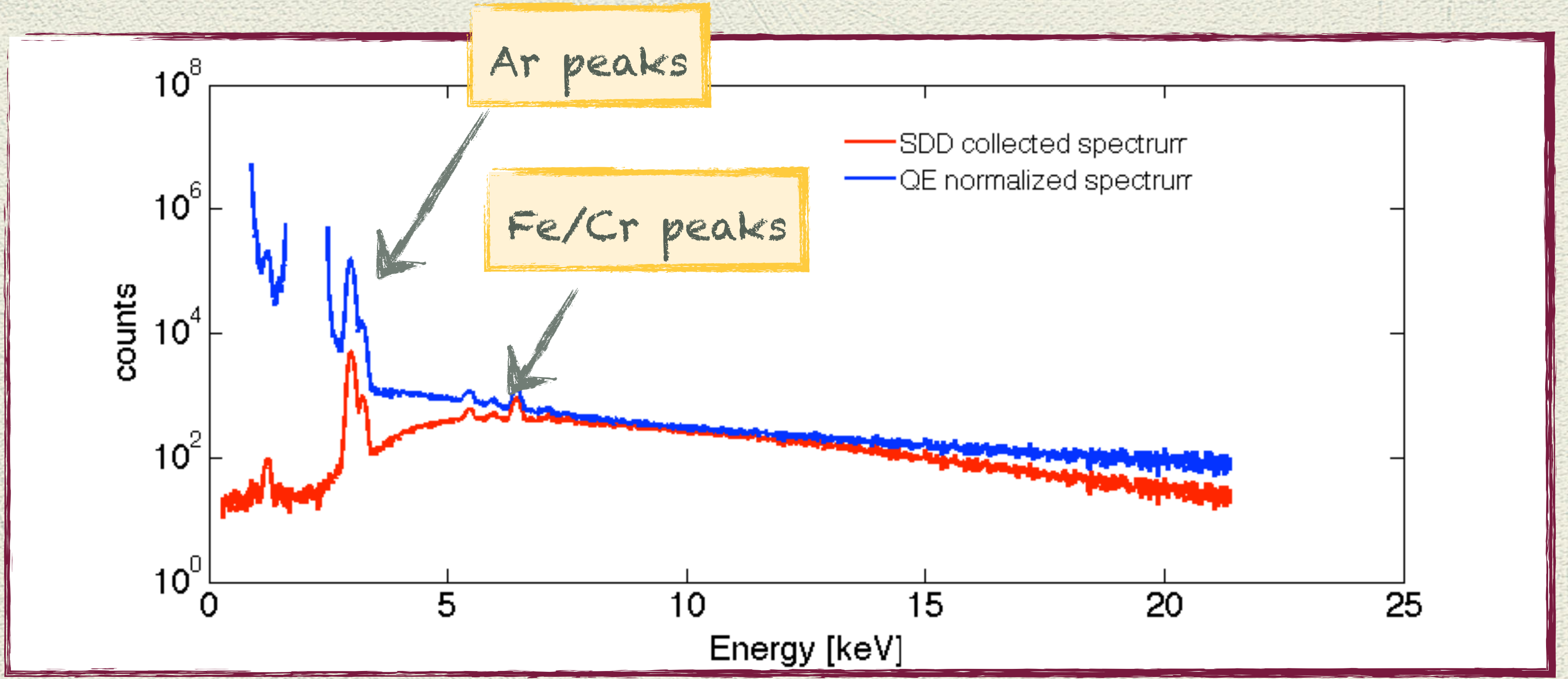

Spectral renormalization for the SDD setup

SDD – Data Analysis

Analysis procedure consists in evaluating the ***Experimental Emissivity*** *after ε_g calculation, that must be then compared to the* ***Theoretical Emissivity*** *by fitting procedure.*

Exp. Emissivity

$$J(h\nu) = h\nu \frac{N^{ch}(h\nu)}{\varepsilon_g t} \frac{4\pi}{\Delta E V_p \Omega_{Tot}}$$

Theor. Emissivity

$$J_{M-K}(h\nu) = \boxed{N_i N_e} (Z\hbar)^2 \left(\frac{4\alpha}{\sqrt{6m_e}}\right)^3 \left(\frac{\pi}{kT_{Mw}}\right)^{1/2} e^{\left(-h\nu / \boxed{kT_{Mw}}\right)}$$

Plasma density

Plasma temperature

(SDD) F.T.E. study

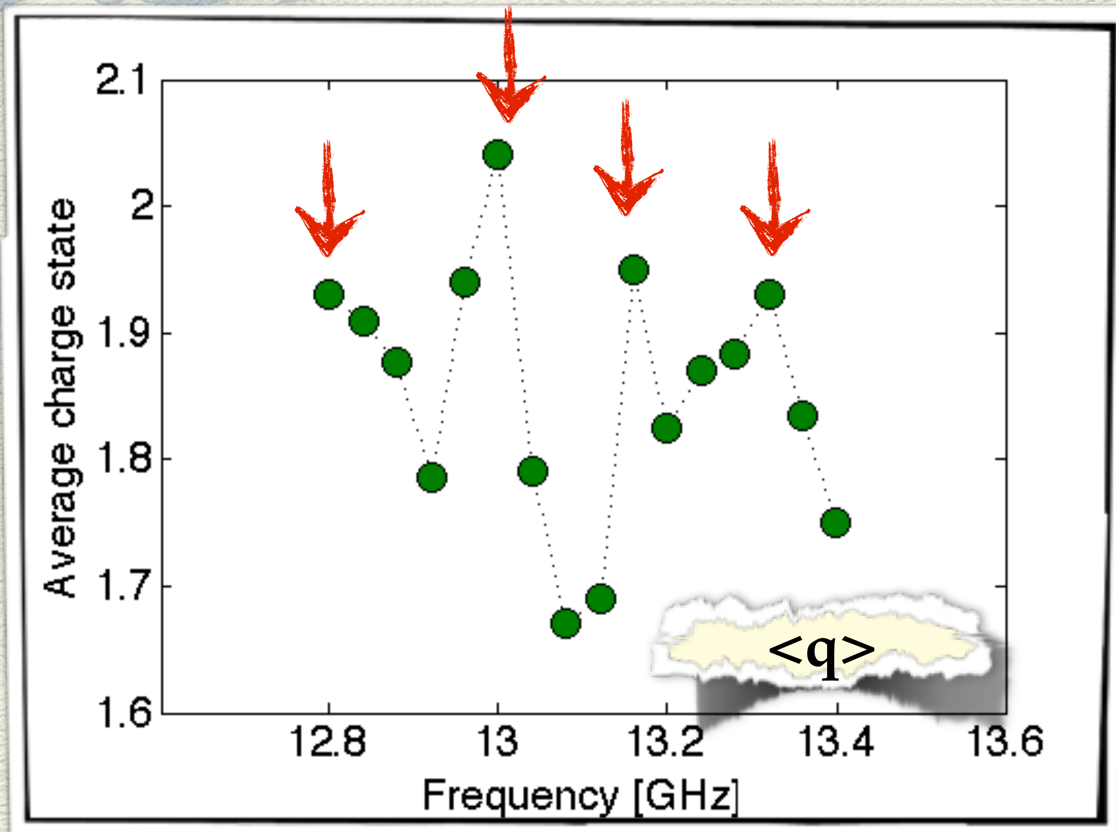

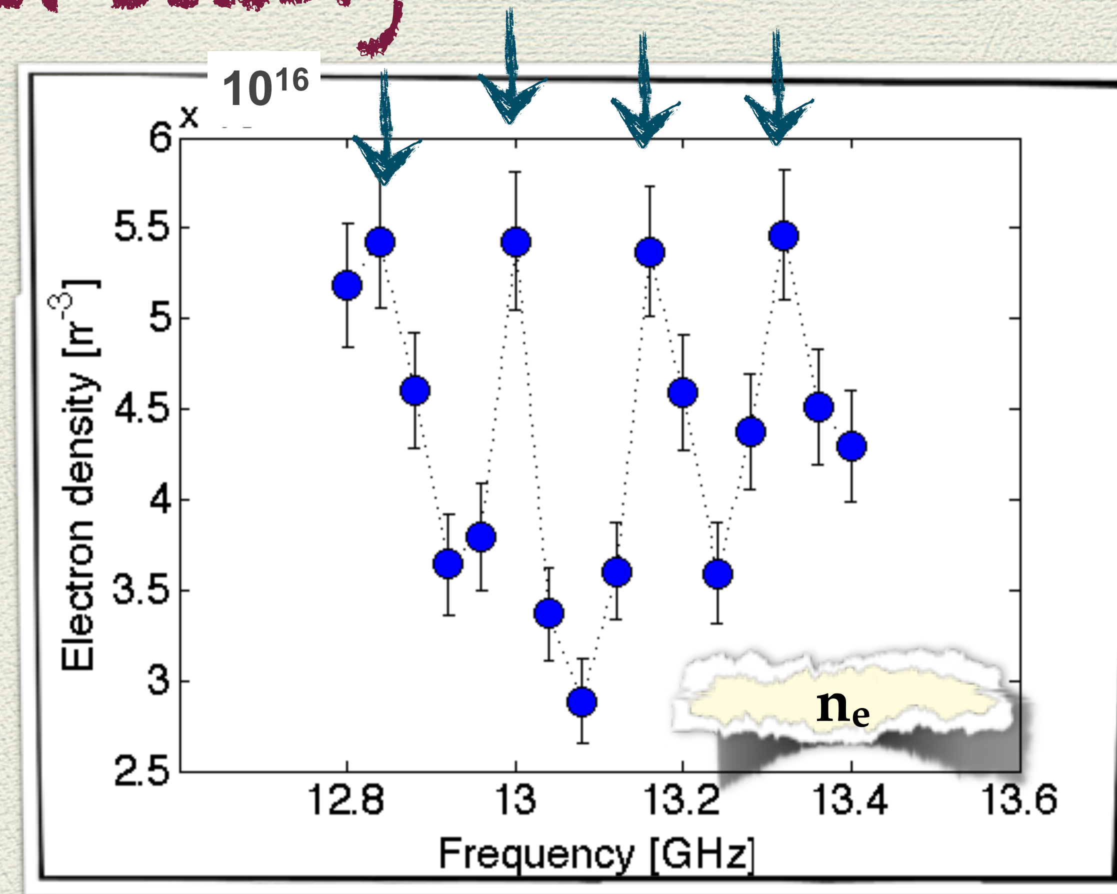

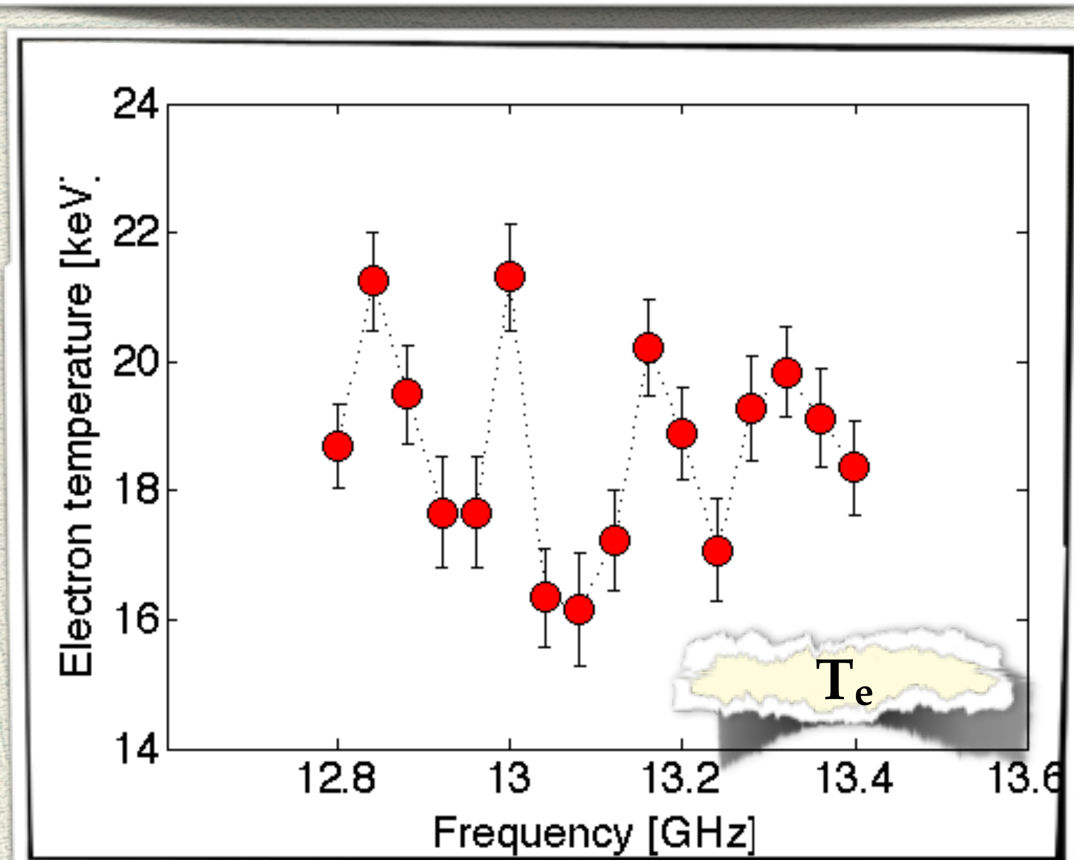

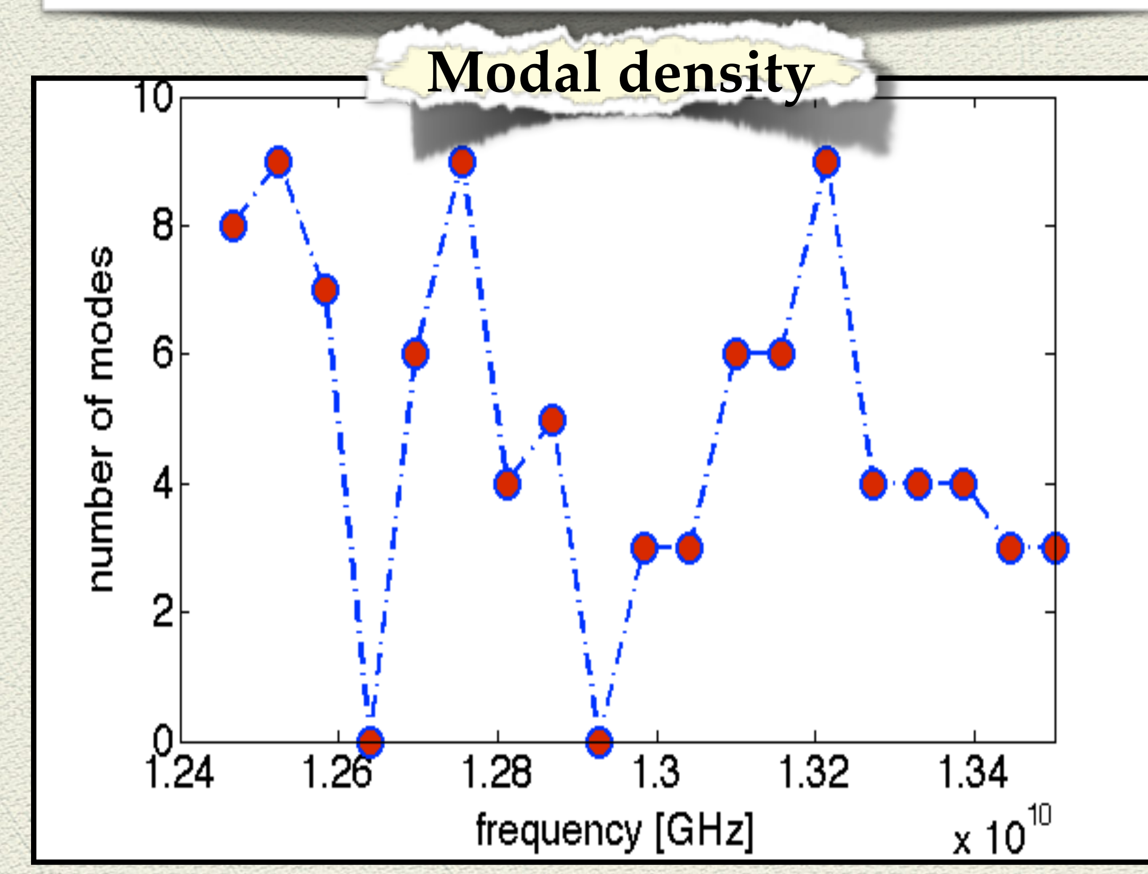

CCD camera Set-up

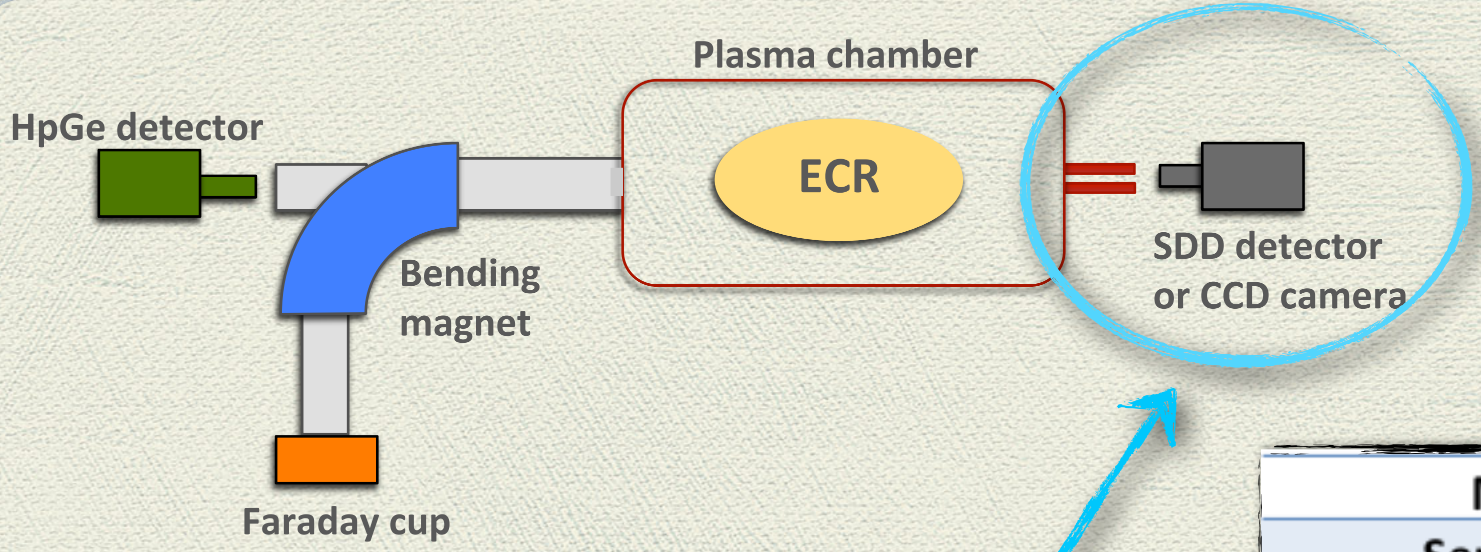

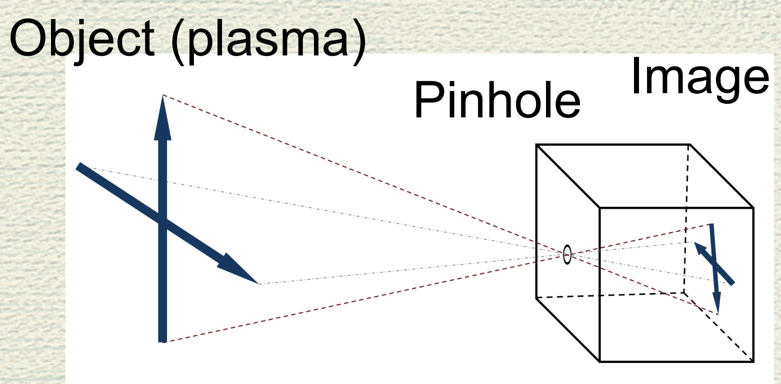

Model	Andor Technology - Newton
Sensor size	27.6 mm x 6.9 mm
Pixels	1024 x 255 (0.3 MP)
Energy Resolution	150 eV
Energy range	1-10 keV
Magnification	0.082-0.124-0.158
Pin-hole diameters	75 um and 100 um (W and Pb)

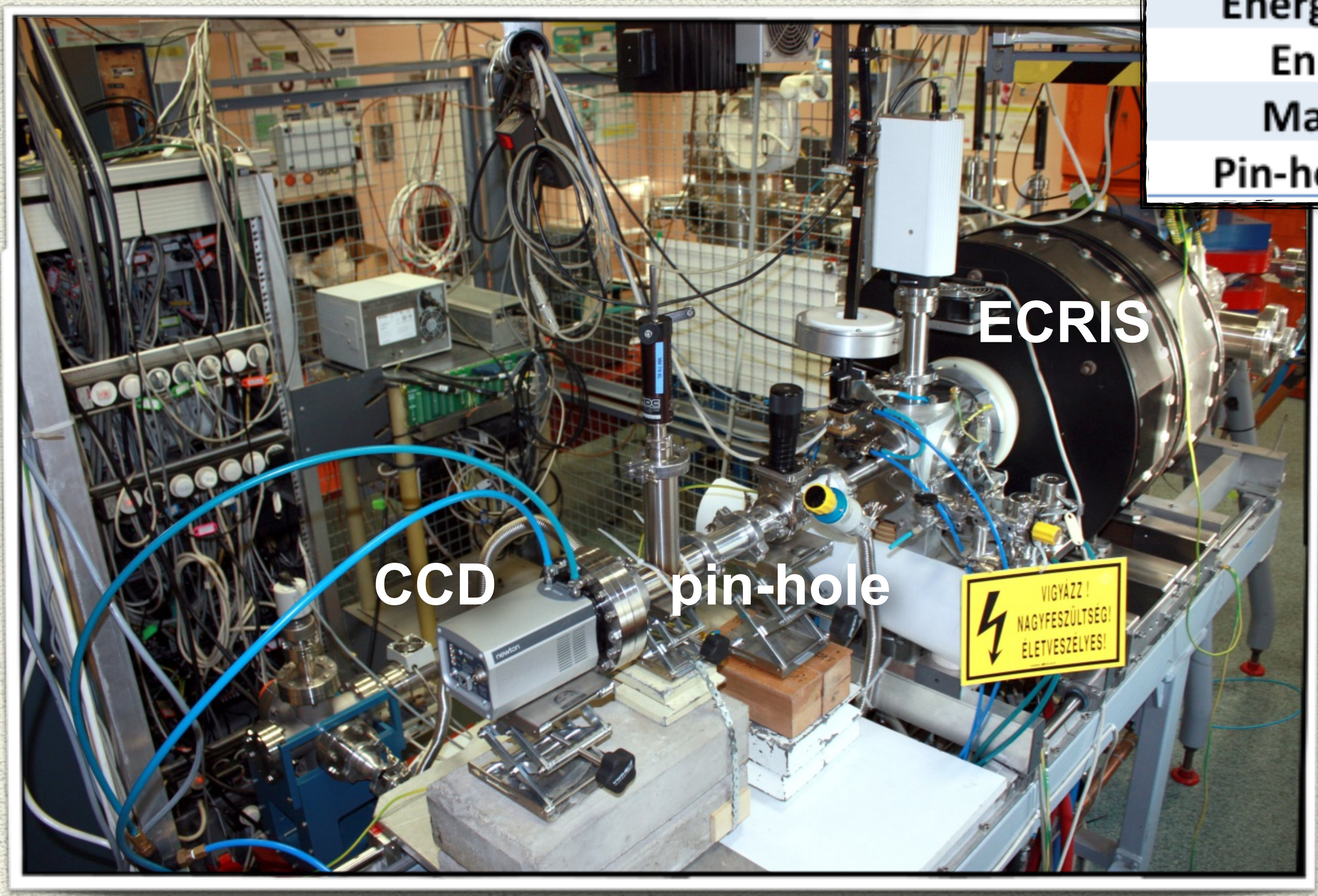

Pin-hole holder

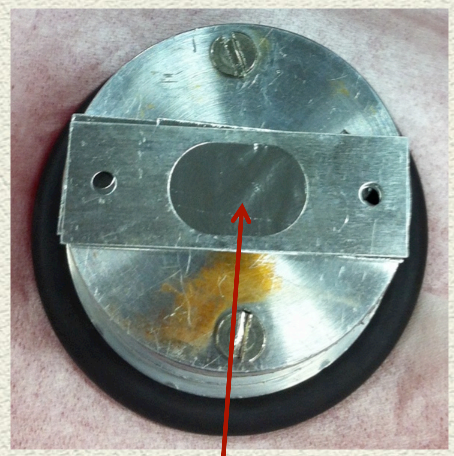

Aluminum Window

X-ray imaging

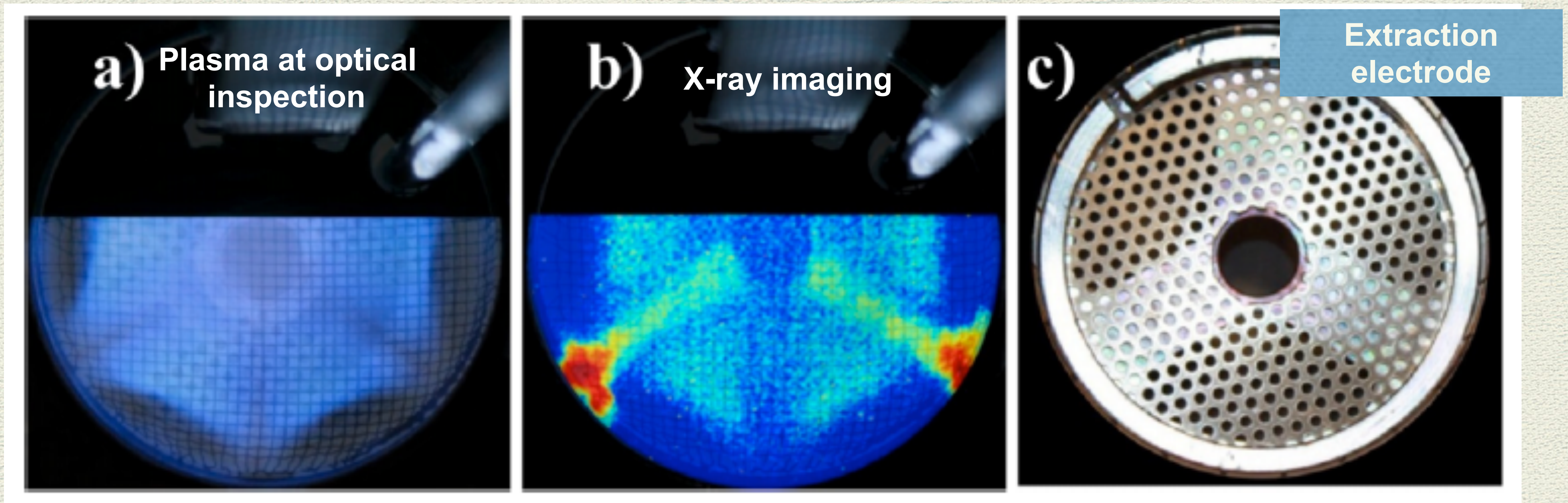

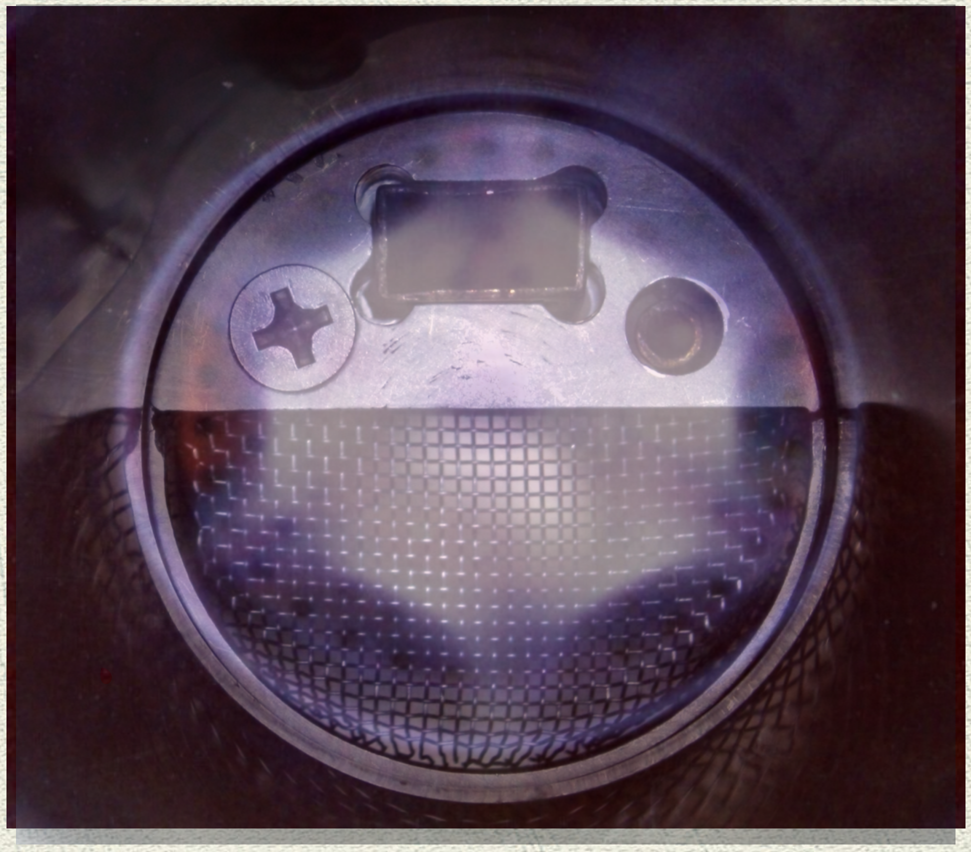

- X-ray imaging: single frame acquisition, up to 30-40 sec. needed, no energy information;
- Photon Counting mode: from 10^{-6} to 0.3 sec., depending on the ROI.
- A Stainl-Steel grid was placed at injection edplate allowing plasma inspection
- Spatial resolution is high enough to find the mesh in X-ray images

X-ray imaging

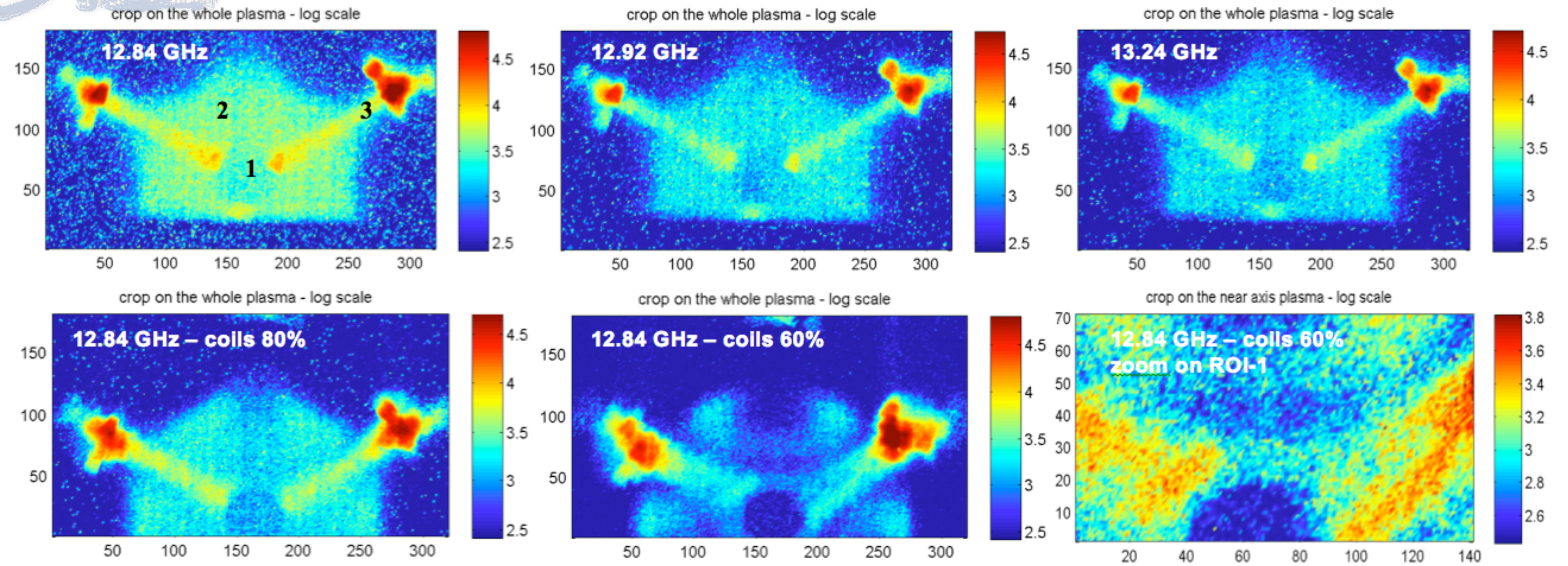

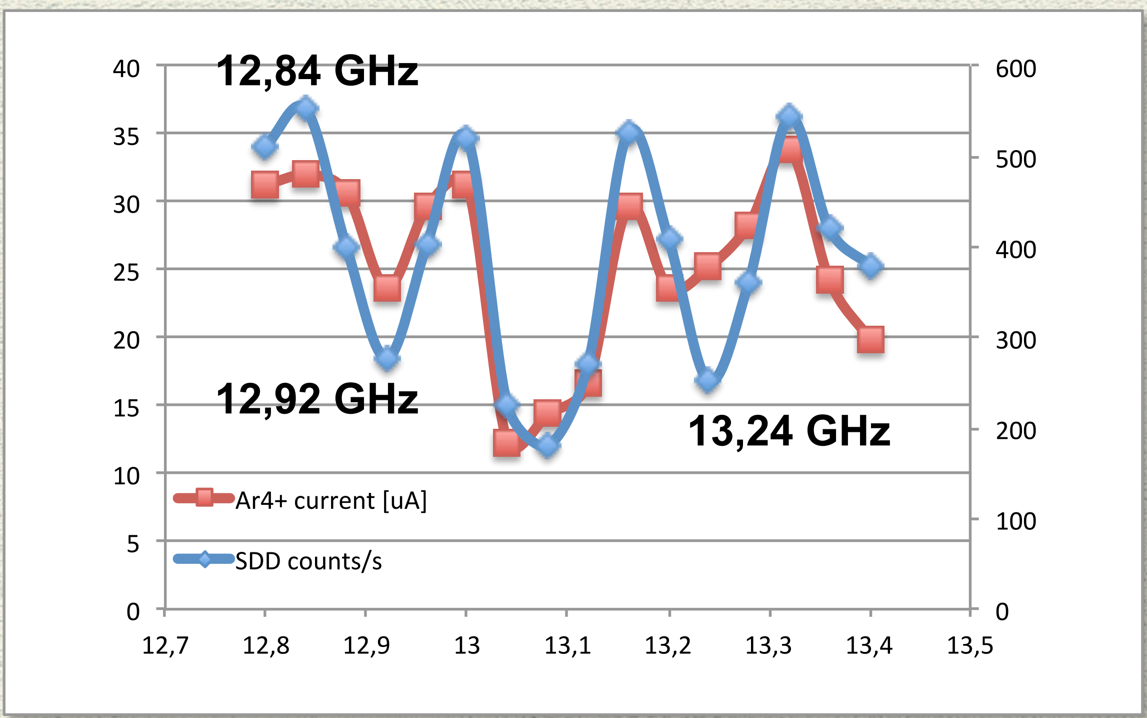

From a general inspection of the pictures, it is clearly visible the structure of the plasma:

- the hole in the near axis region
- the branches due to the electrons escaping from the confinement
- he hot spots due to lost electrons producing bremsstrahlung radiation when impinging on the chamber walls.

2D resolved X-ray spectroscopy

Preliminary tests carried out with a multi-metals matrix:

- energy resolution
- spatial resolution

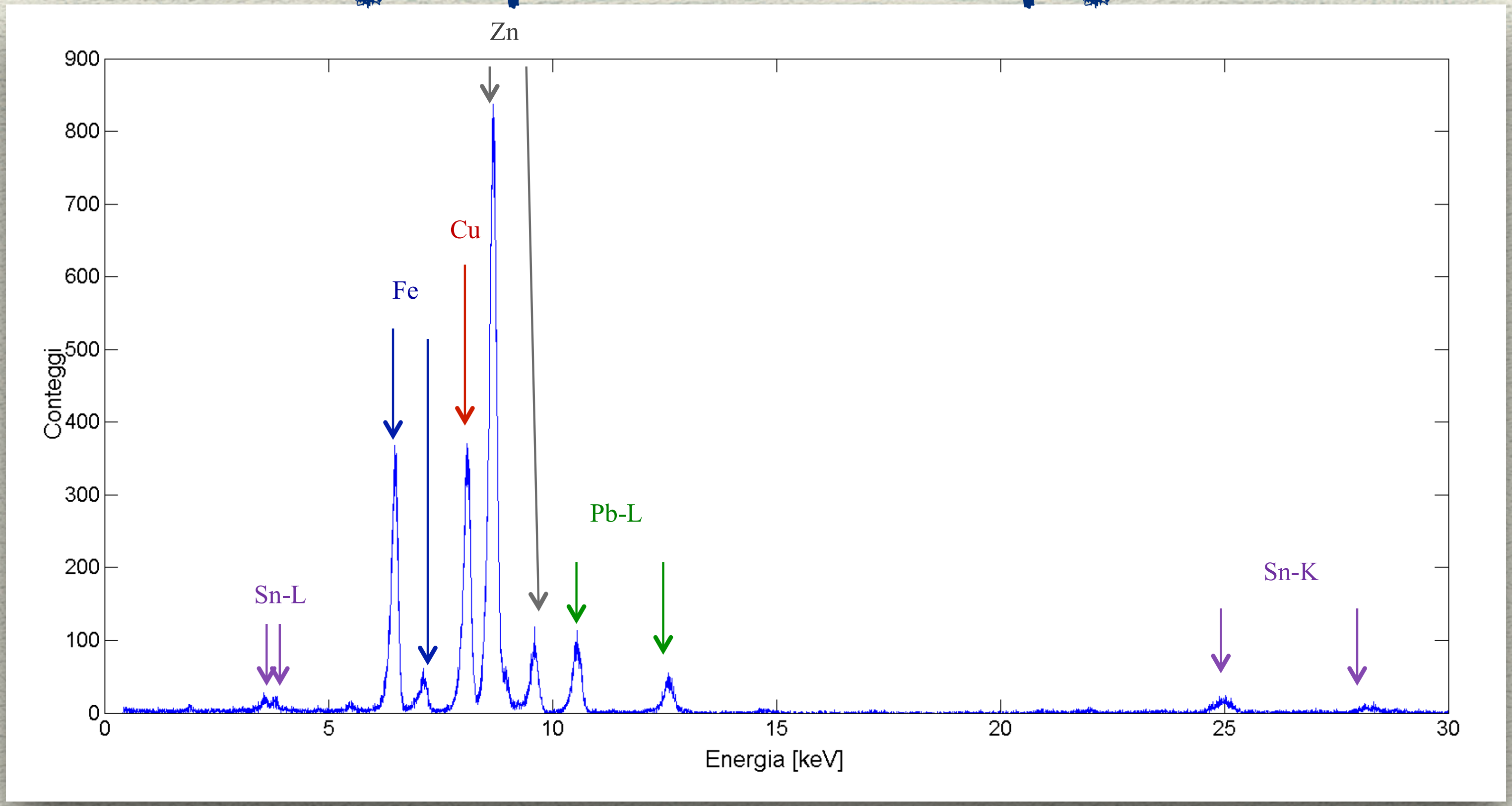

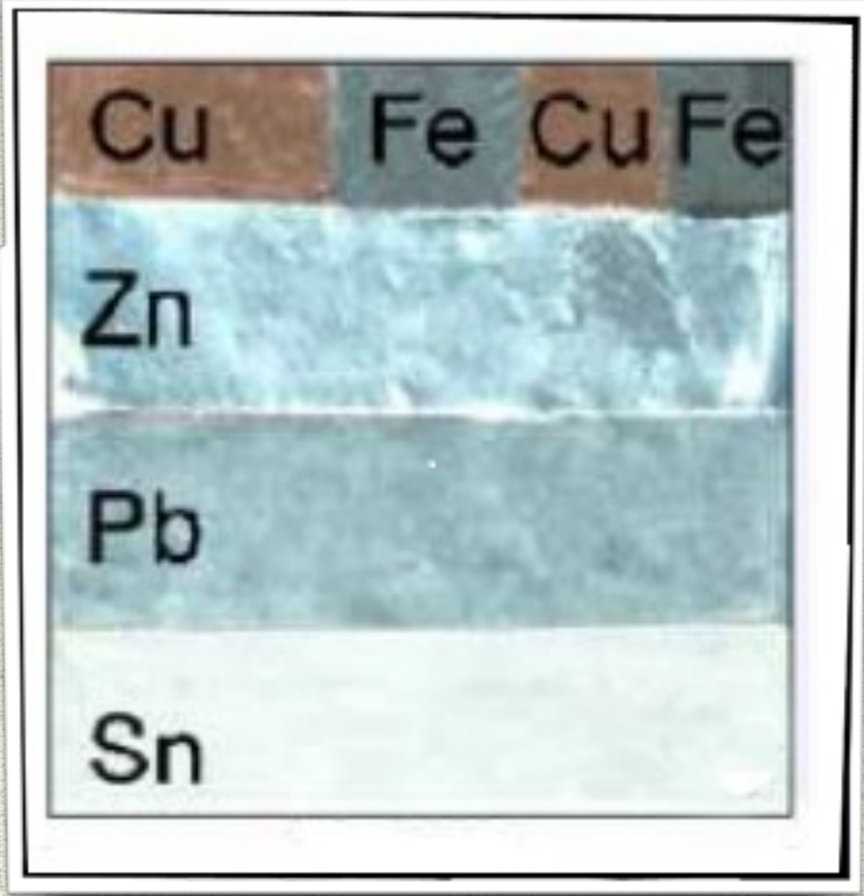

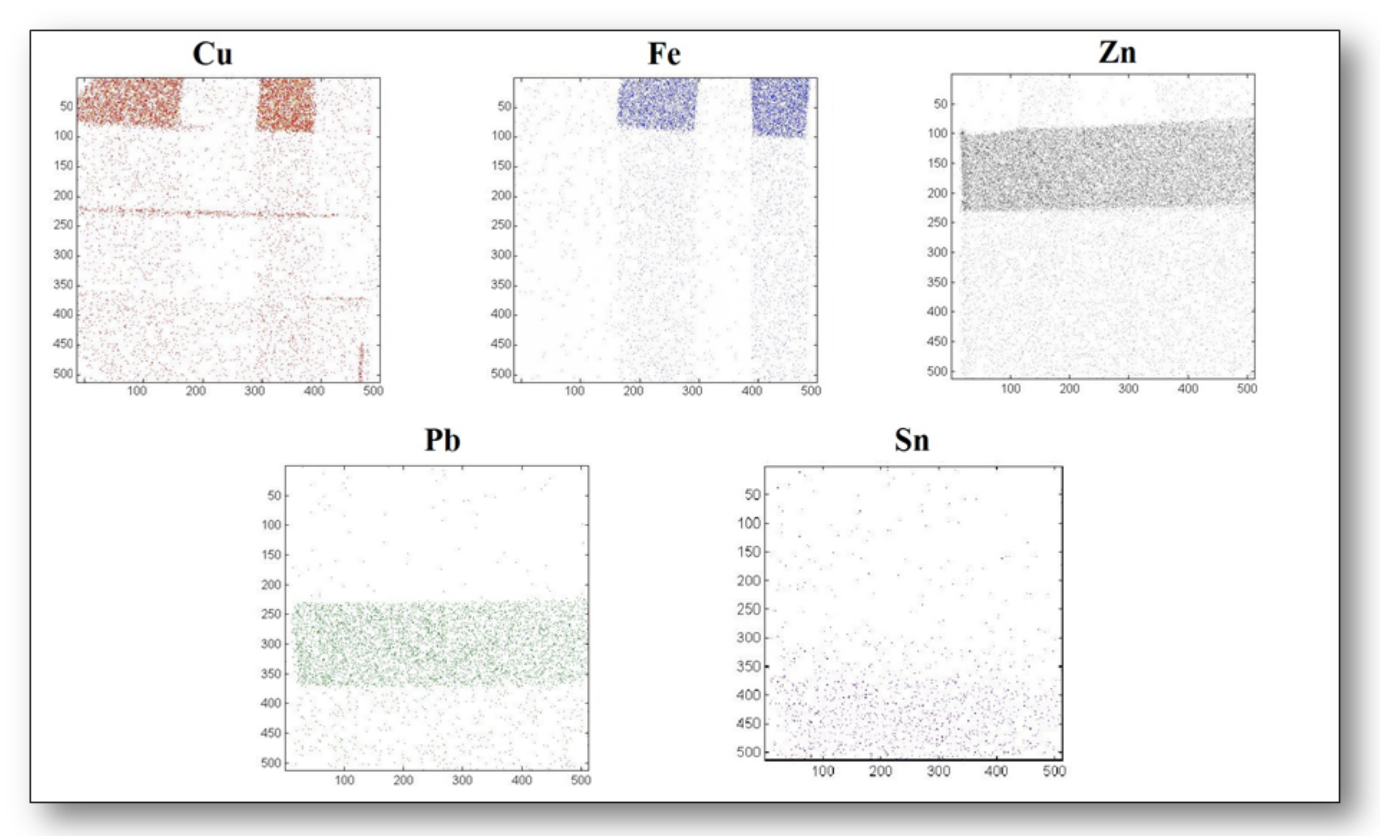

Plasma inspection by energy filtering

CCD camera Spectrum – ***Space resolved Specctroscopy***

X-ray Plasma Spectrum detected by using a CCD Camera like a common X-ray detector

AIR Plasma *@ Pressure:* ***1.5 10^{-4} mbar*** *Frequency:* ***3,7475 GHz*** *Power:* ***100 W***

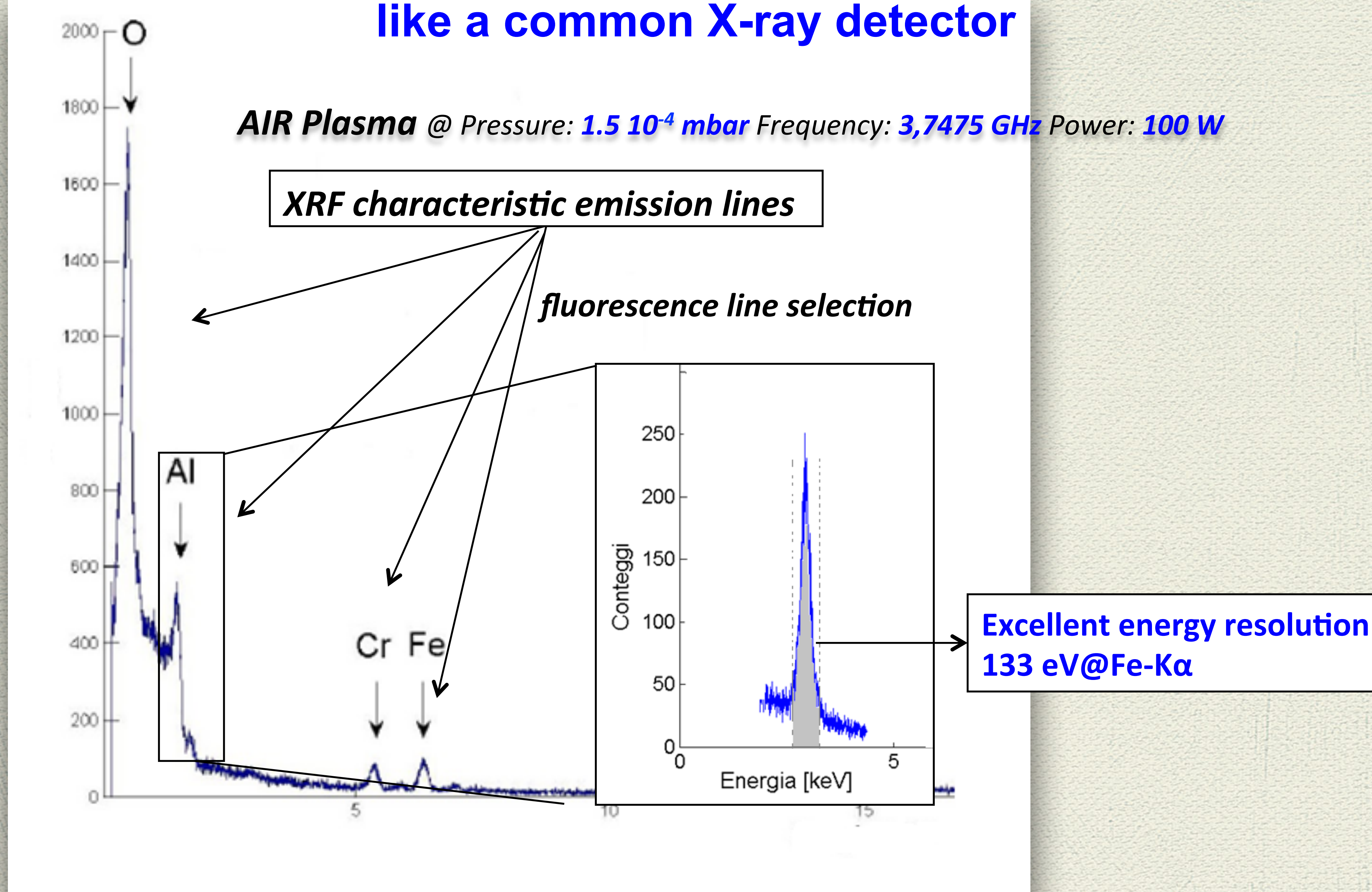

Plasma inspection after energy filtering

12.84 GHz - distribution at different energies

(equalized pseudocolor maps)

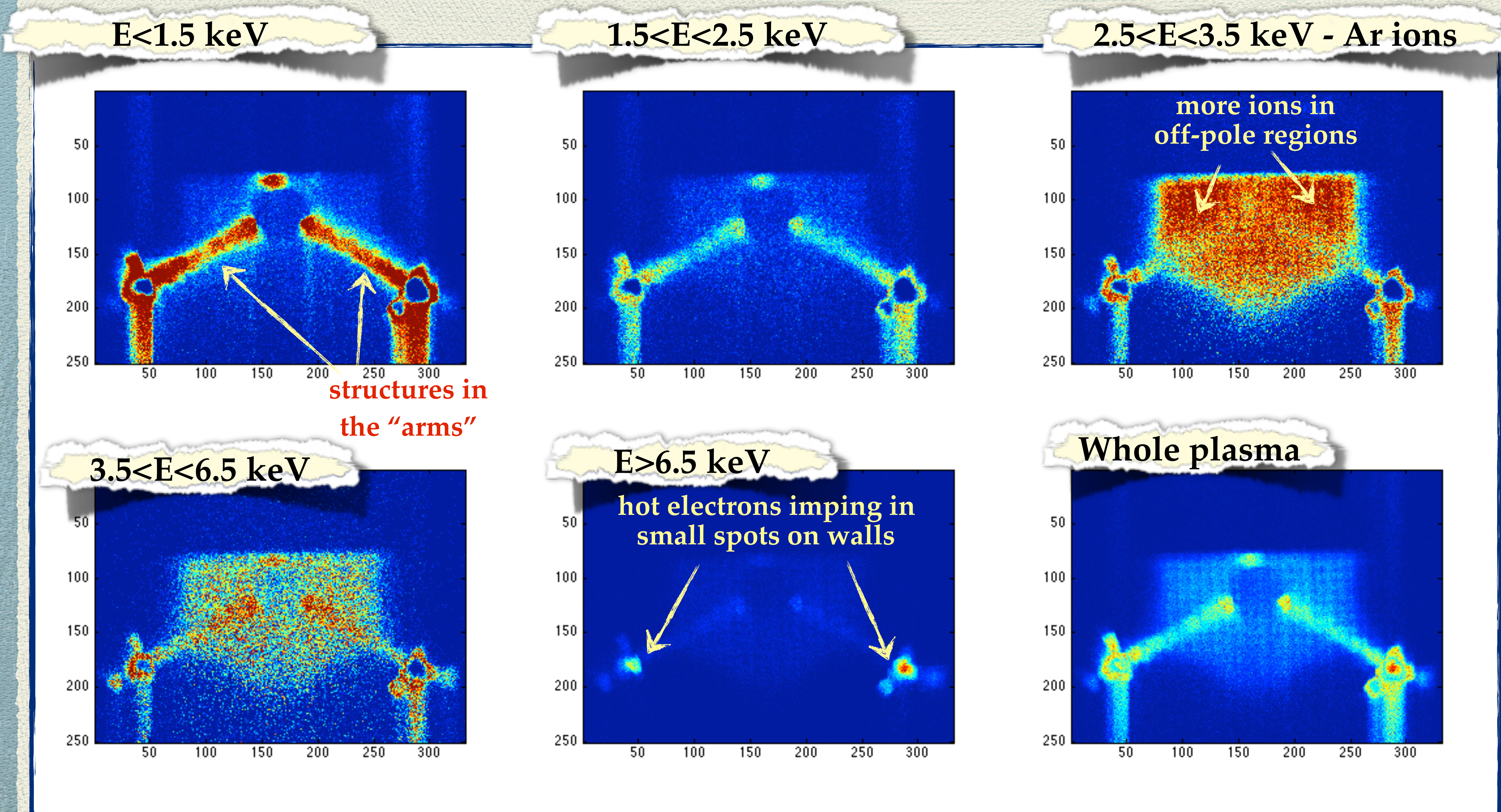

Plasma inspection after energy filtering

12.92 GHz - distribution at different energies

(equalized pseudocolor maps)

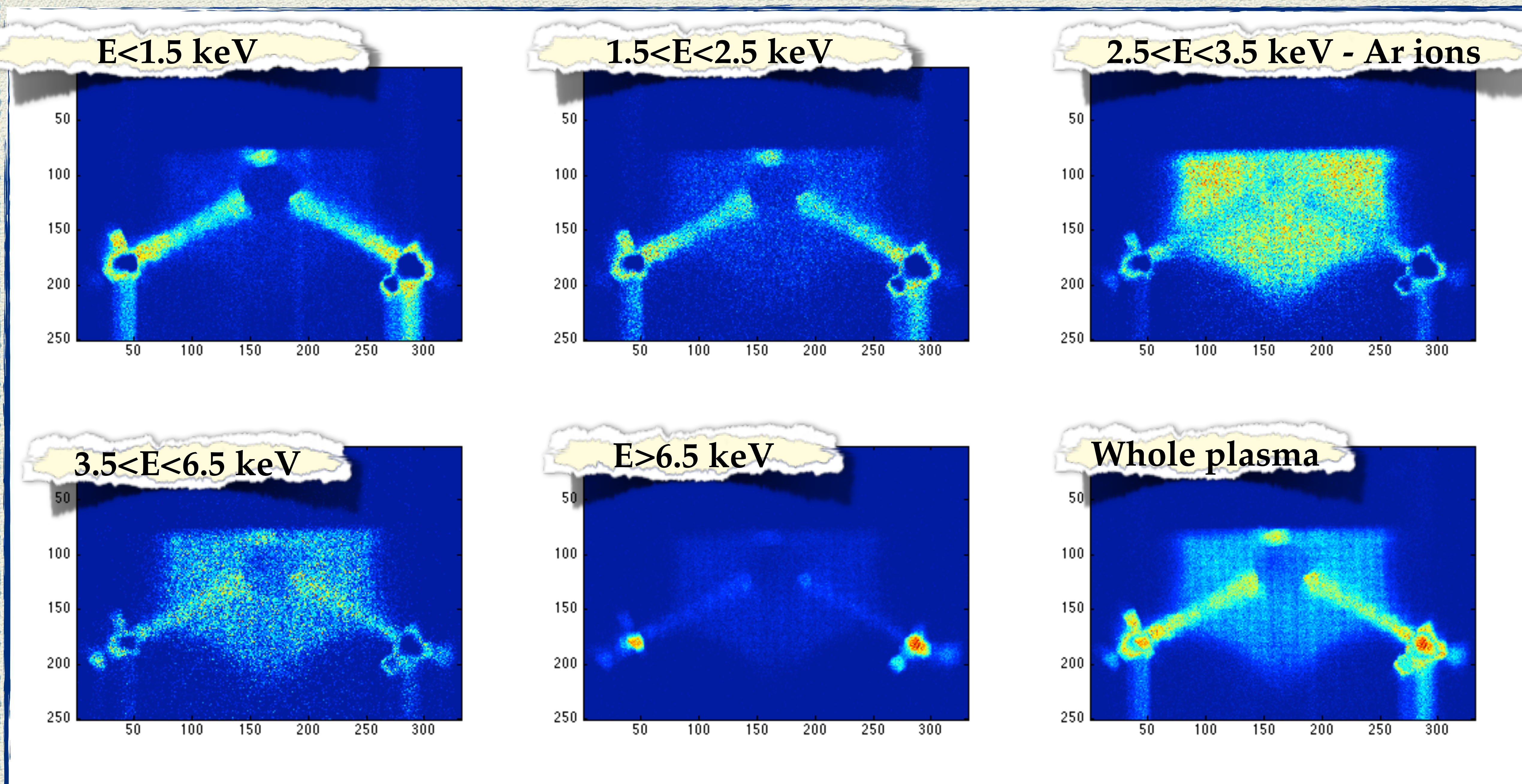

Analysis of plasma morphology

2.8<E<3.5 keV

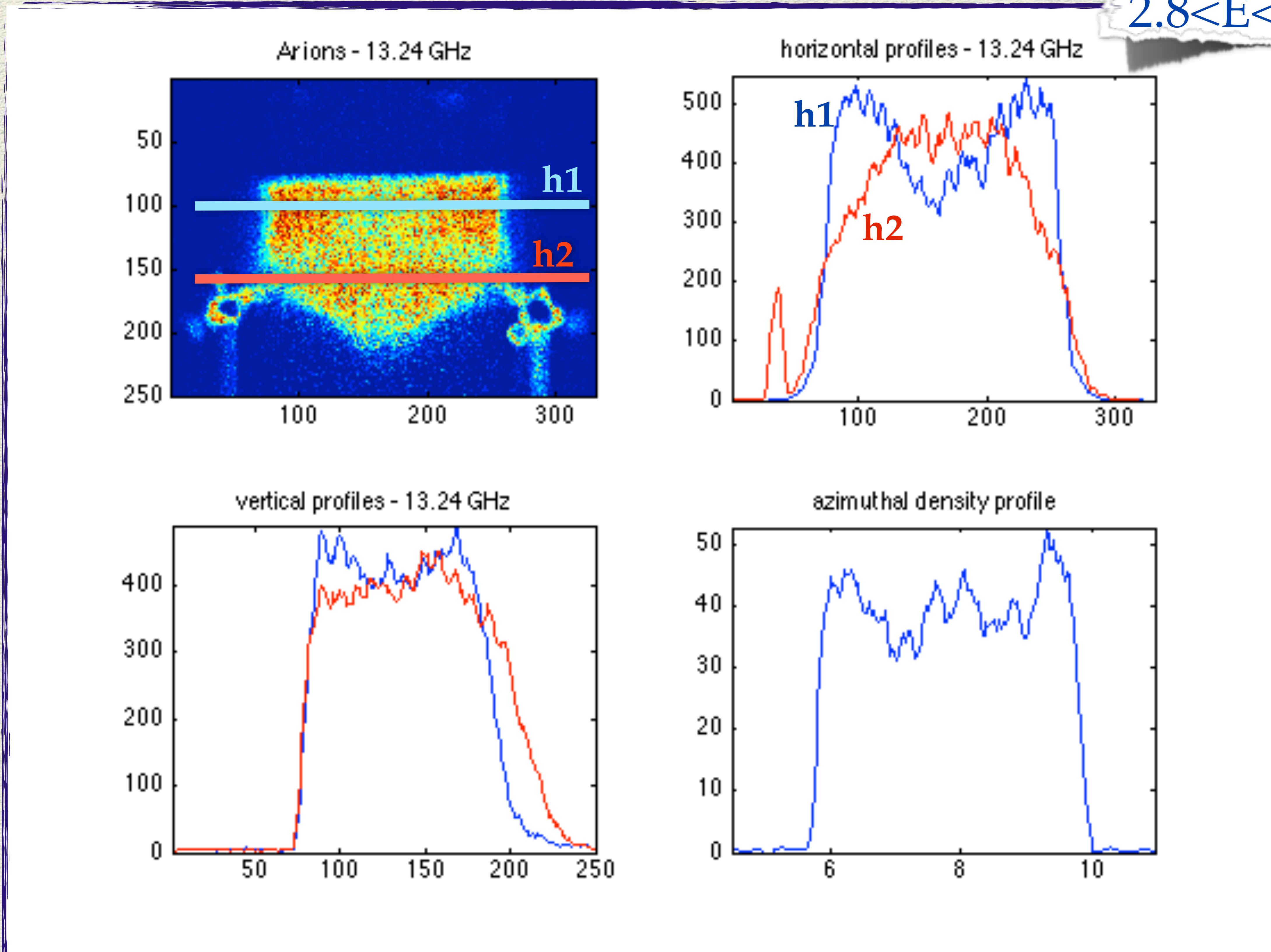

Comparison with self-consistent simulations

$$\frac{d\vec{v}}{dt} = \frac{q}{m_0\gamma}\left[\vec{E} + \vec{v}\times B - \frac{\vec{v}\cdot\vec{E}}{c^2}\vec{v}\right]$$

Solving the ***time-dependent Vlasov equation****, including single particle collisions*

$$\frac{\partial f_\alpha}{\partial t} + \vec{v}\cdot\vec{\nabla} f_\alpha + \frac{q_\alpha}{m_\alpha}\left(\vec{E} + \frac{\vec{v}\times\vec{B}}{c}\right)\cdot\vec{\nabla}_{\vec{v}} f_\alpha = 0$$

Step-by-step current

Step-by-step plasma density

$$\begin{aligned}
\vec{\nabla}\cdot\vec{E} &= 4\pi\sum_\alpha \overline{n}_\alpha q_\alpha \boxed{\int f_\alpha d\vec{v}} + 4\pi\rho_{ext} \\
\vec{\nabla}\times\vec{B} &= \frac{1}{c}\frac{\partial\vec{E}}{\partial t} + \frac{4\pi}{c}\sum_\alpha \overline{n}_\alpha q_\alpha \boxed{\int \vec{v} f_\alpha d\vec{v}} + \frac{4\pi}{c}\vec{J}_{ext} \\
\vec{\nabla}\times\vec{E} &= -\frac{1}{c}\frac{\partial\vec{B}}{\partial t}
\end{aligned}$$

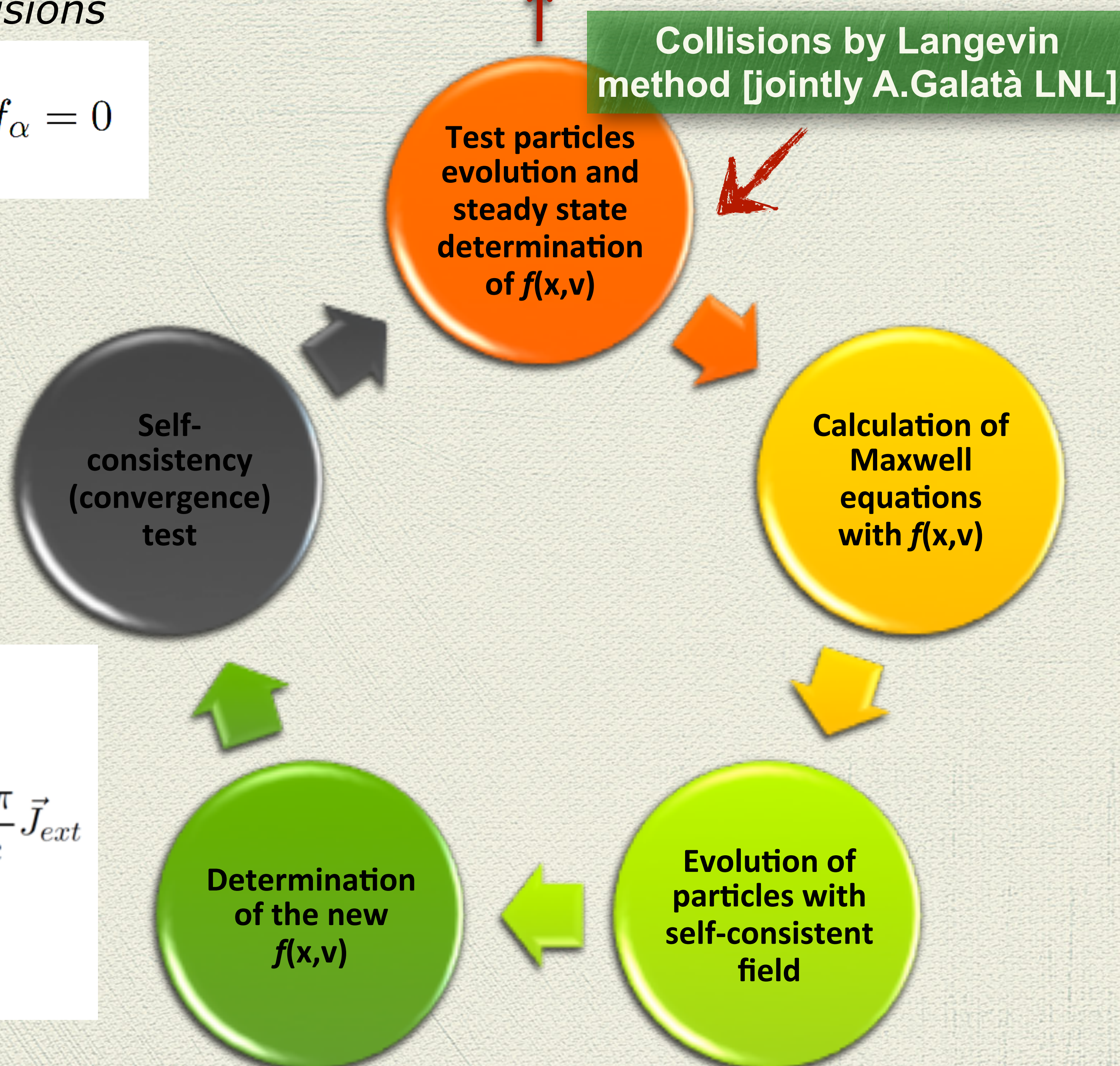

Comparison with self-consistent simulations

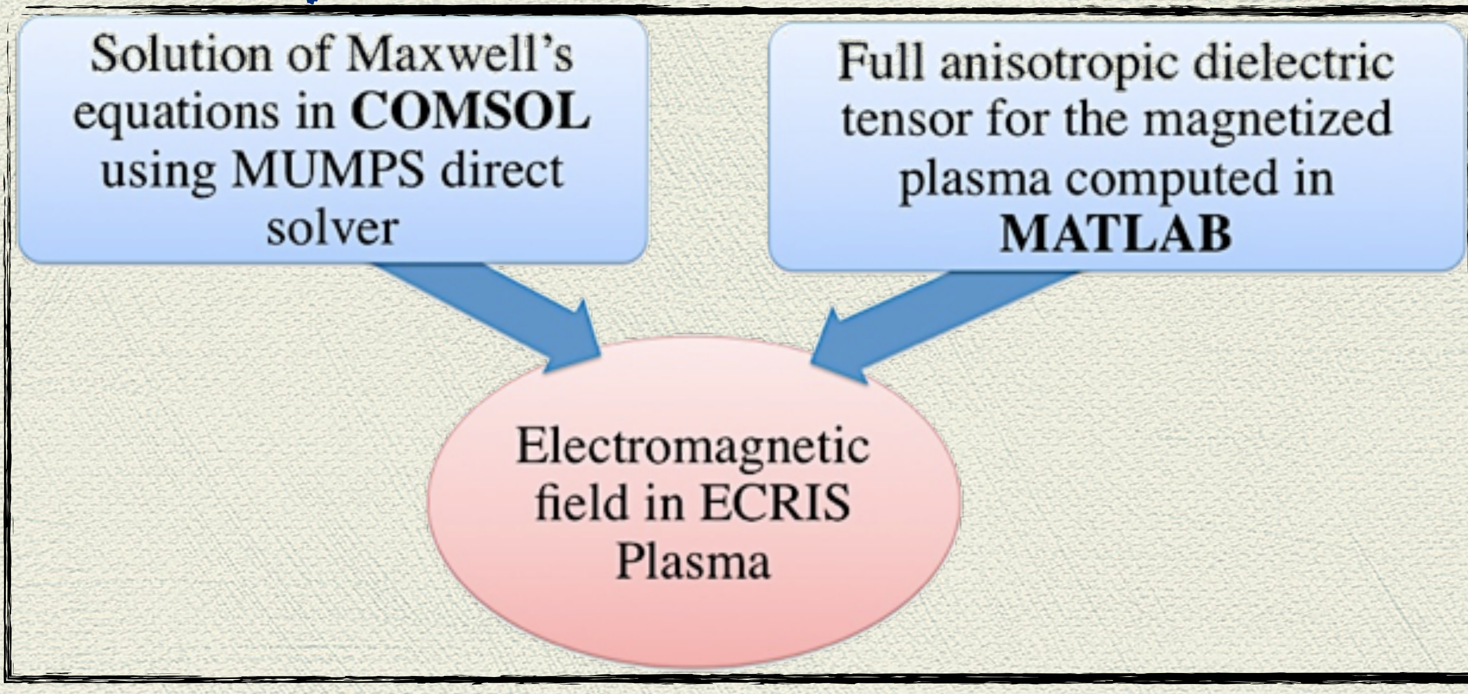

$$\nabla \times \nabla \times \boldsymbol{E} - \frac{\omega^2}{c^2}\overline{\overline{\epsilon_r}} \cdot \boldsymbol{E} = 0$$

Wave equation with tensorial permittivity

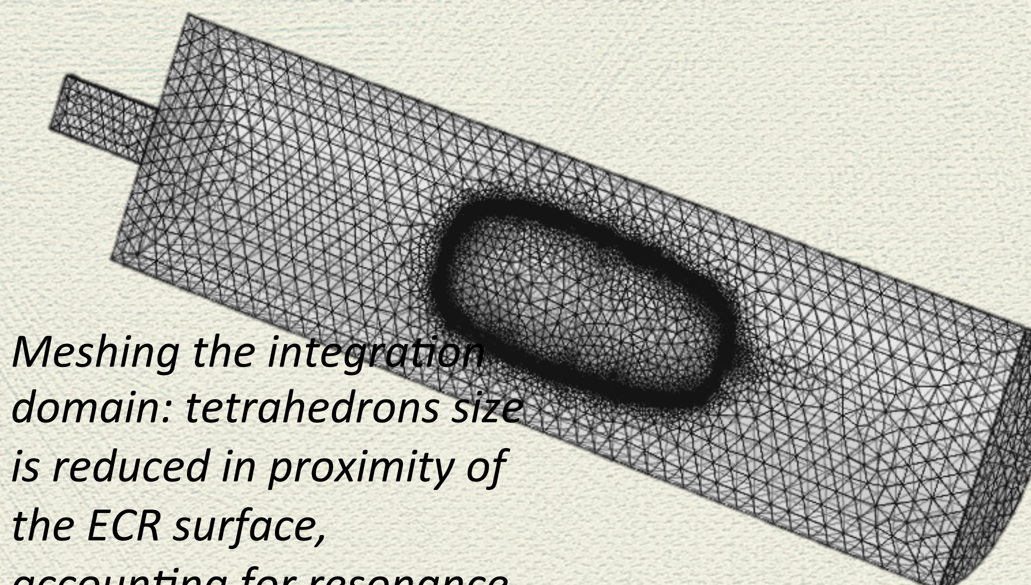

Meshing the integration domain: tetrahedrons size is reduced in proximity of the ECR surface, accounting for resonance.

$$\overline{\overline{\epsilon}} = \epsilon_0 \overline{\overline{\epsilon}}_r = \epsilon_0 \left(\overline{\overline{\epsilon'}} - i\overline{\overline{\epsilon''}}\right) = \epsilon_0 \left(\overline{\overline{I}} - \frac{i\overline{\overline{\sigma}}}{\omega\epsilon_0}\right)$$

$$= \epsilon_0 \begin{bmatrix} 1 + i\frac{\omega_p^2}{\omega}\frac{a_x}{\Delta} & i\frac{\omega_p^2}{\omega}\frac{c_z + d_{xy}}{\Delta} & i\frac{\omega_p^2}{\omega}\frac{-c_y + d_{xz}}{\Delta} \\ i\frac{\omega_p^2}{\omega}\frac{-c_z + d_{xy}}{\Delta} & 1 + \frac{i\omega_p^2}{\omega}\frac{a_y}{\Delta} & i\frac{\omega_p^2}{\omega}\frac{c_x + d_{yz}}{\Delta} \\ i\frac{\omega_p^2}{\omega}\frac{c_y + d_{xz}}{\Delta} & i\frac{\omega_p^2}{\omega}\frac{-c_x + d_{zy}}{\Delta} & 1 + i\frac{\omega_p^2}{\omega}\frac{a_z}{\Delta} \end{bmatrix}$$

Full-3D non homogeneous dielectric permittivity
Tensor depends on local density and B-field

Full-wave solution of the electromagnetic field

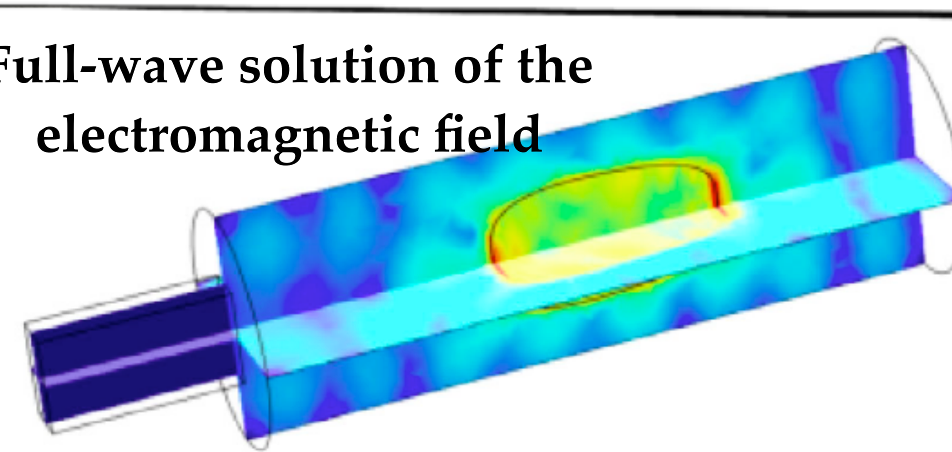

Searching self-consistency

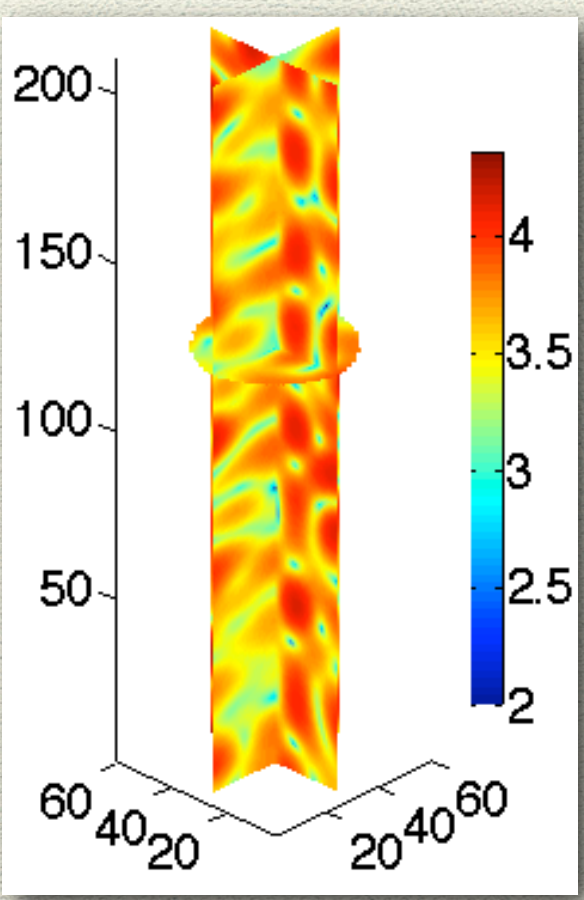

Freq. dom. solution
step 0
(vacuum cavity)

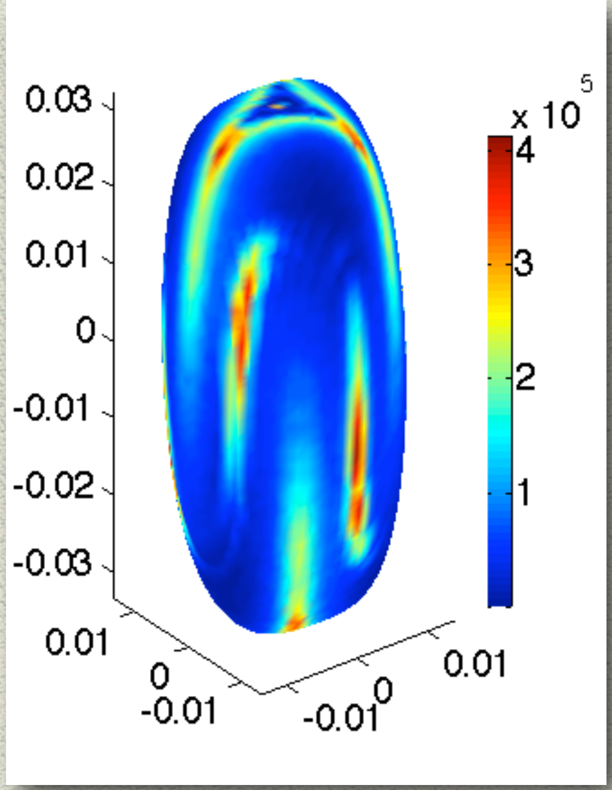

Particle Tracking
step 1
(vacuum field
+plasmoid-halo initial
density distr.)

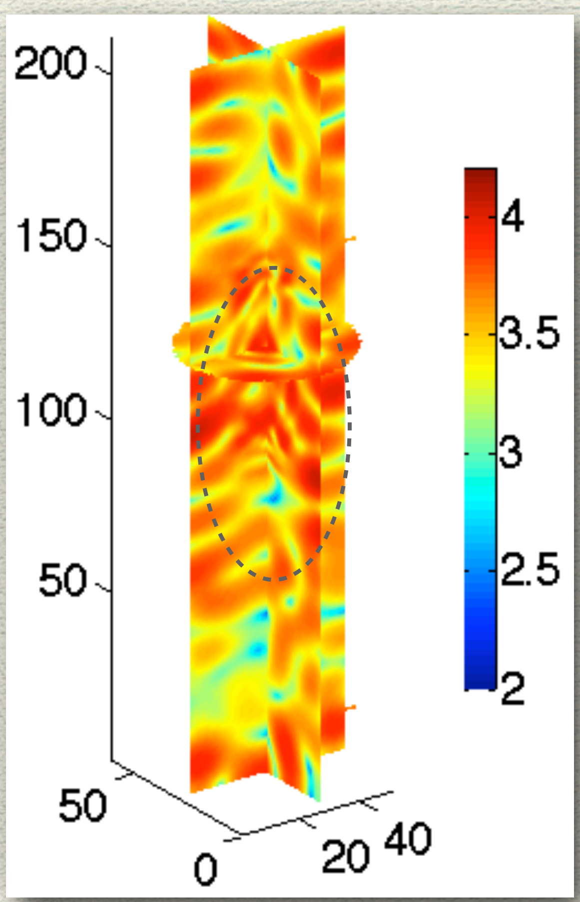

Freq. dom. solution
step 1
(70% density from
plasmoid halo model
+30% step-1 density
structure)

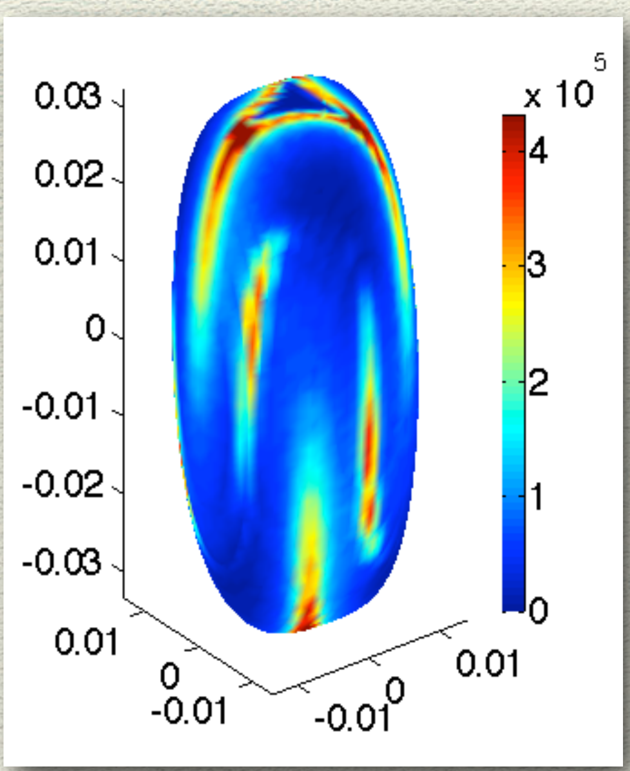

Particle Tracking
step 2
(70% vacuum field +
30% step-1 full-wave
calculated field)

Plasma shape at different energy domains

12.84 GHz

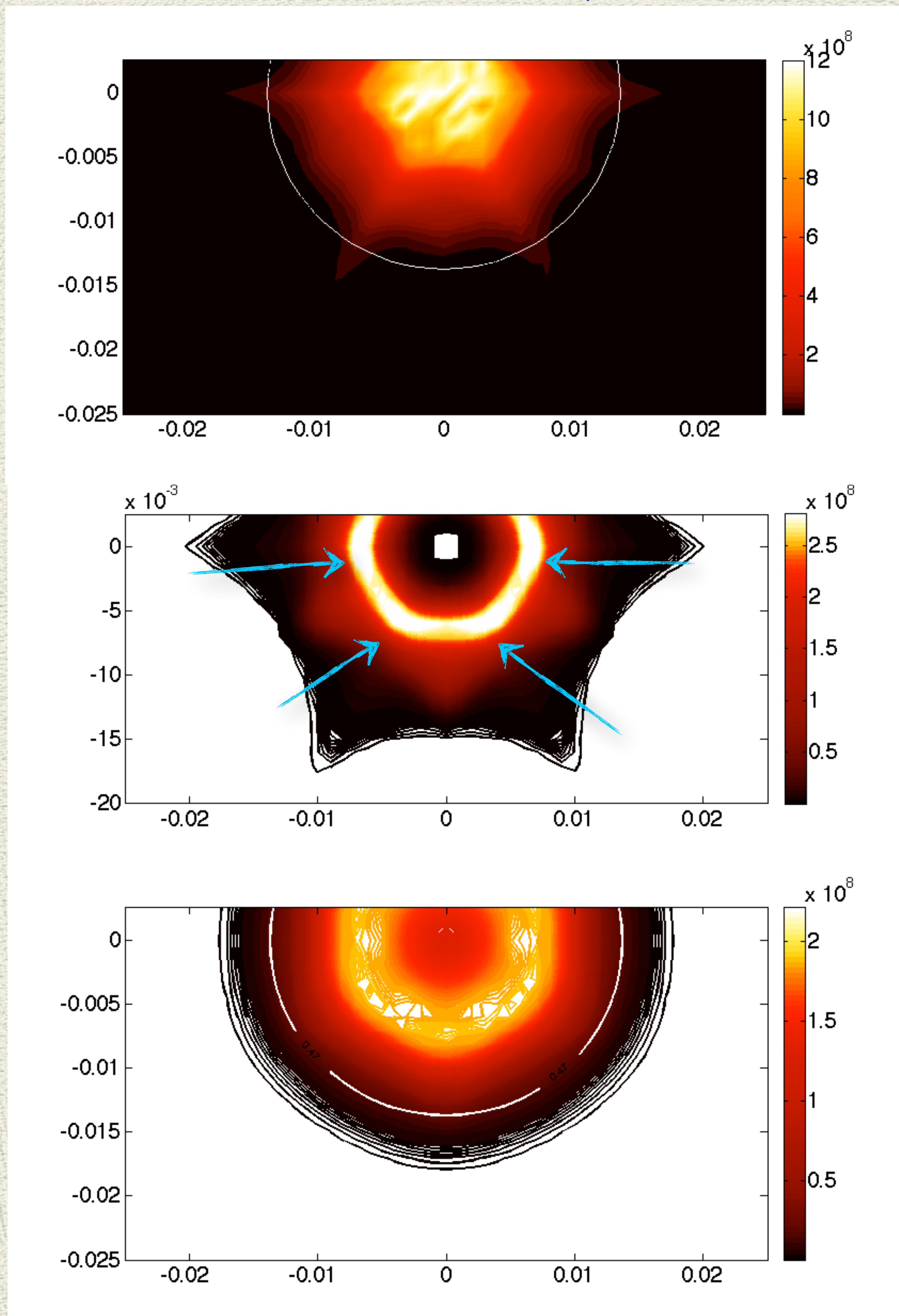

Cold Electrons

E<1 keV

concentration in the near axis region

Warm electrons

2 keV<E<30 keV

bright annulus with intense spots in off-pole region

Hot electrons

E>30 keV

broad annulus well inside the resonance layer

Comparison to self-consistent simulations
12.92 GHz

Experimental result Ar-fluor. 3 keV

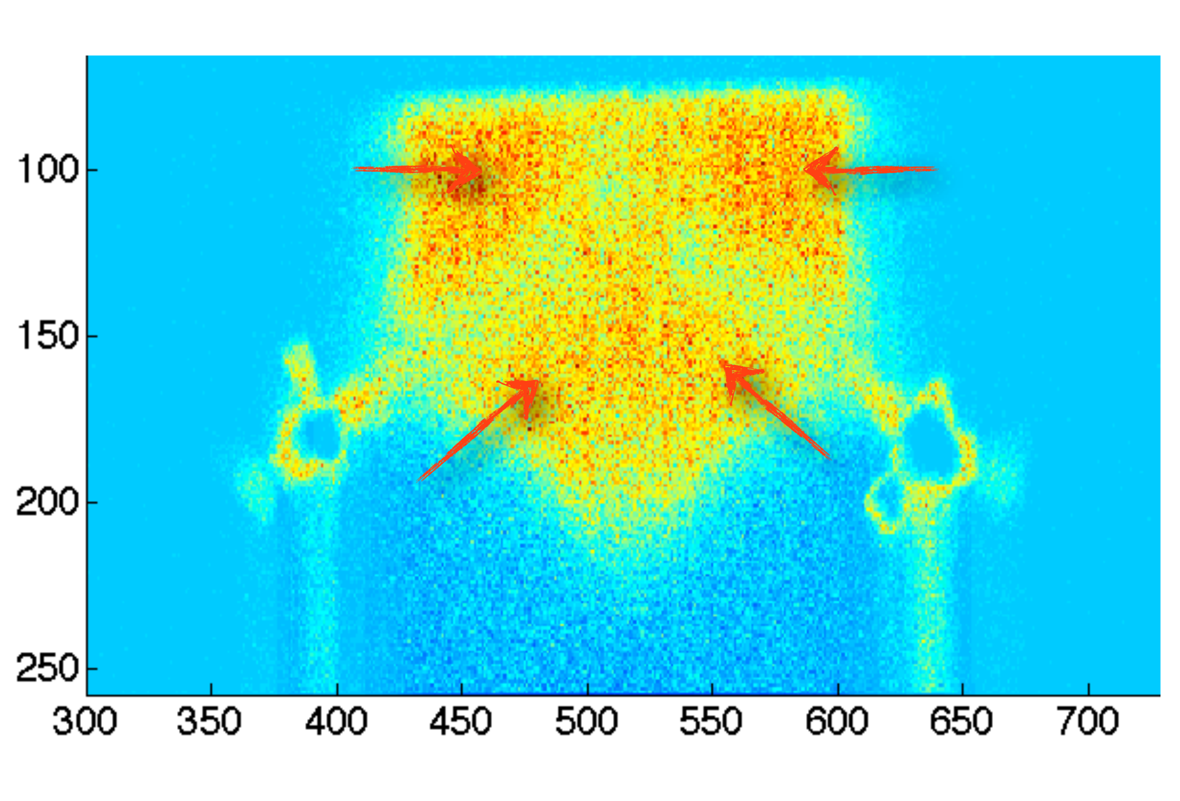

Simulations - warm electrons at 2<E<30 keV

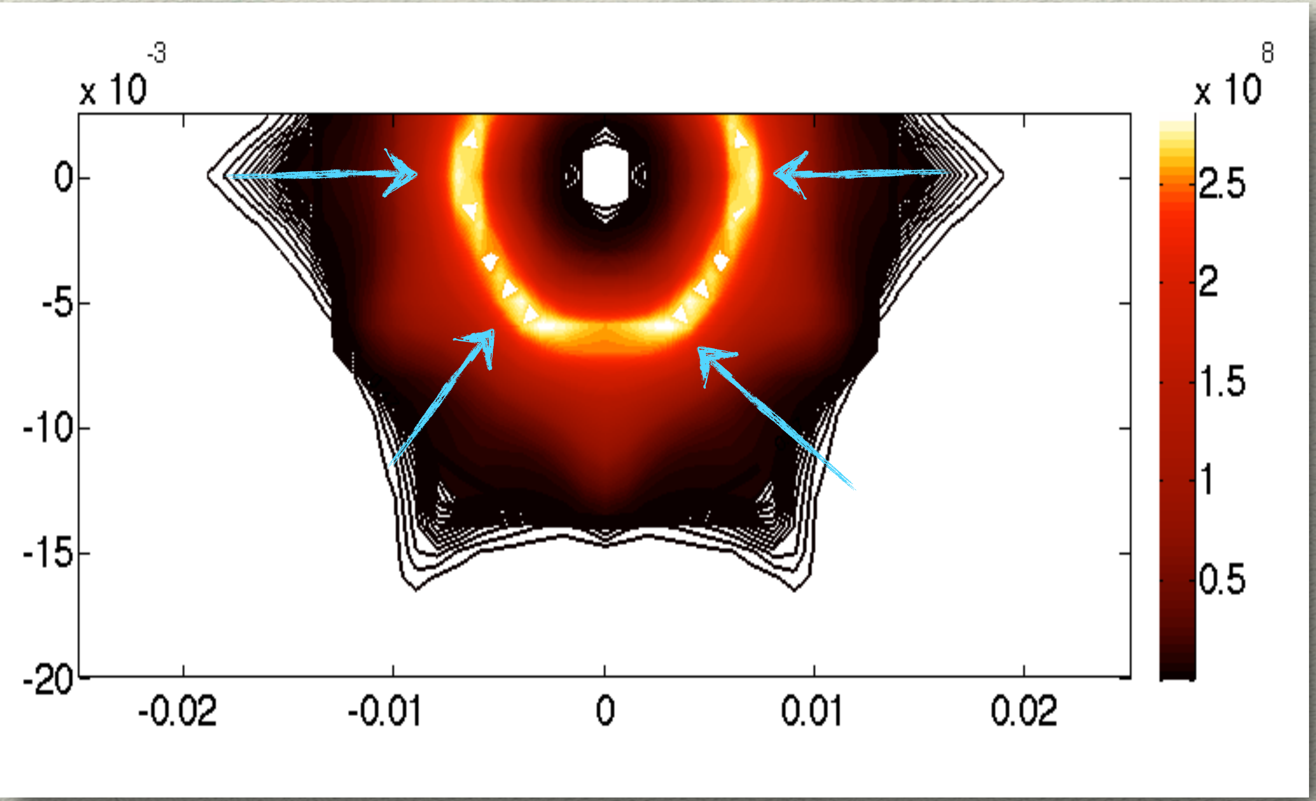

- Argon ions occupy far-from-poles positions: from comparison to simulations it comes out there warm electrons (having enough energy for ionisation and excitation) are placed
- Next step: comparison of two frequencies

Comparison to self-consistent simulations

12.84 + 12.92 GHz

12.92 GHz
warm-electrons

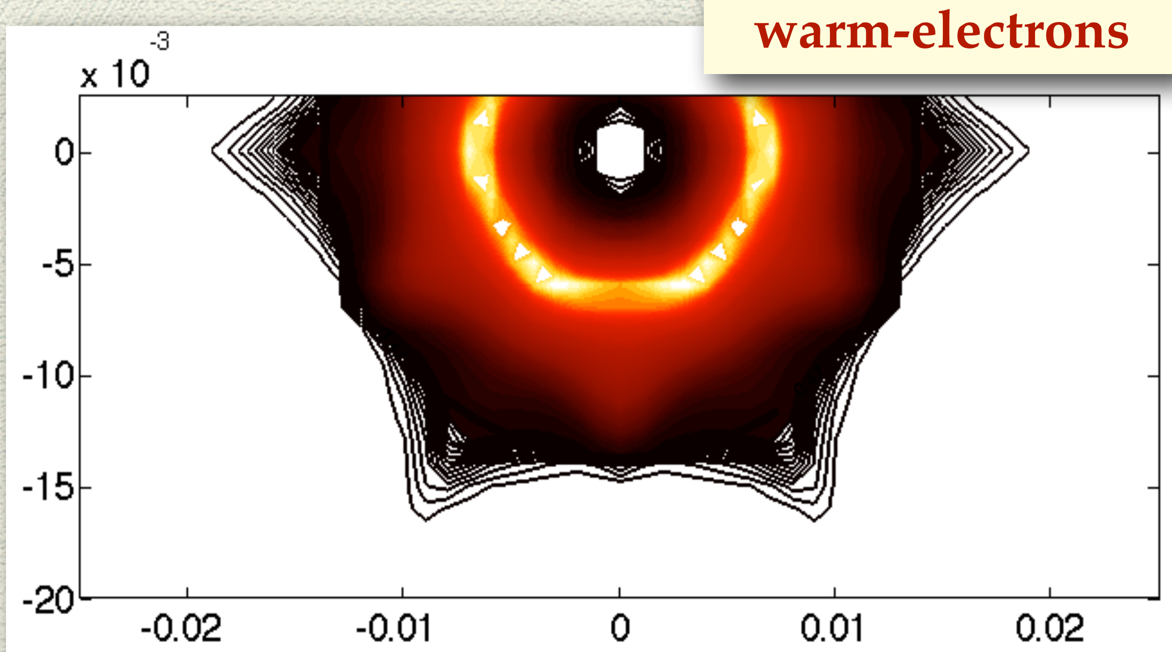

12.84 GHz
warm-electrons

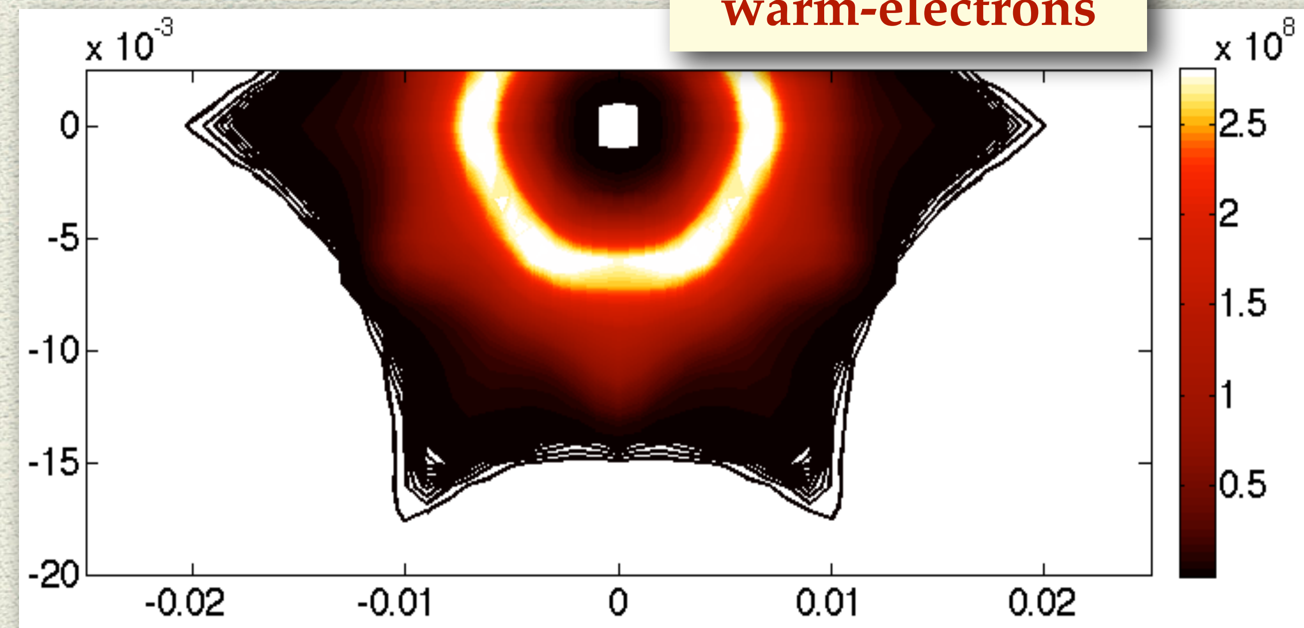

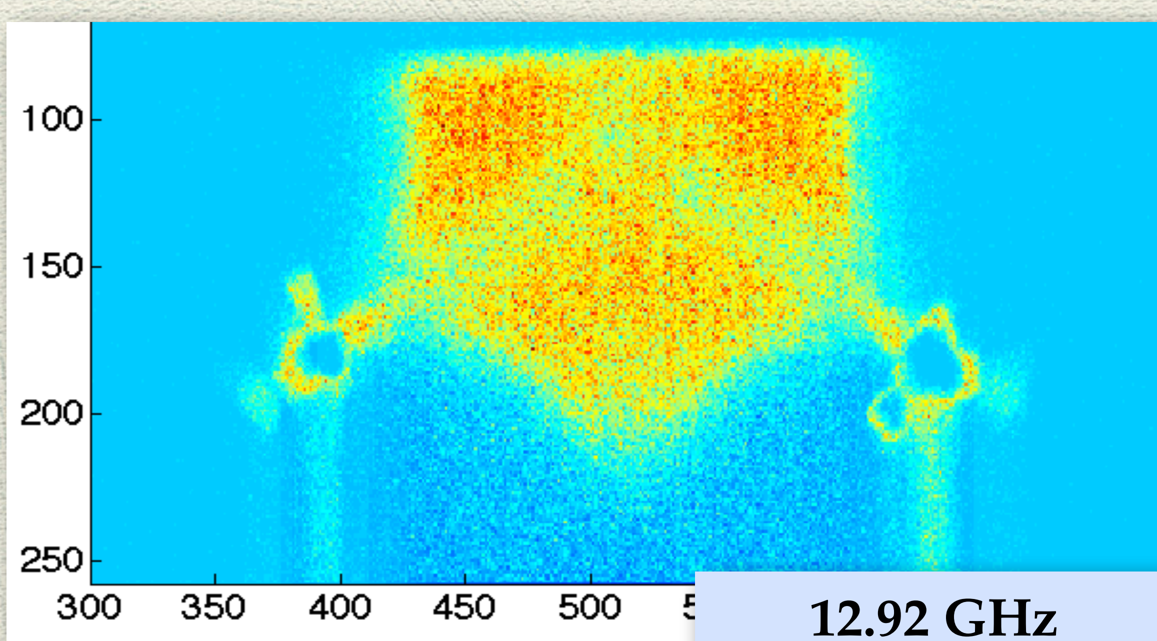

12.92 GHz
Ar fluor. lines

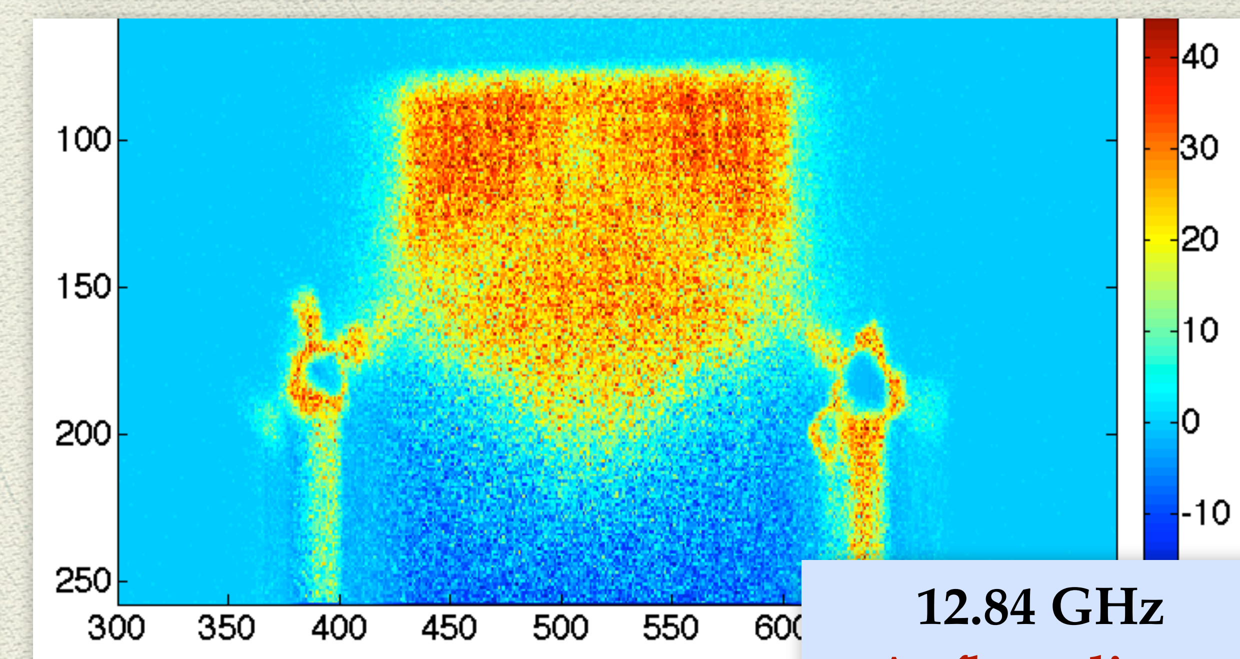

12.84 GHz
Ar fluor. lines

Comparison to self-consistent simulations

12.84 GHz

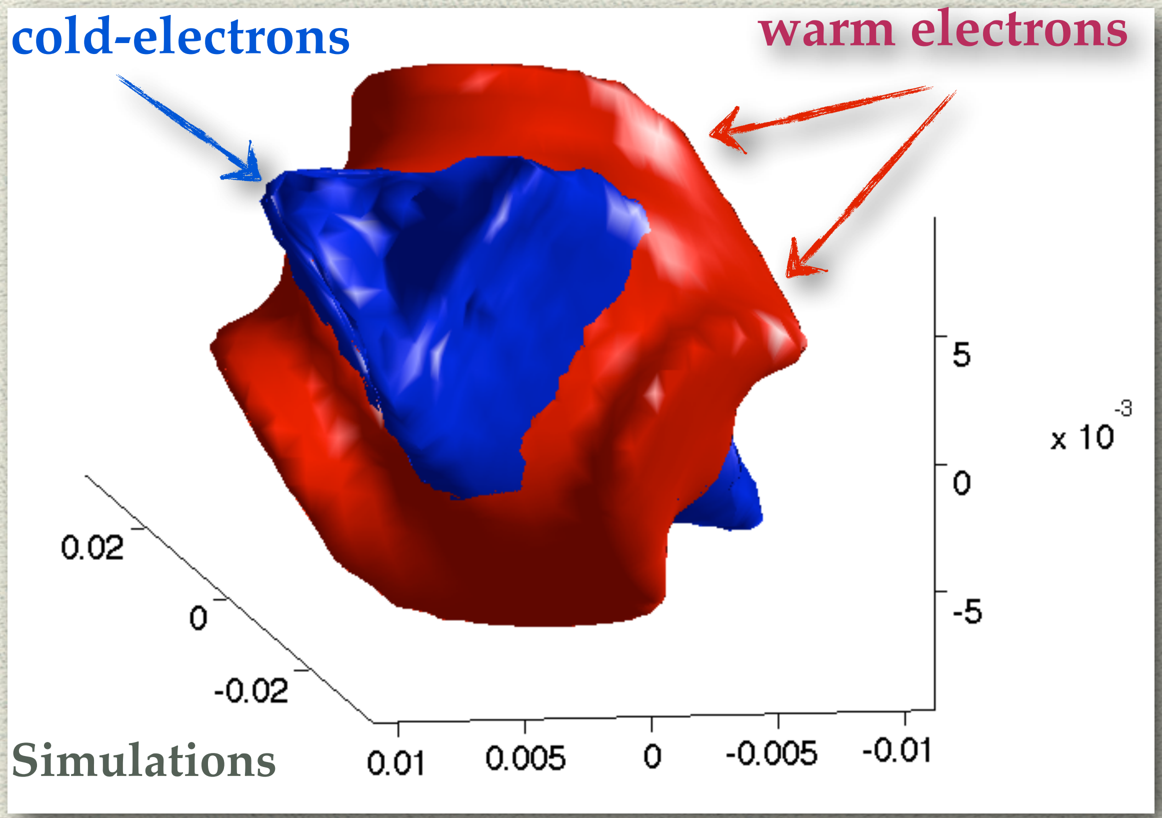

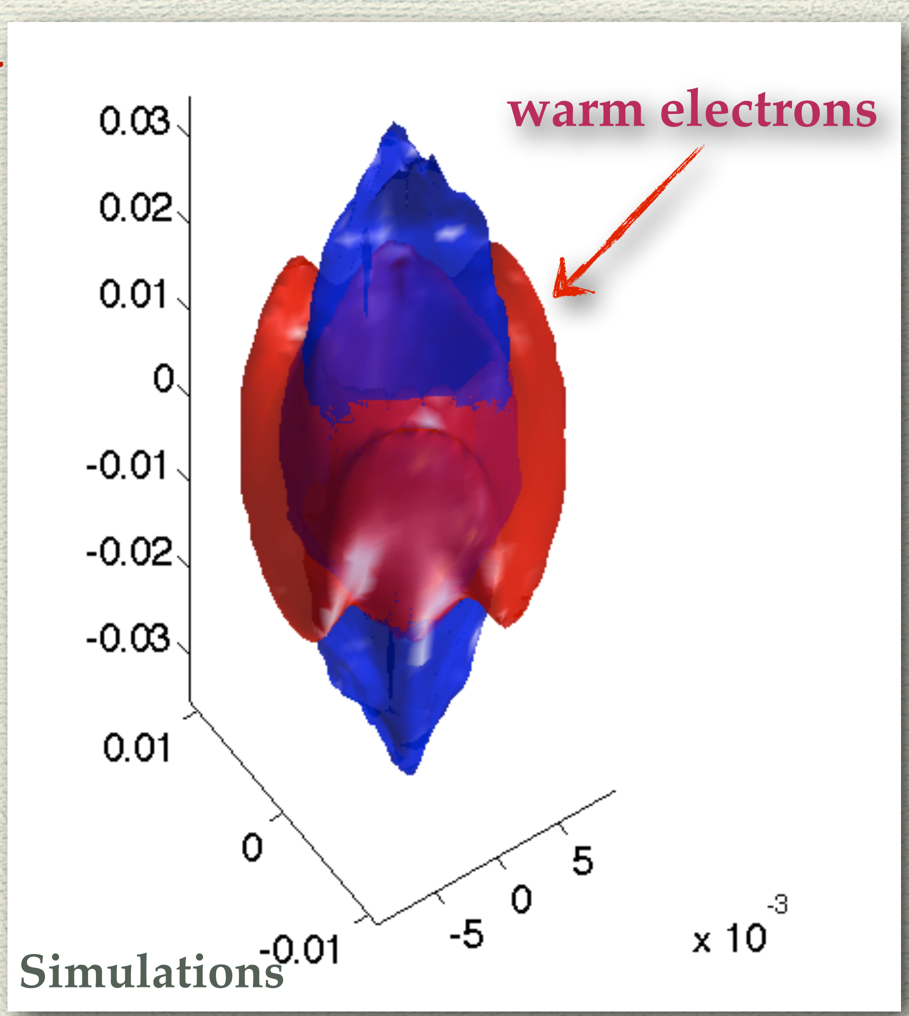

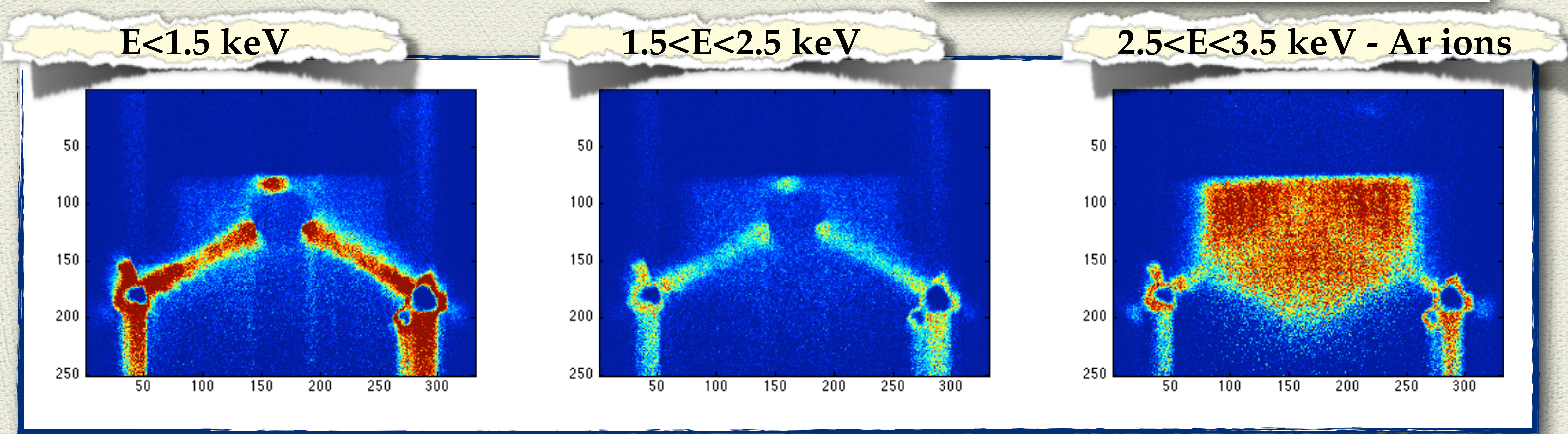

Comparison to self-consistent simulations

12.84 + 12.92 GHz

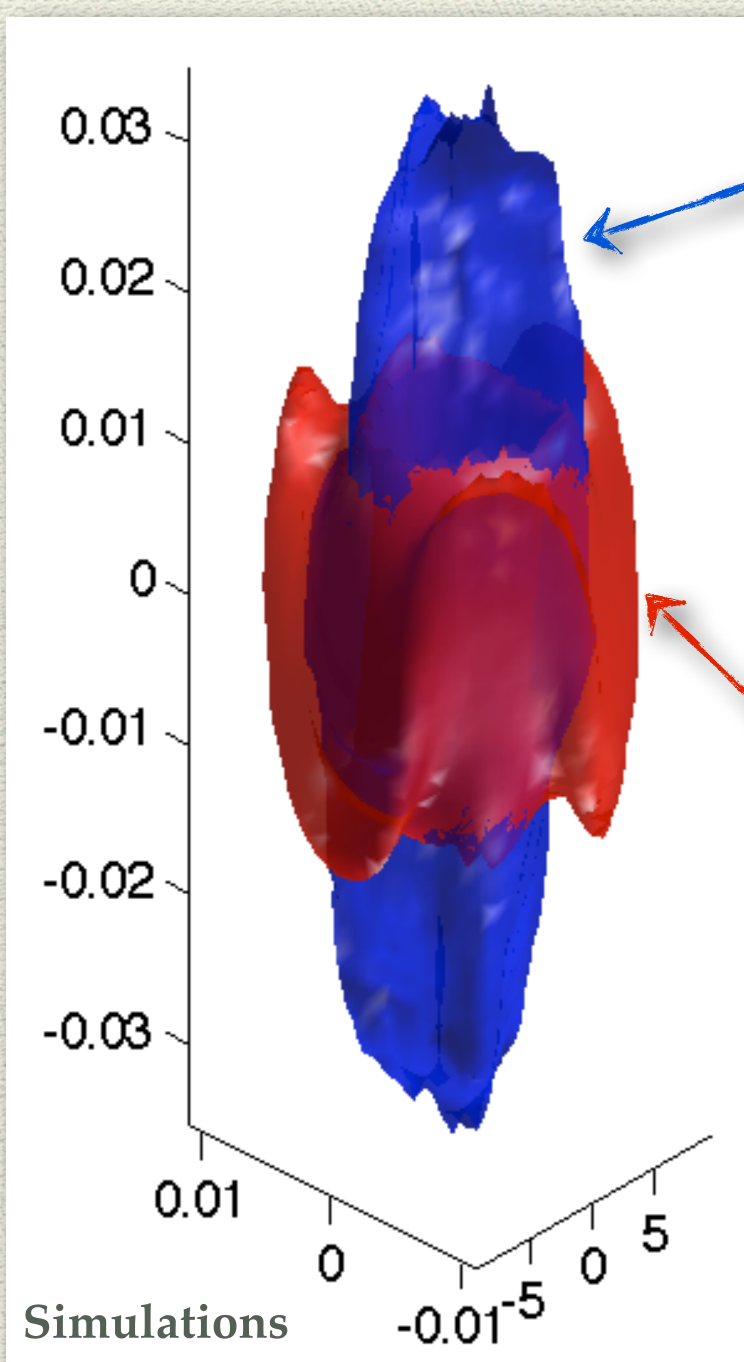

cold-electrons

warm electrons
have different
morphology

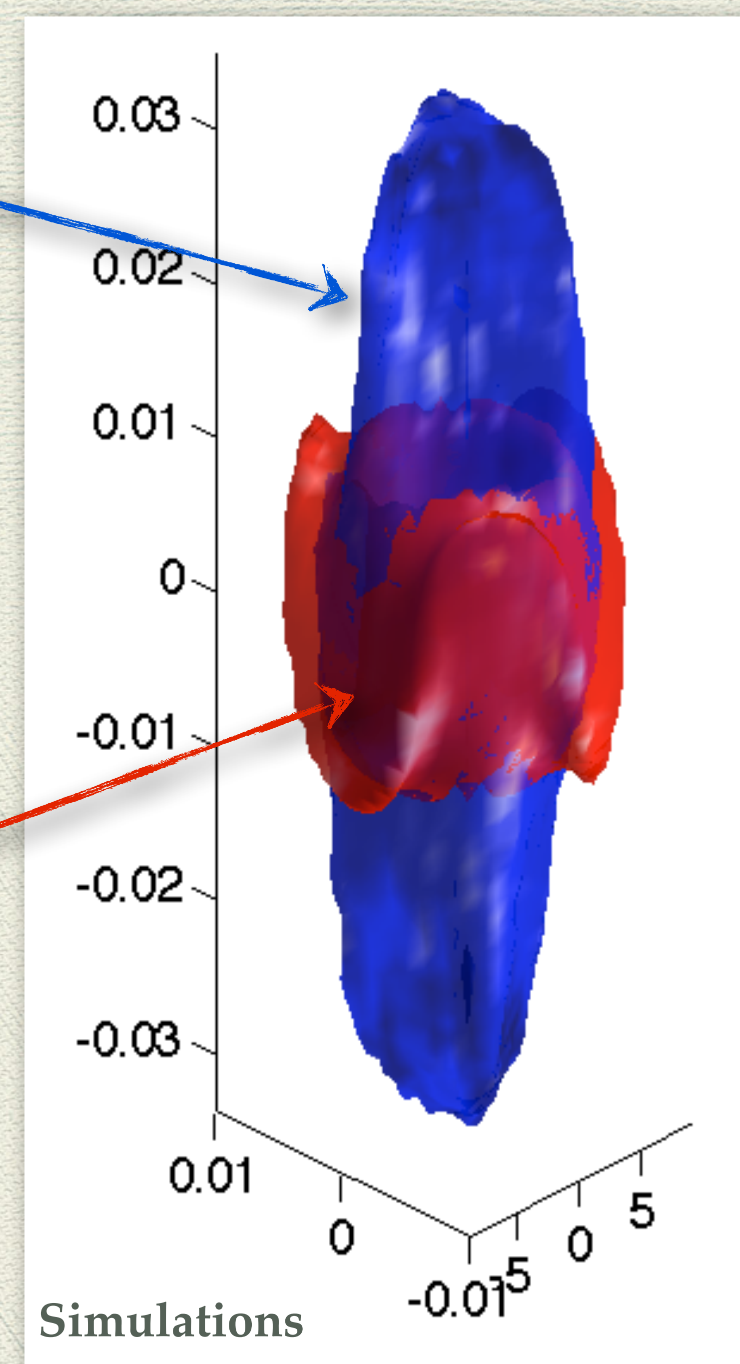

12.84 GHz
cold & warm electrons

12.92 GHz
cold & warm electrons

Achievements and Perspectives

- We are now able to see what happens into the plasma and to model through numerical simulations how it could be happen differently (and in a better way)

- Microwave absorption oriented design is needed: Power deposition into the plasma must be done in a highly controlled way → **Single pass absorption**

Some ideas

- STILL IN ECR-heating paradigm: are cylindrical shapes of the plasma chamber still mandatory?
- OVERCOMING ECR-heating paradigm: on-purpose design of launchers

Overdense Plasma generation
axial launching in off-resonance mode

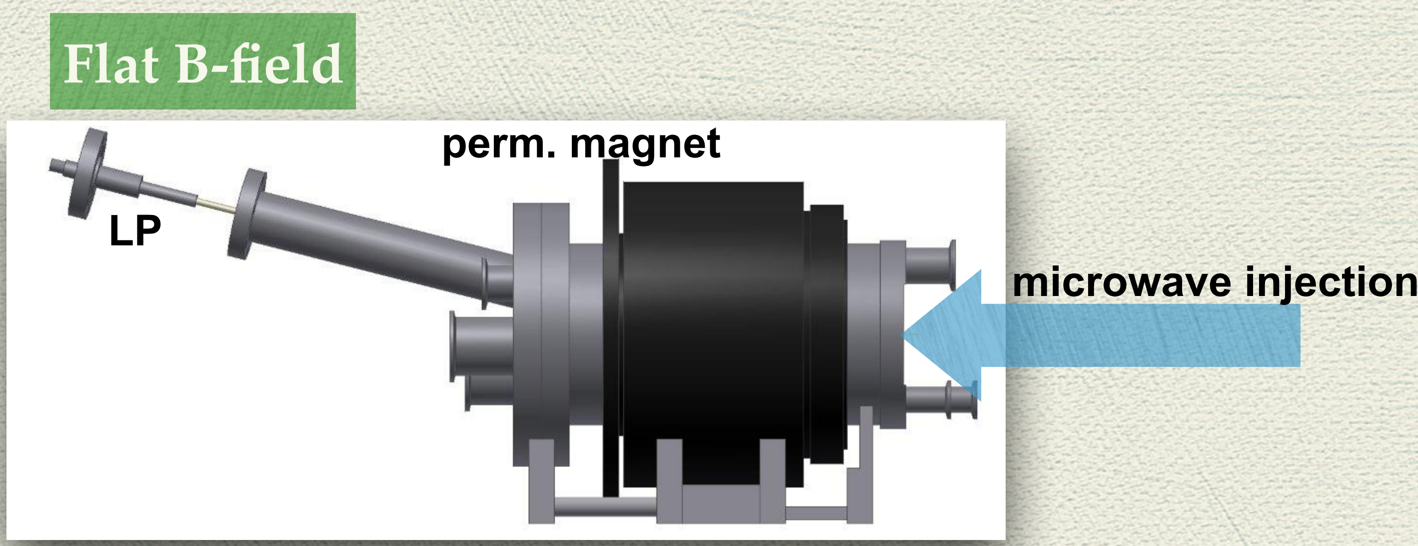

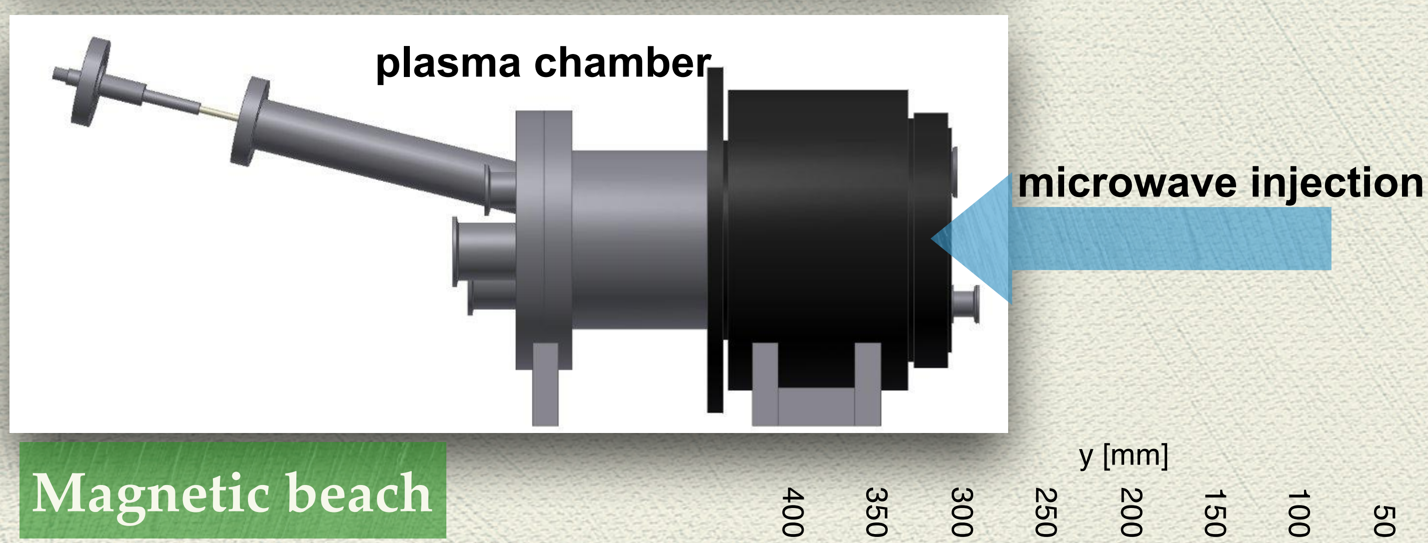

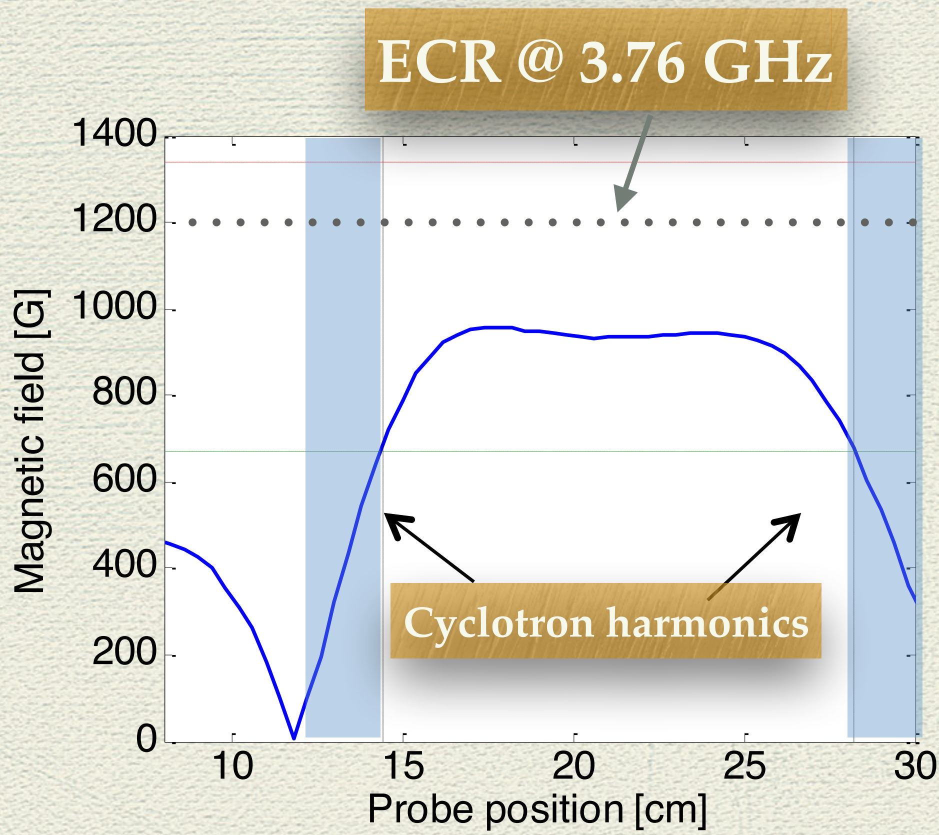

At first step: ray tracing calculations show non-axial components of the injected radiation are formed due to a refractive-like effect

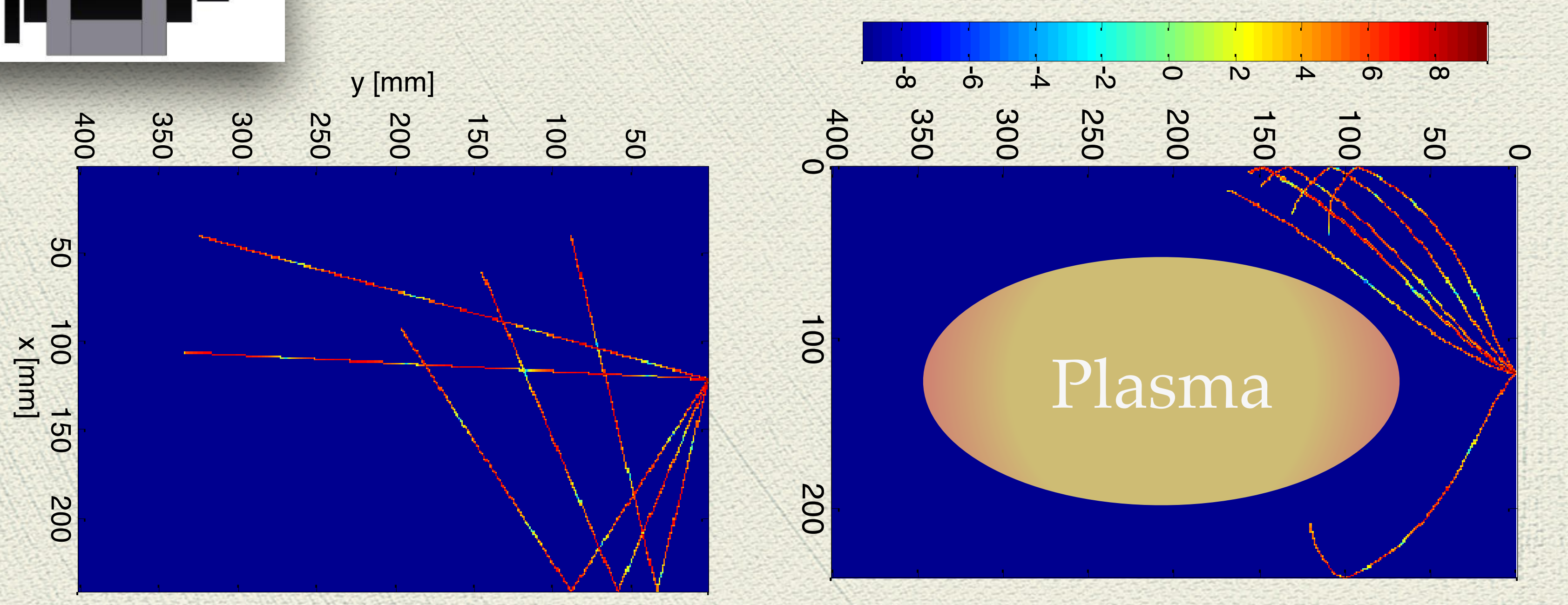

Test-bench for exploring modal conversion at 2.45÷3.75 GHz

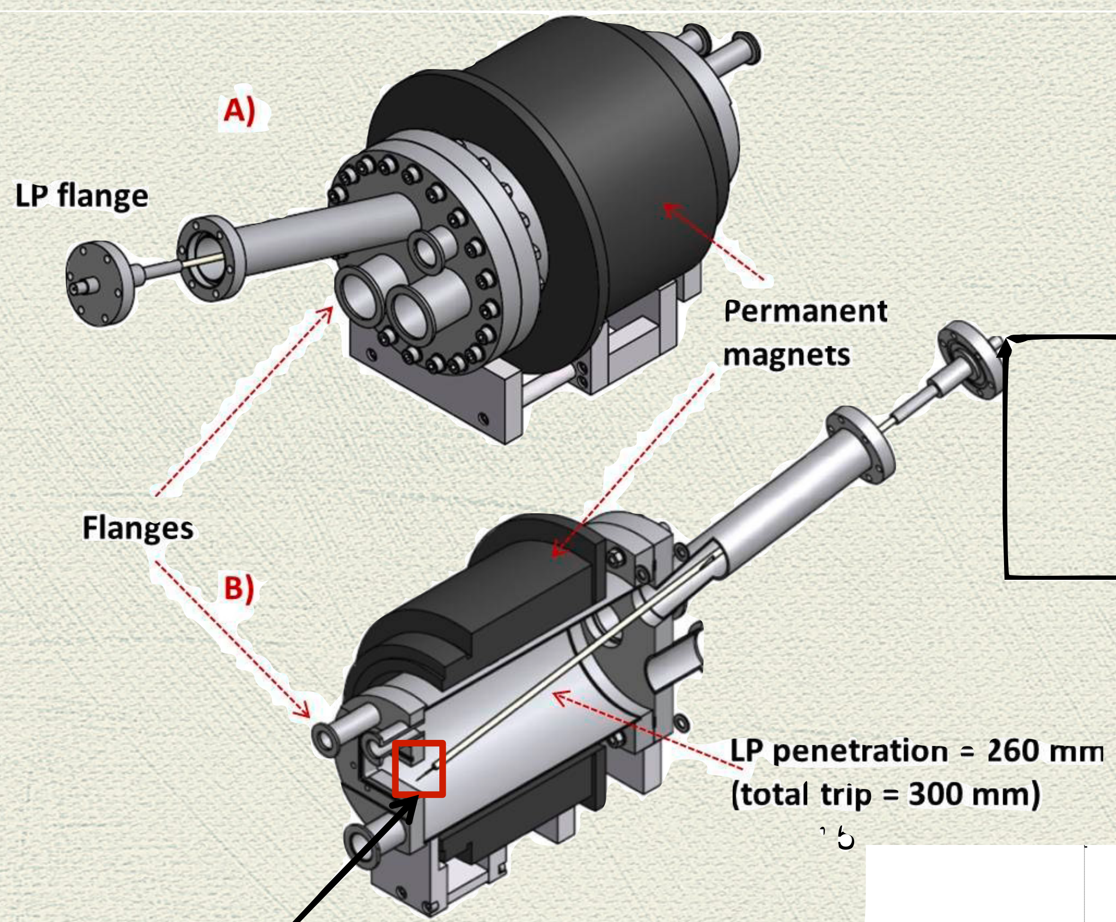

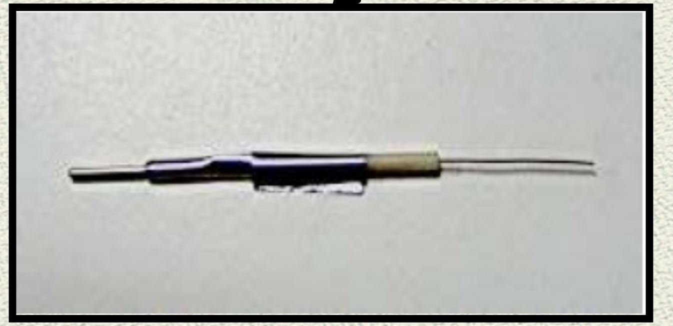

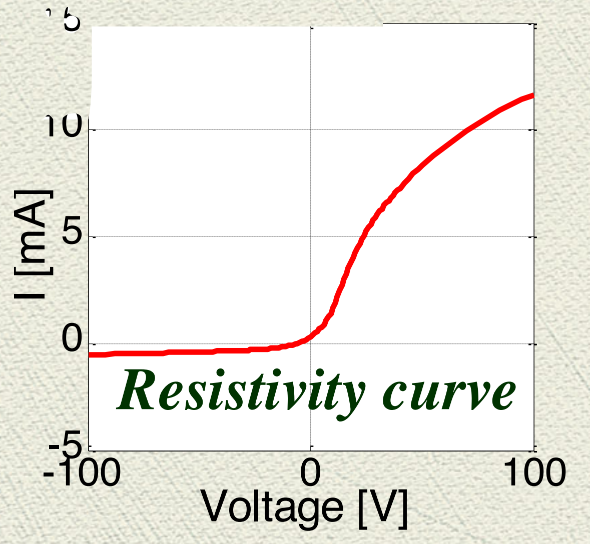

Spectrum analyzer for inner plasma electromagnetic spectrum detection

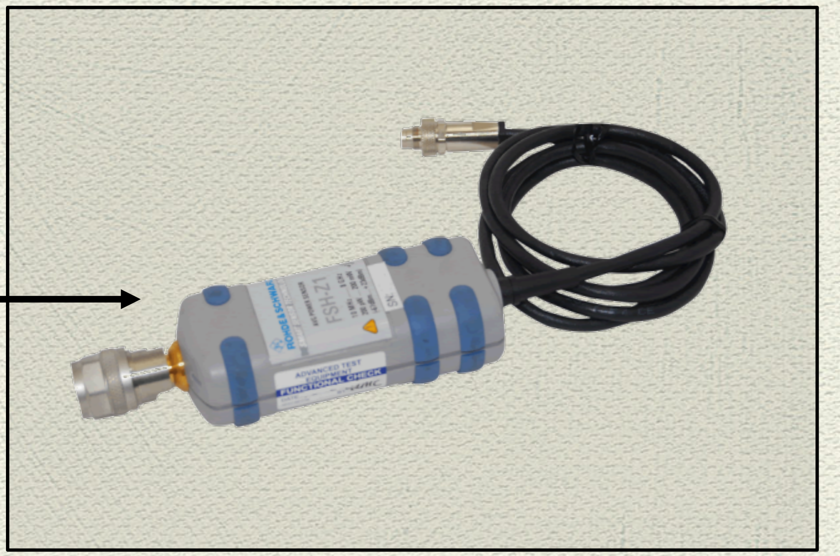

Power meter for intra-plasma EM power measurements

X-ray detectors and X-ray pin-hole camera

X-ray pi-hole camera

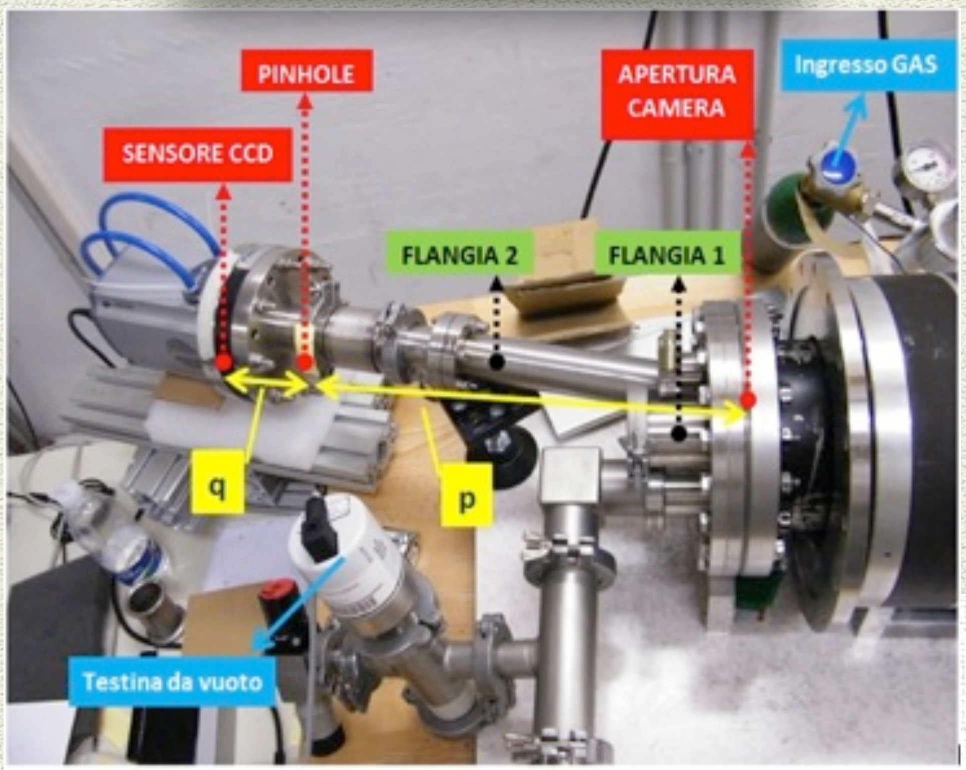

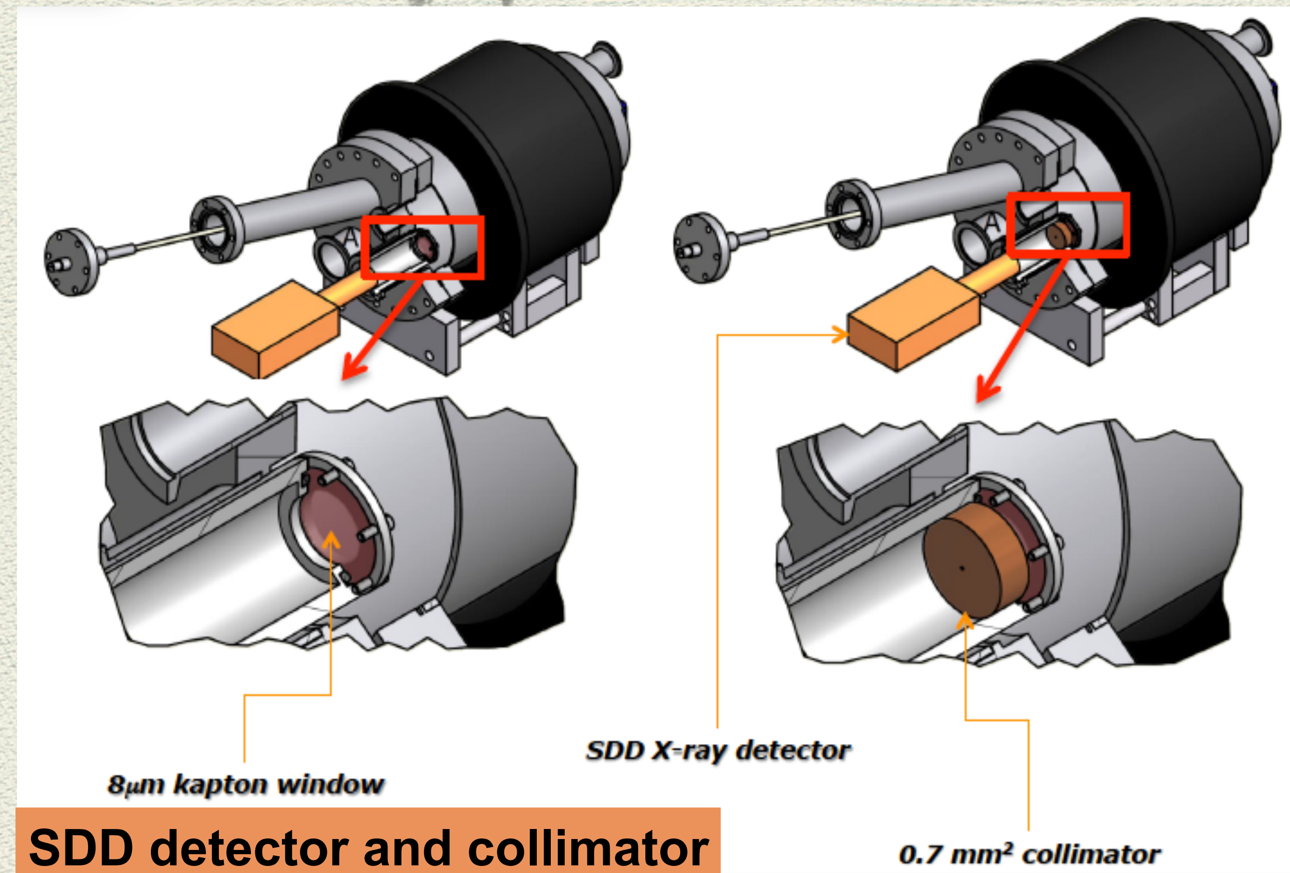

SDD detector and collimator

X-ray sensitive CCD - camera

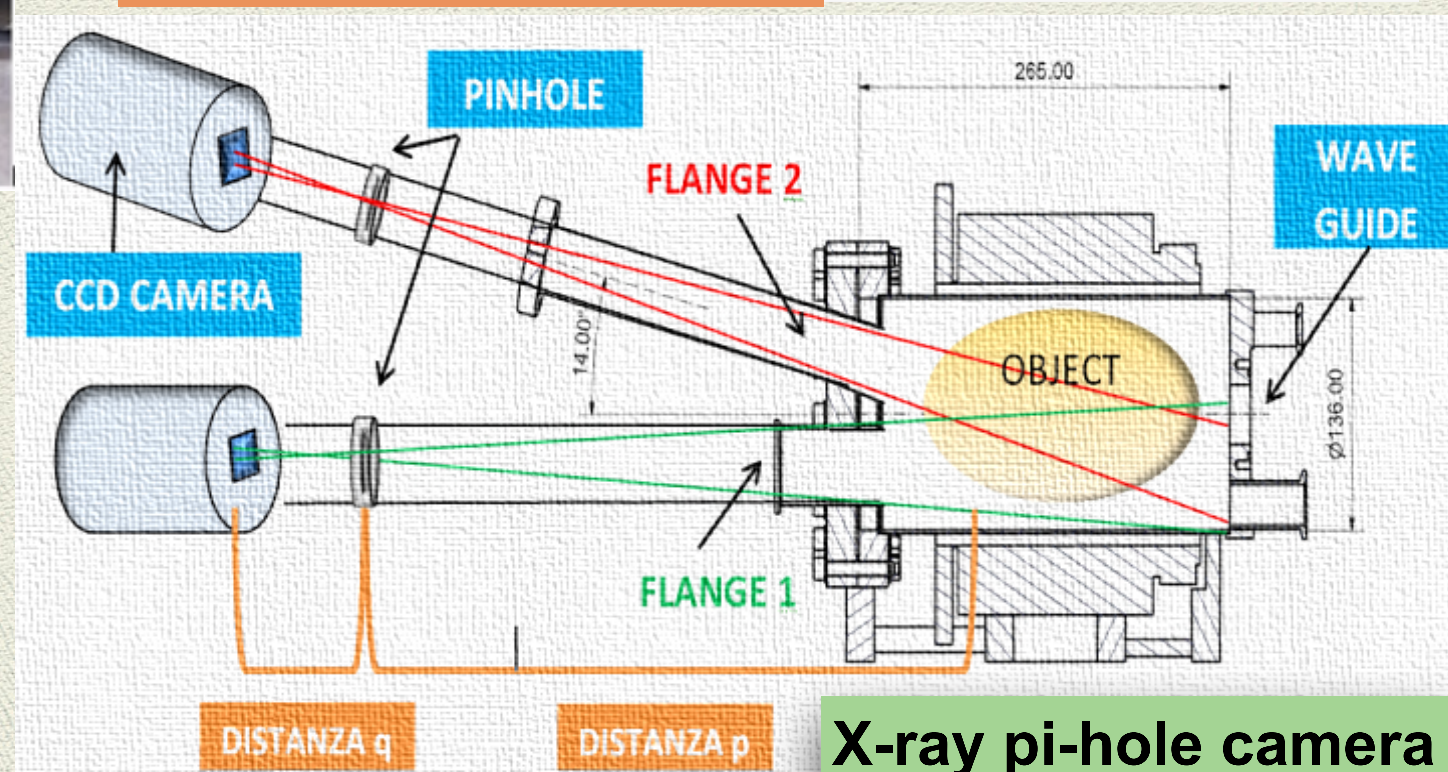

X-ray pi-hole camera

Plasma X-ray emission and density/temperature boost

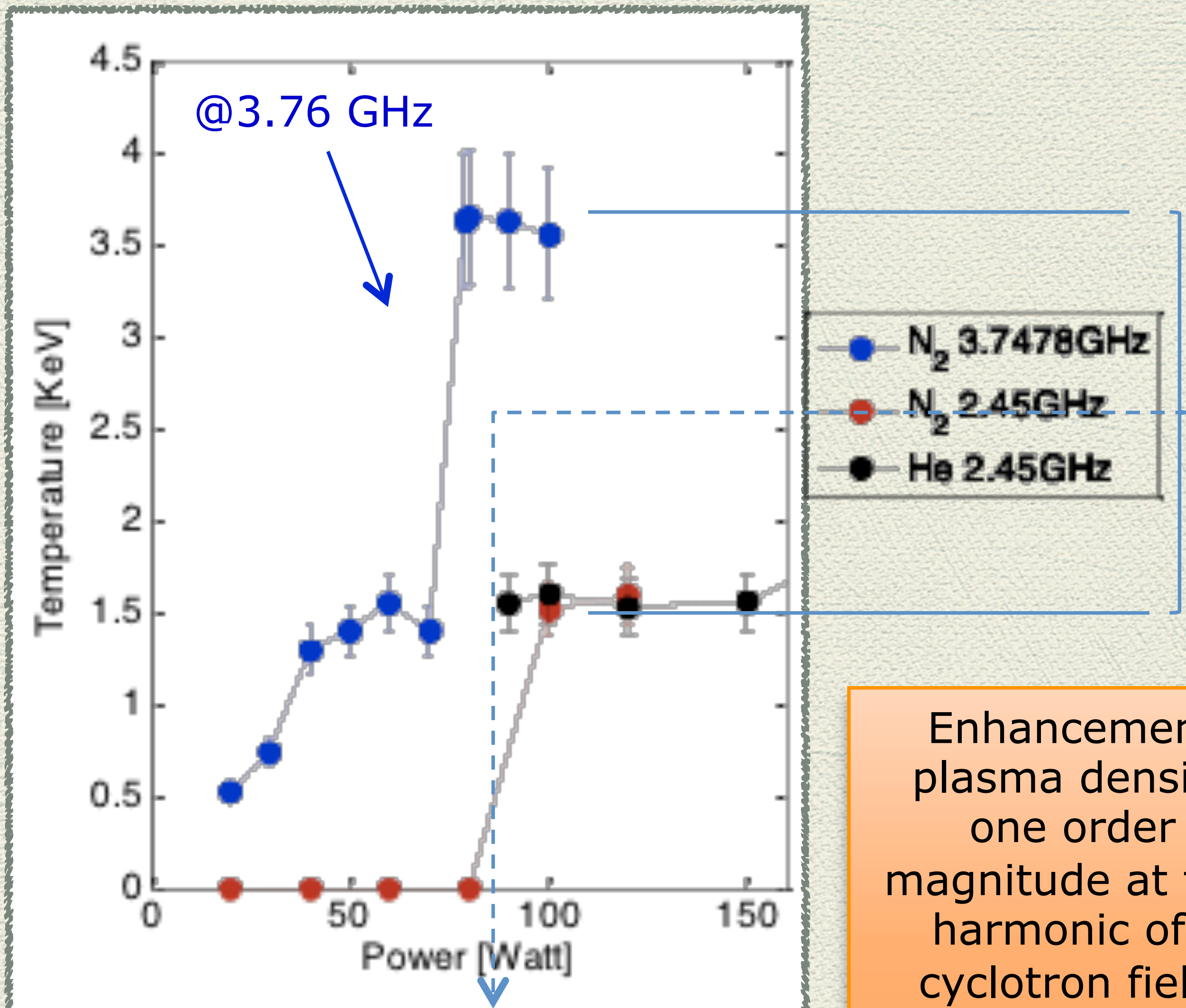

Evidence of strong non linear heating above a critical threshold

Enhancement of plasma density of one order of magnitude at the 1° harmonic of the cyclotron field !!!

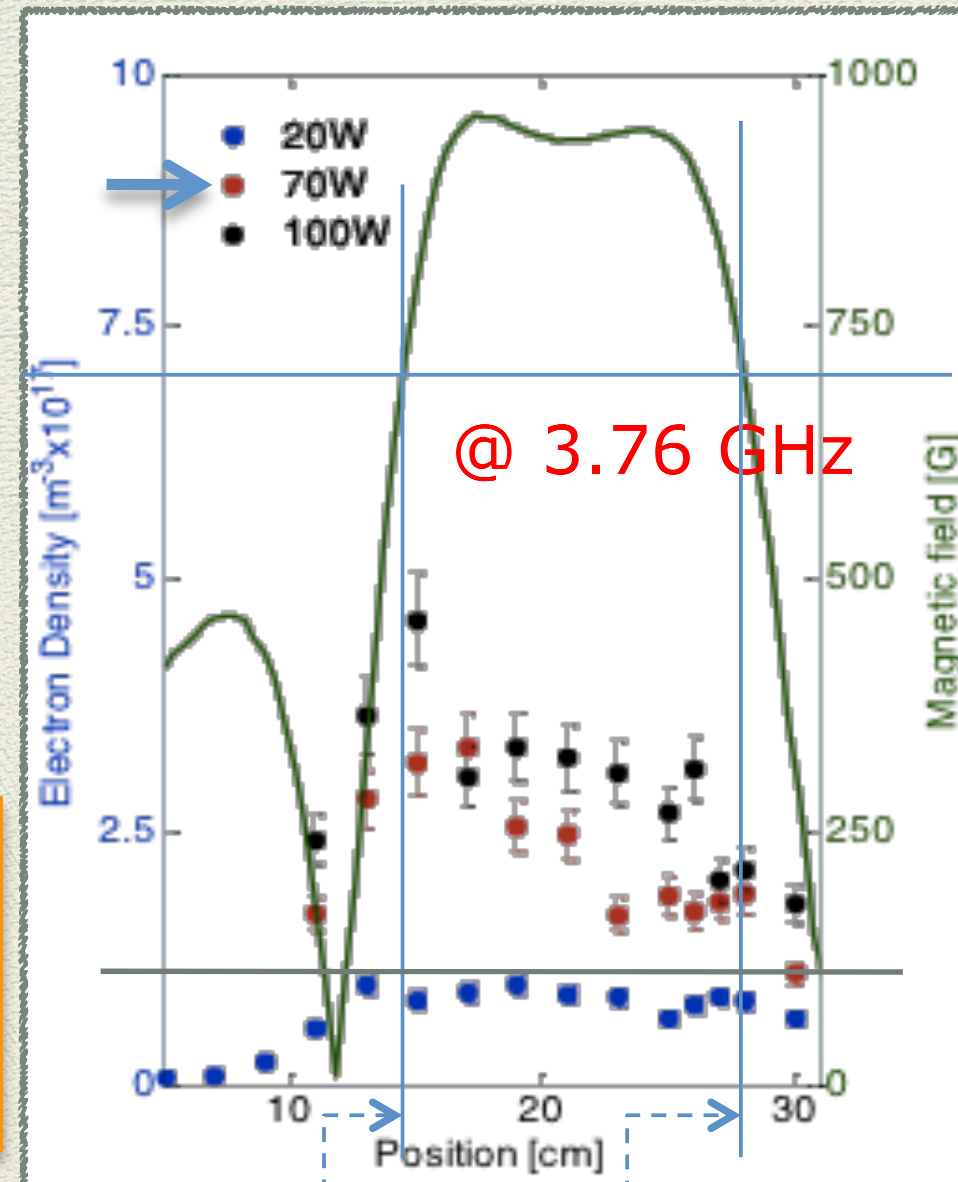

First harmonic

Experimental observation shows a non-linear growing of plasma temperature and density, with a JUMP above a certain threshold of the RF power.

From optical to -ray inspection
the X-ray pin-hole camera

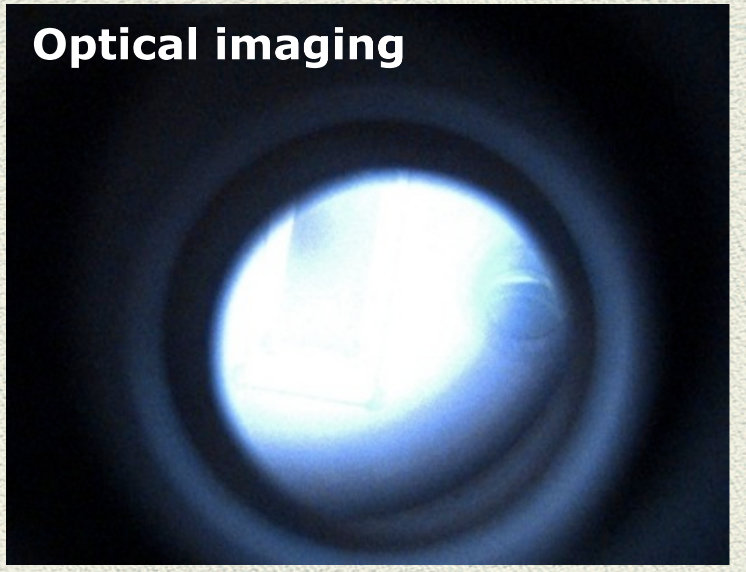

Images in the optical window, taken through an off-axis DN40 flange, evidence the generation of a high-brightness annulus surrounding a dark hole.

X-ray imaging evidences that the pumping power is deposited in the annulus, where the energetic electrons are generated

Transversal reconstruction of the plasma structure in X-ray domain (1-30 keV).

A high brightness strip appears due to electrons impinging on the chamber walls (bremsstrahlung through the stainless steel walls)

gas:Argon
pressure:3*10-4 mbar
RF power:100W
100 frames - 1sec exposure for each one

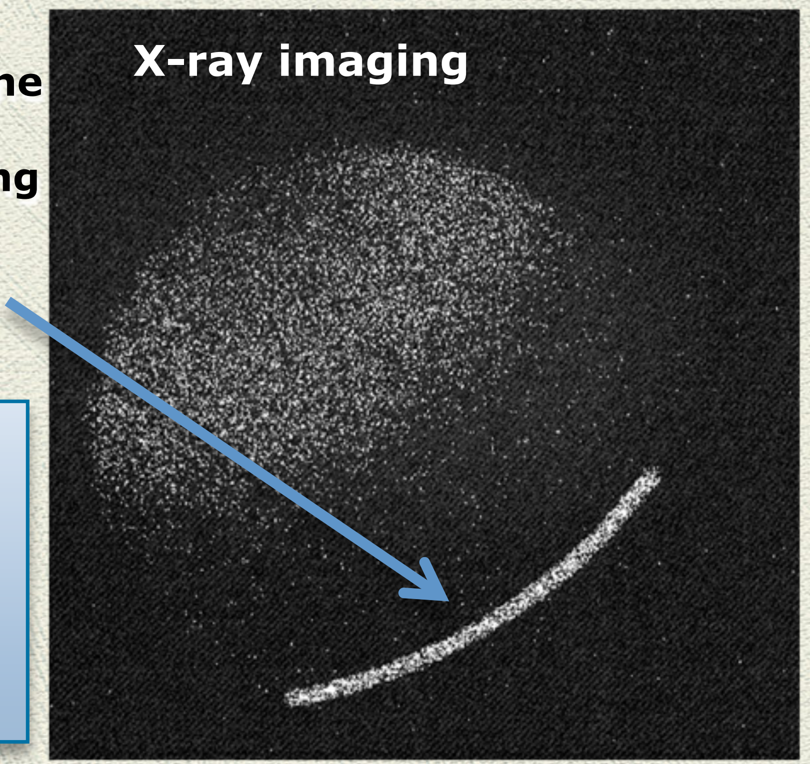

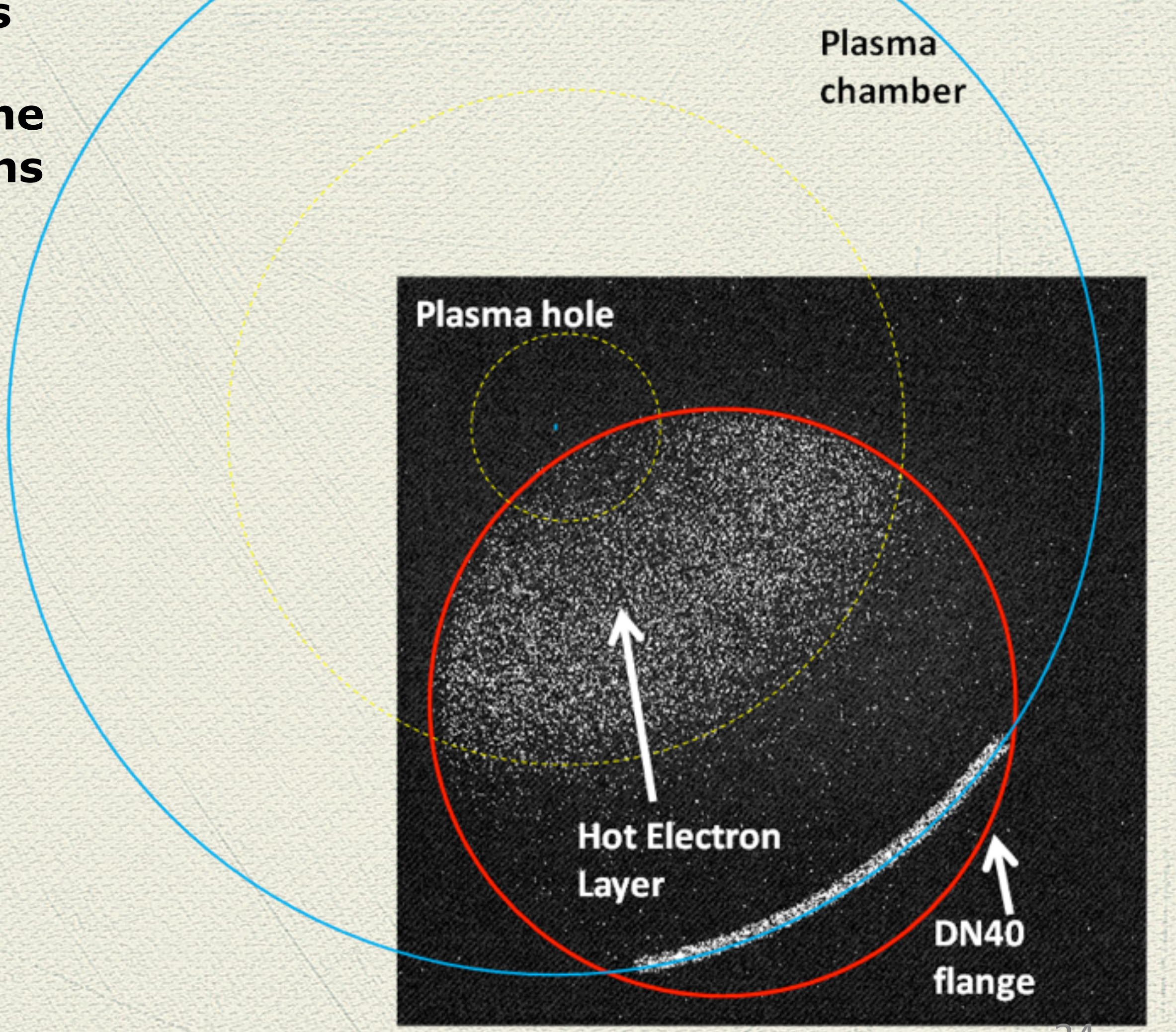

24

Probing the plasma density in all the energy domains

VESPRI

VEry Sensitive evaluation of Plasma density by micRowave Interferometry

Probing the plasma density in all the energy domains

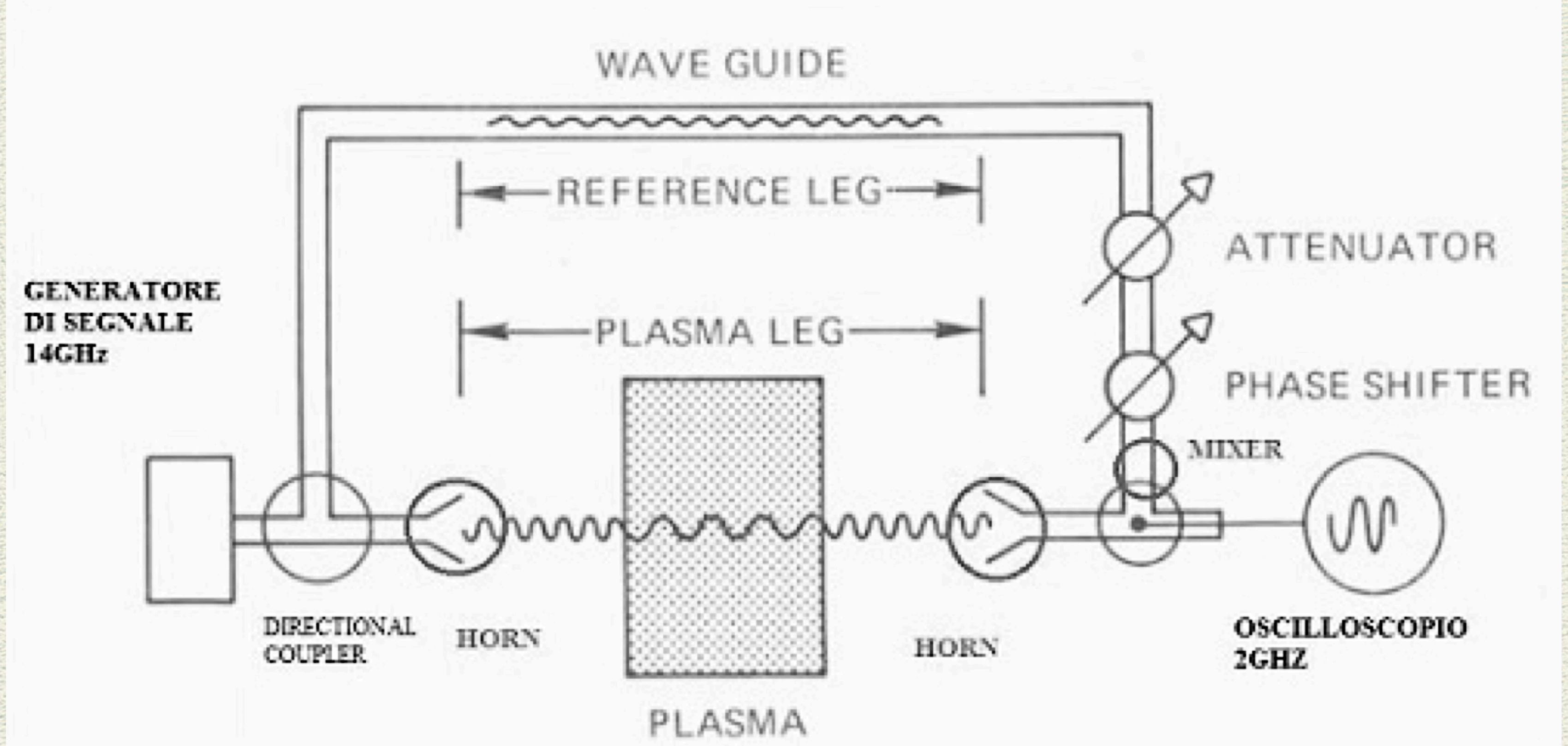

Classical Scheme of Interferometer

How to calculate the density n of the plasma

$$\Delta\varphi = \frac{\omega}{c}\left[1 - \left(1 - \frac{\omega_p{}^2}{\omega^2}\right)^{\frac{1}{2}}\right] L \quad \rightarrow \quad \omega_p{}^2 = \frac{4\pi n e^2}{m\varepsilon_0} \quad \rightarrow$$

In plasmas the phase variation depends on the " natural plasma frequency"

The plasma frequency depends on the density

Microwave interferometry measures plasma density through a measurement of phase shift.

The main challange: "downsizing"

JET Tokamak for nuclear fusion (energy production)

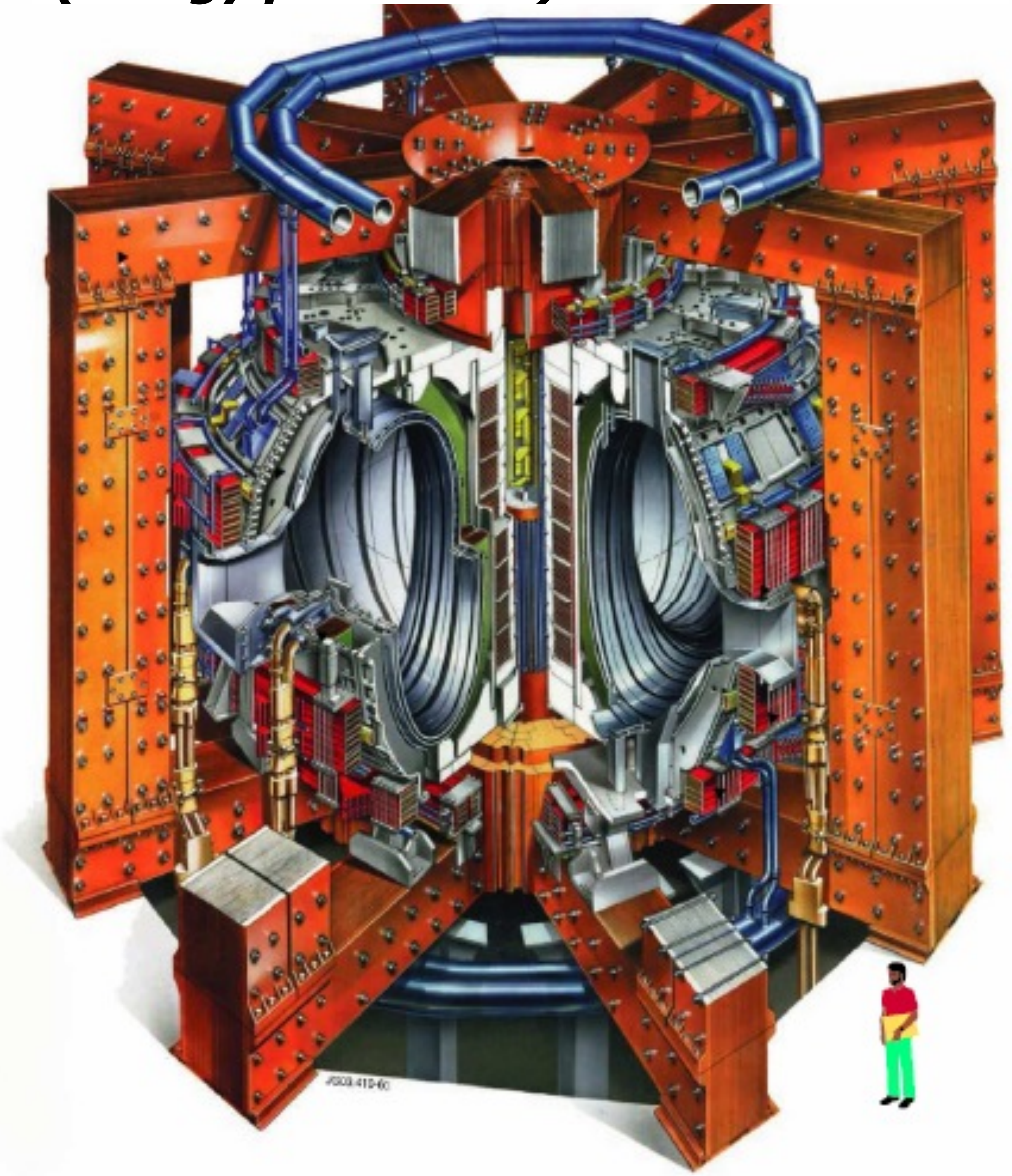

ECR ION Source: extremely compact plasma machine

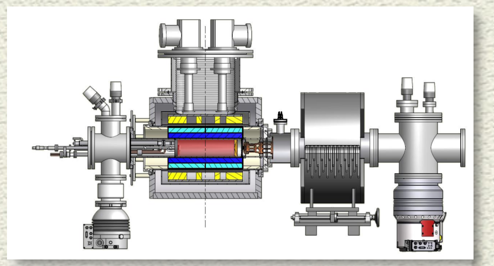

Probing the plasma density in all the energy domains

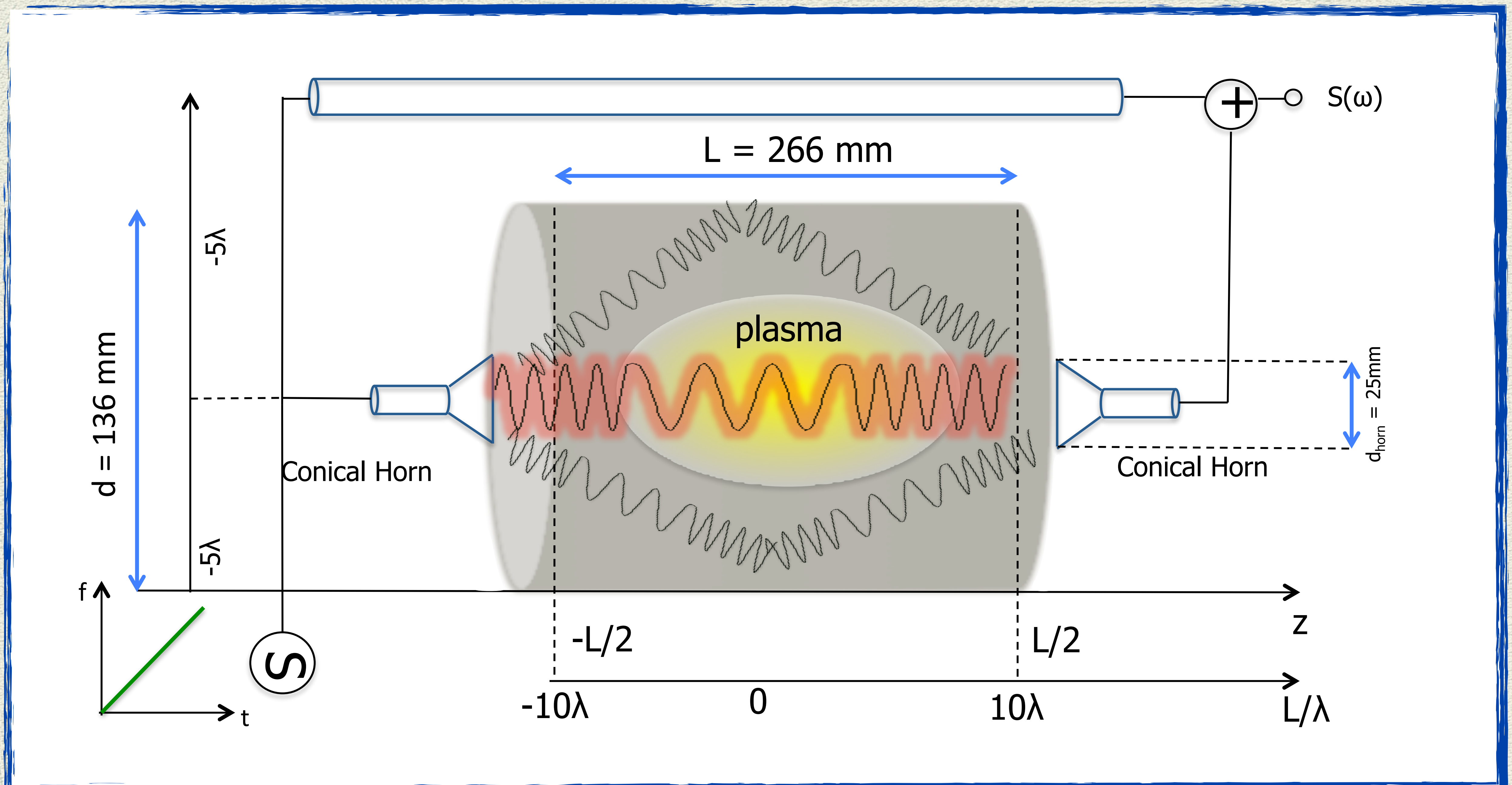

Drawbecks →

- **Limited ECRIS access probing port**
- **Multi-paths introduce spurious signals**

Interferometry in ECRIS: simulations

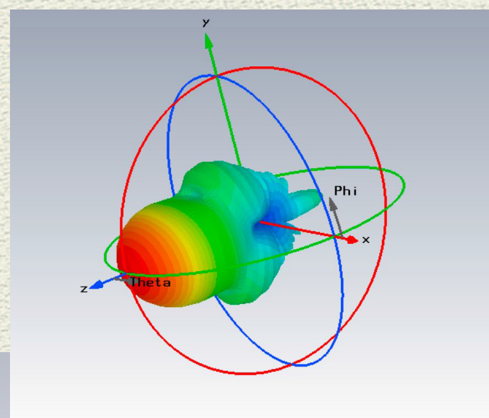

- Antenna directivity

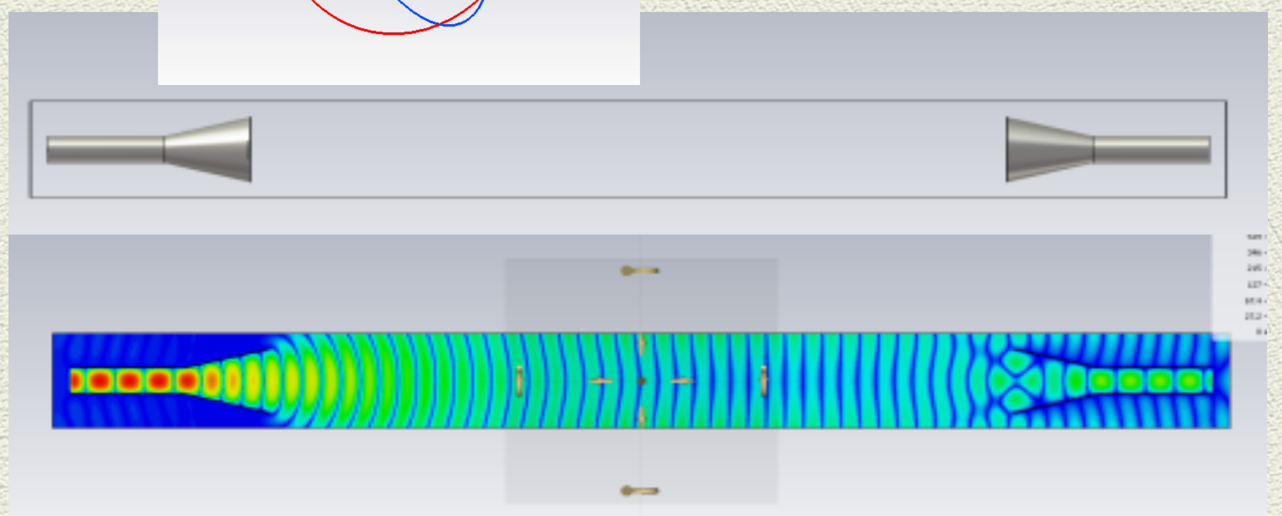

Horn-to-horn transmission for antennas facing each other in vacuum

Numerical simulations (COMSOL+CST) put in evidence cavity walls effects

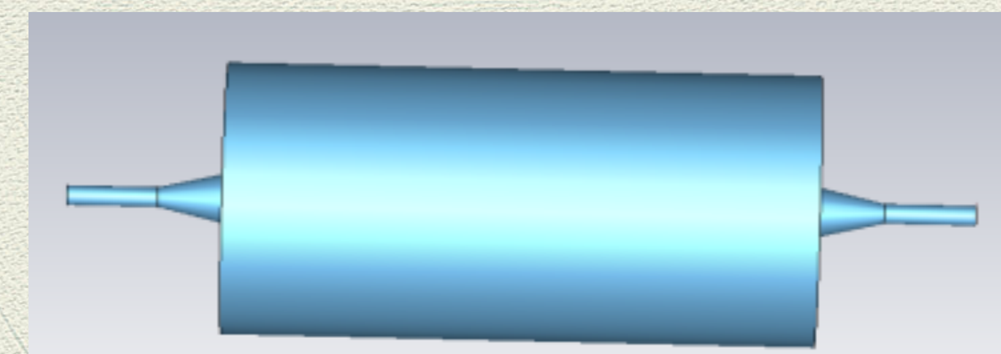

Horn connected to the plasma cavity

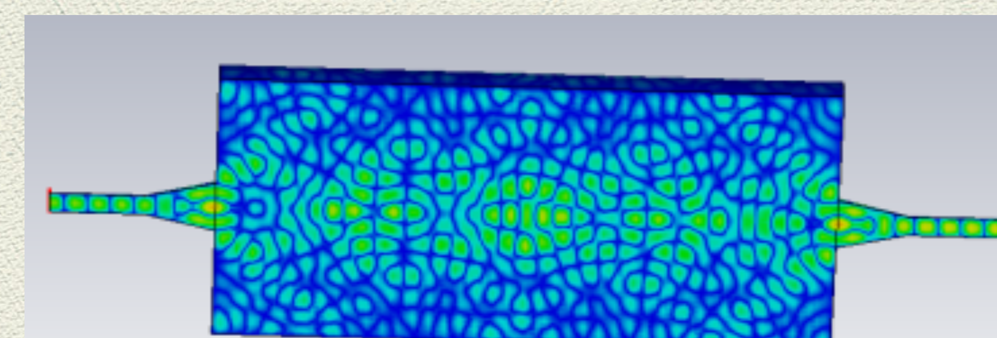

Electric field

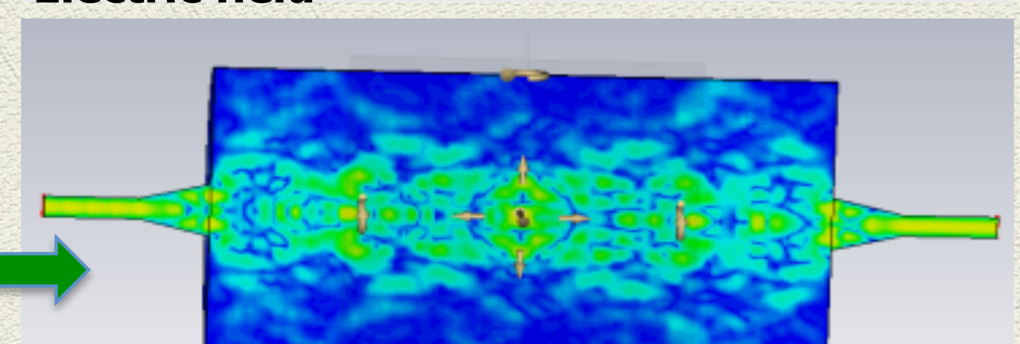

Power flow

Interferometry in ECRIS: the strategy

Multipath suppression

High antennas directivity

Specific antenna design L_{horn}

Use of High frequencies

Non conventional antennas:
Horn
Antenne

"Frequency swept" method with post-filtering procedure of the beating signal S(ω)

Interferometry in ECRIS:
"Sizing" of the different tools

Parameters		Values
Frequency MIN	f_{min}	20 GHz → down to 18 GHz
Frequency MAX	f_{max}	24.5 GHz → up to 26 GHz
Frequency CENTRAL	f	22 Ghz
Wavelength	λ	13 mm
Horn aperture radius	R_horn	12.5 mm
Standard WG radius	R_guida	5.03 mm
	l_{opt}	16 mm
	L_horn_{opt}	9.57 mm

$$l = \frac{(d)^2}{3\lambda} \qquad L_{horn} = l\left(1 - \frac{R_{guida}}{R_{horn}}\right)$$

Interferometry in ECRIS:
Mechanical assembly

Dimensions :
- 2.5 cm diameter (DN 25)

Vacuum:
- 8 µm layer of Kapton

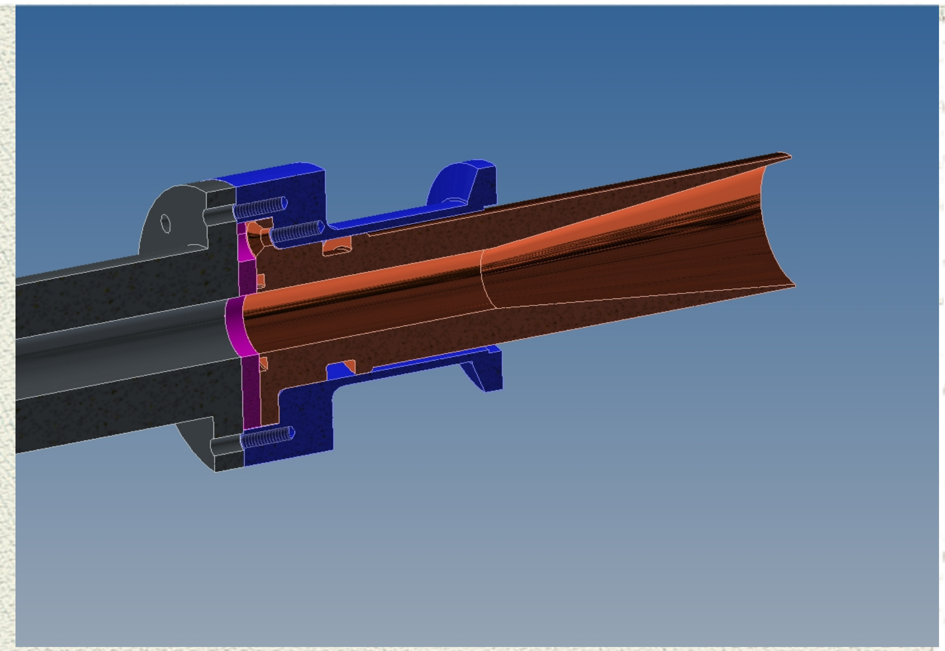

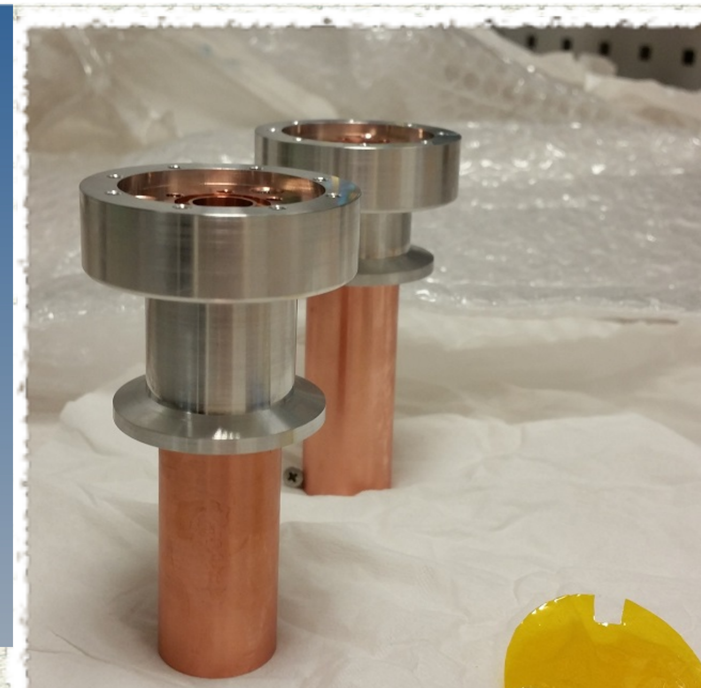

Interferometry in ECRIS: antennas charactetization

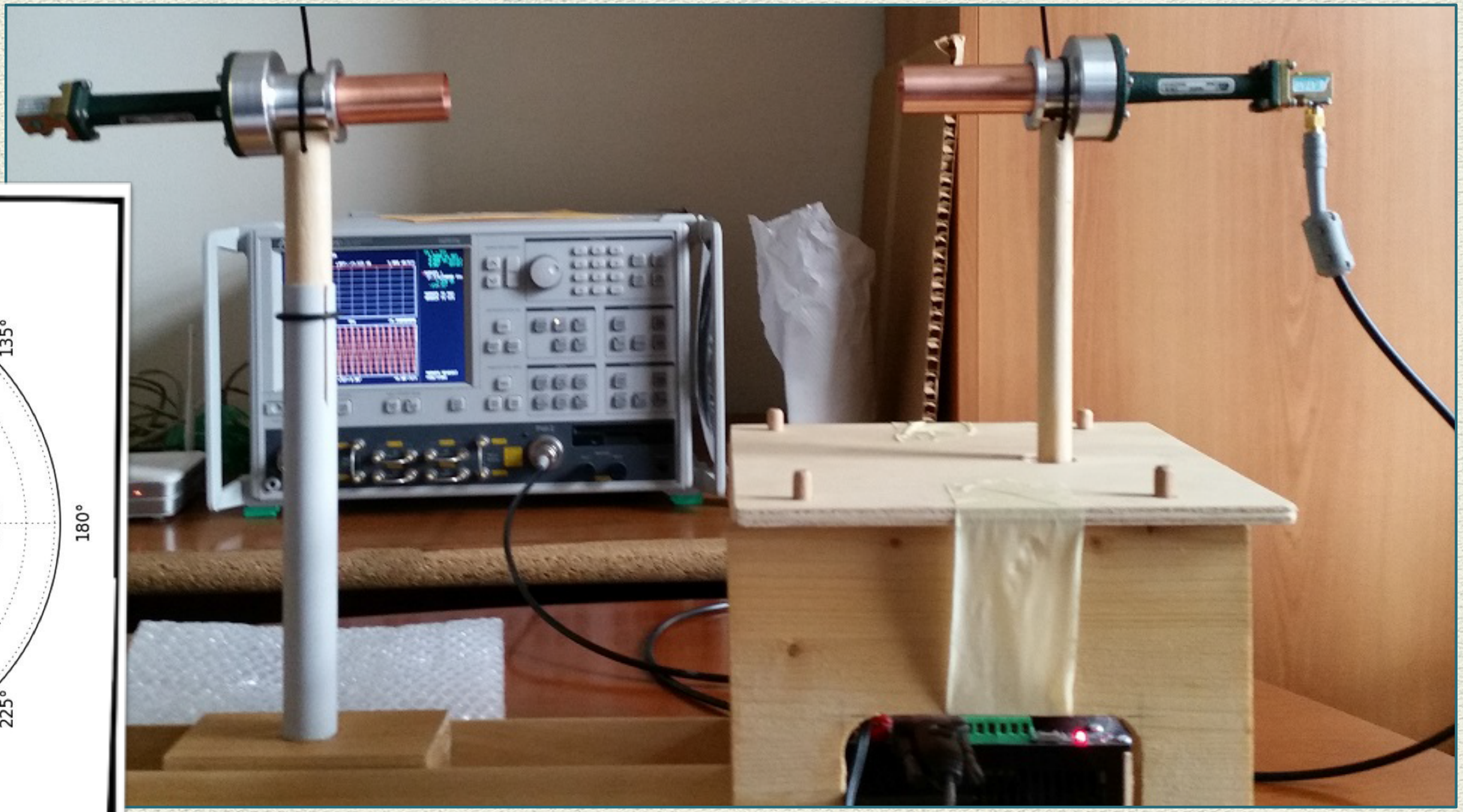

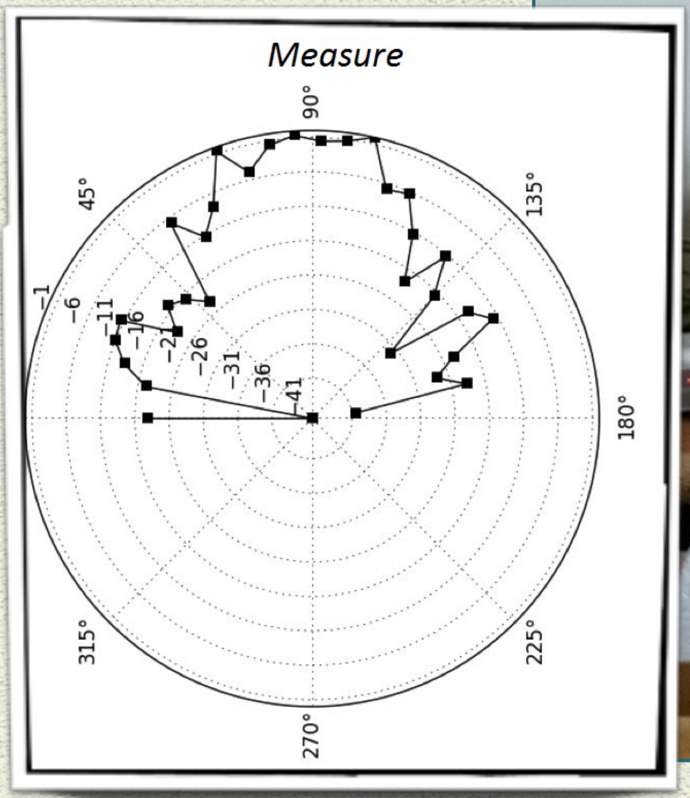

One horn is xed and the other one is placed on a plywood rod, rotating at 3.2 deg steps, for each angle was measured the intensity of the transmitted signal

Interferometry in ECRIS:
antennas characterization

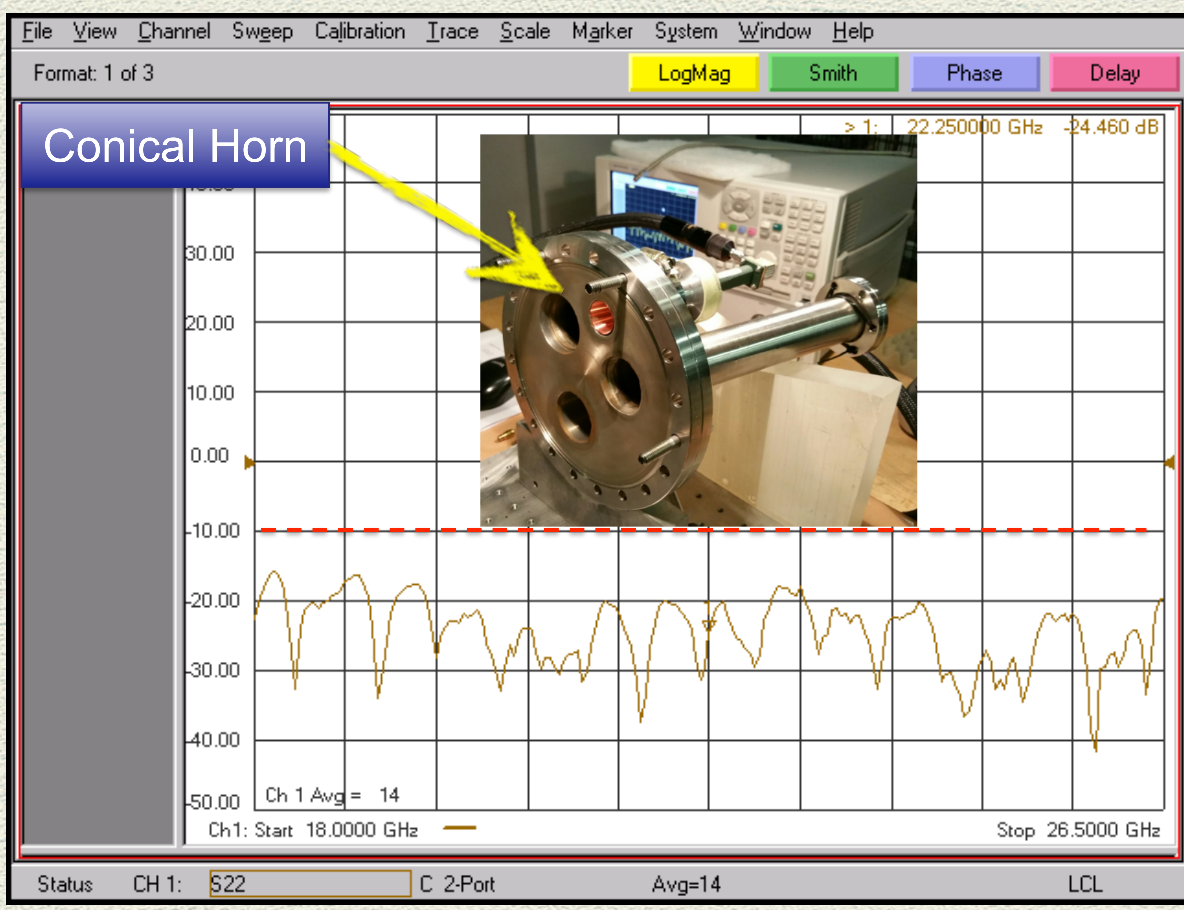

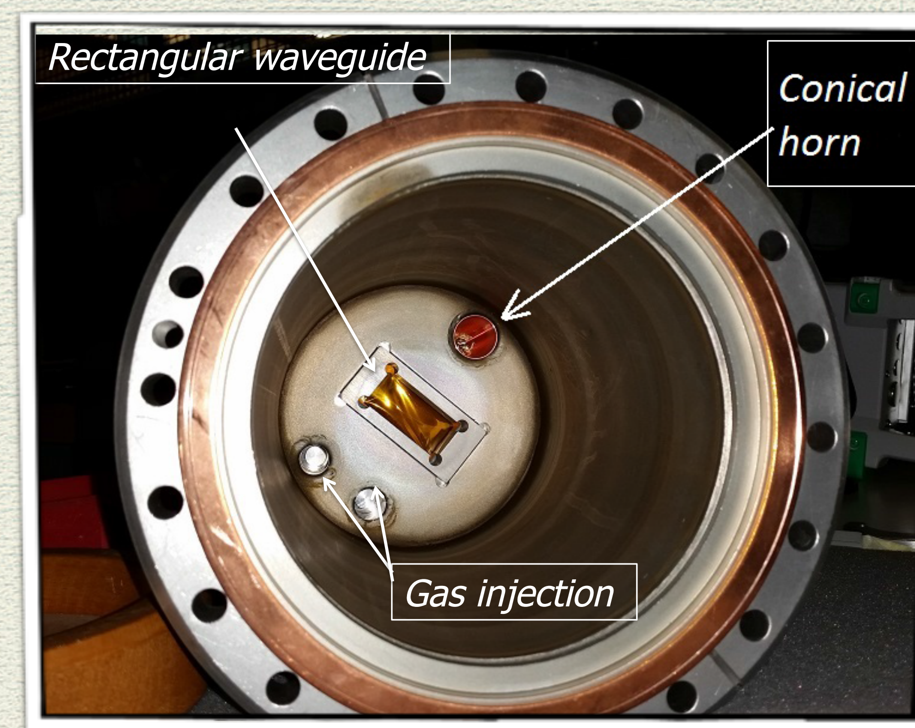

S11 measurements in presence of flanges and cavity

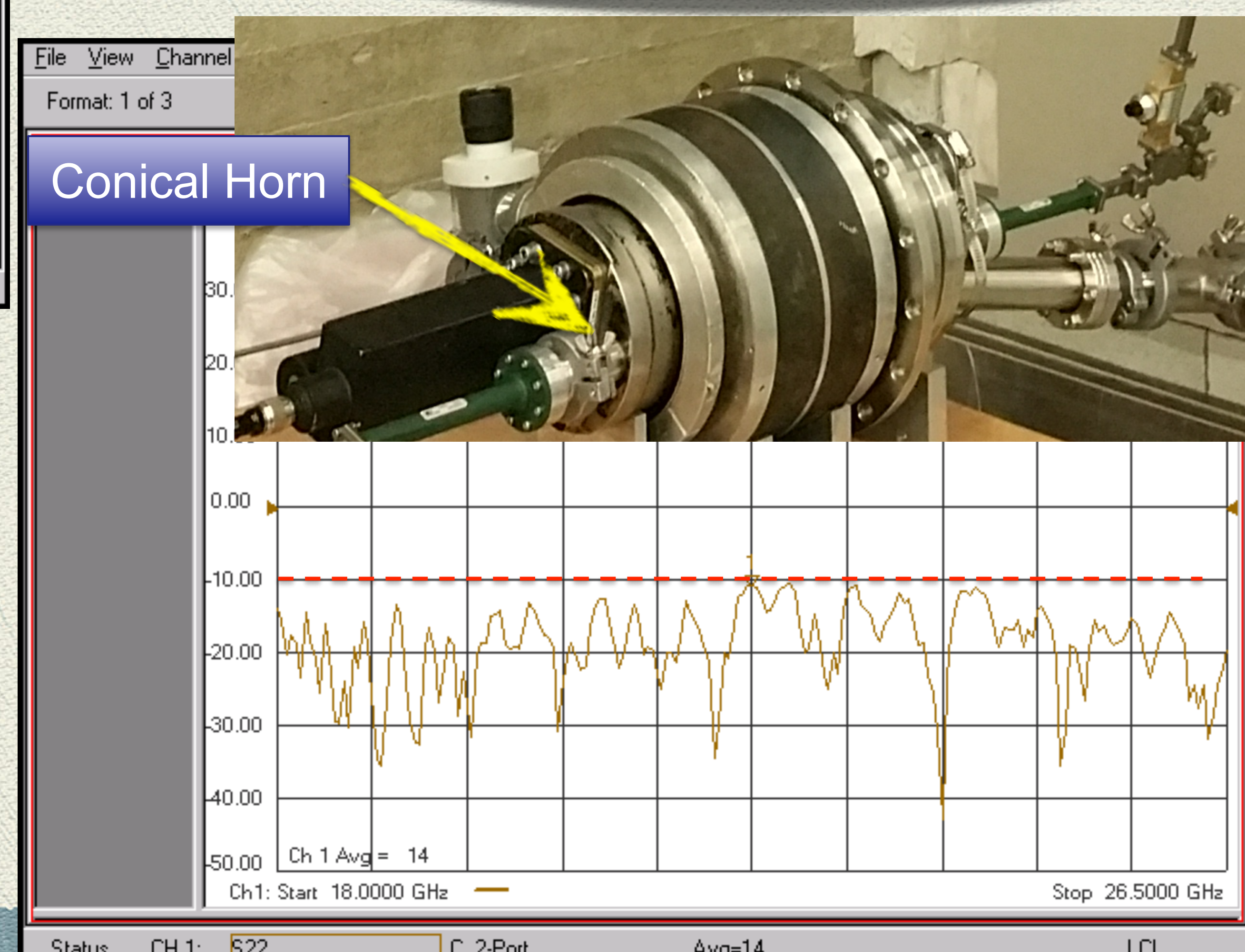

Interferometry in ECRIS:
the frequency sweep method

The method is based on the frequency shift of the beating signal given by the superposition of the reference leg plus the plasma leg waves.

The beating frequency cab be fixed as long as the ramp relation "freq. vs. time" is chosen in the following way:

$$\omega_{B_0} = \frac{\partial \omega}{\partial t}\left(\Delta L \frac{\partial k_g}{\partial \omega} + \frac{2a}{c} \right) = \text{constant}$$

Rapidly increasing frequency produces a beating whose *S(ω(t))* shape function assumes the following form:

$$S(\omega) \propto 2A^2 \cos^2\left\{ \left[\Delta L \sqrt{\omega^2 - \omega_c^2} + \int_{-a}^{a} \sqrt{\omega^2 - \omega_p^2(l)}\, dl \right] \Big/ 2c \right\}$$

The presence of plasma (accounted by the plasma frequency w_p) only shifts the beating frequency, while multipath introduce spurious components in the spectrum

Interferometry in ECRIS: the frequency sweep method

- Only one frequency is visible, corresponding to the beating signal.

Reference signal: Waveguide
Probing signal: free space

Beating signal component

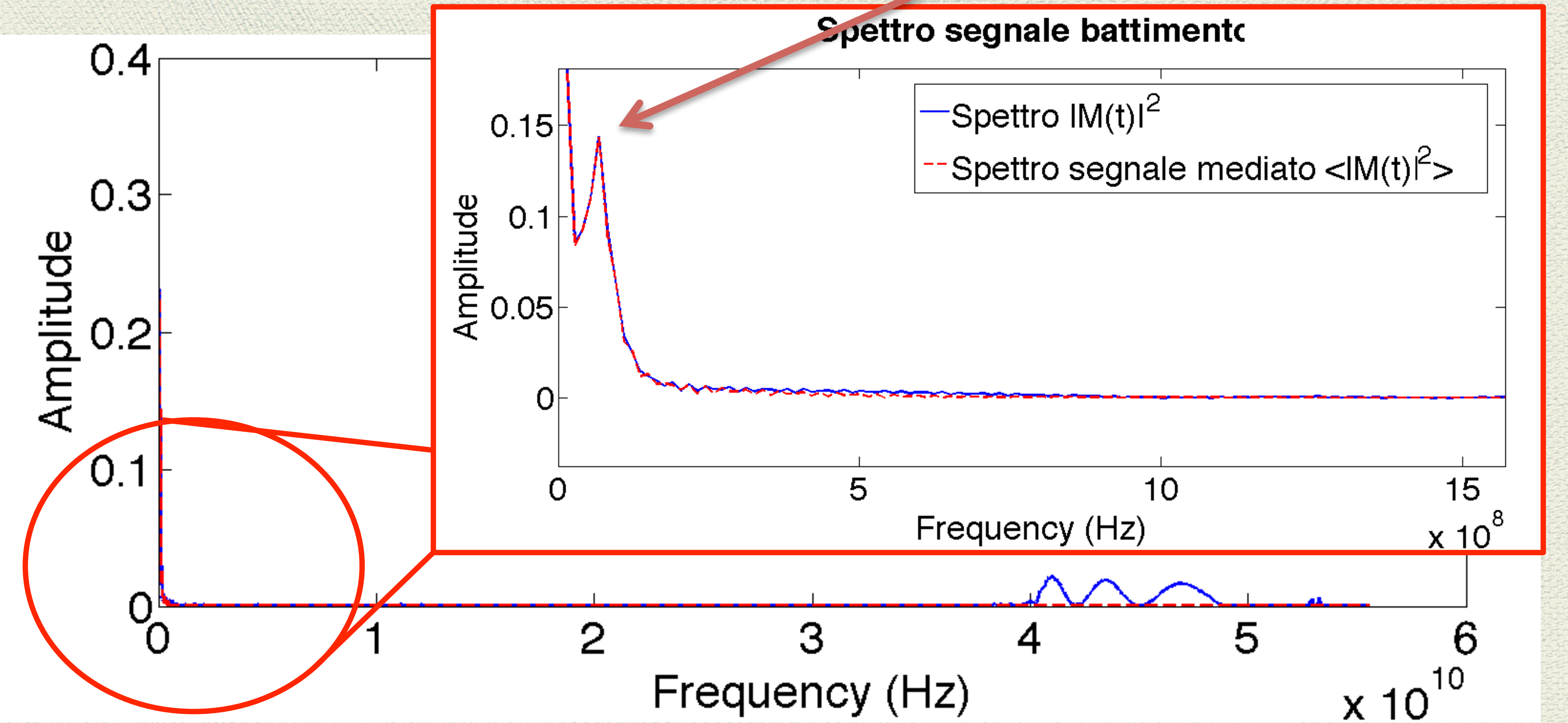

SIMULATION

Interferometry in ECRIS:
the frequency sweep method

Many peaks come out due to multi-reflections at the chamber walls

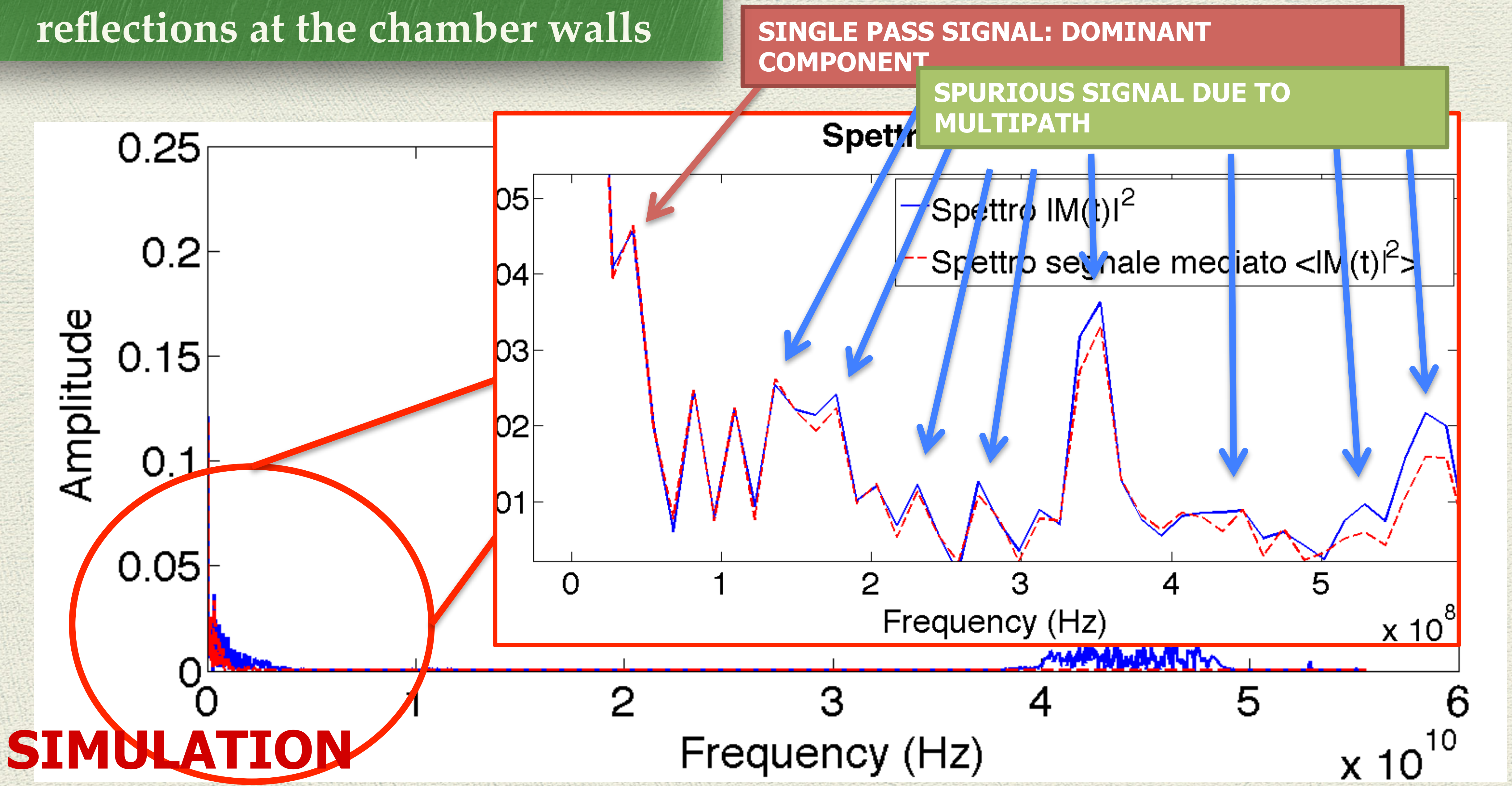

Interferometry in ECRIS:
the calibration phase

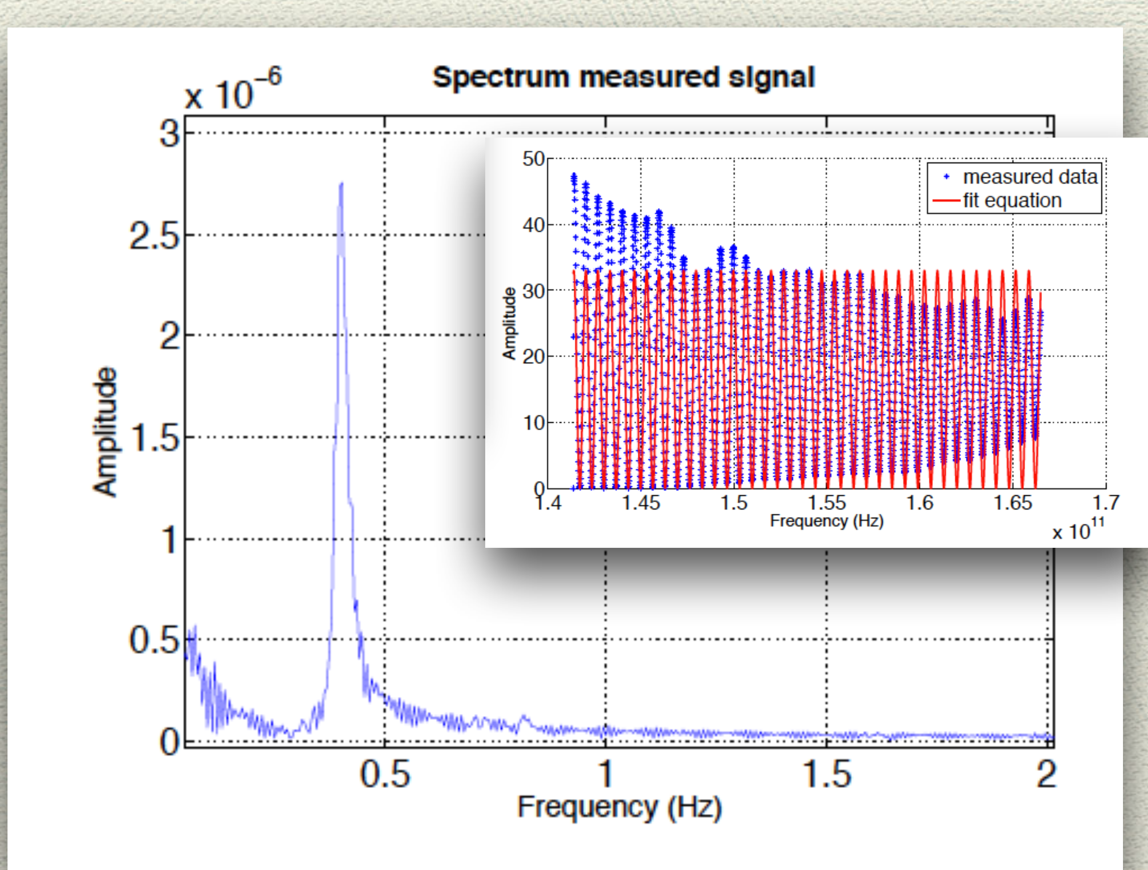

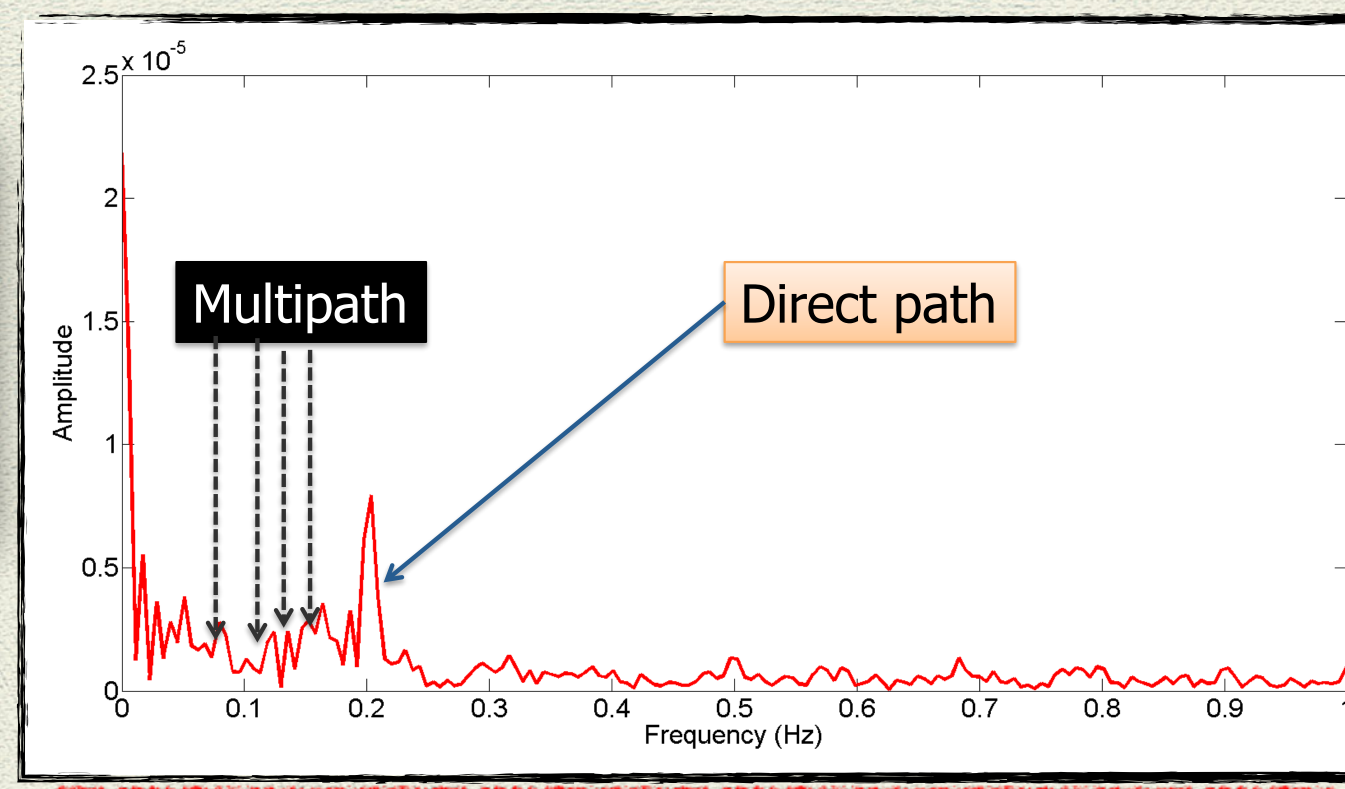

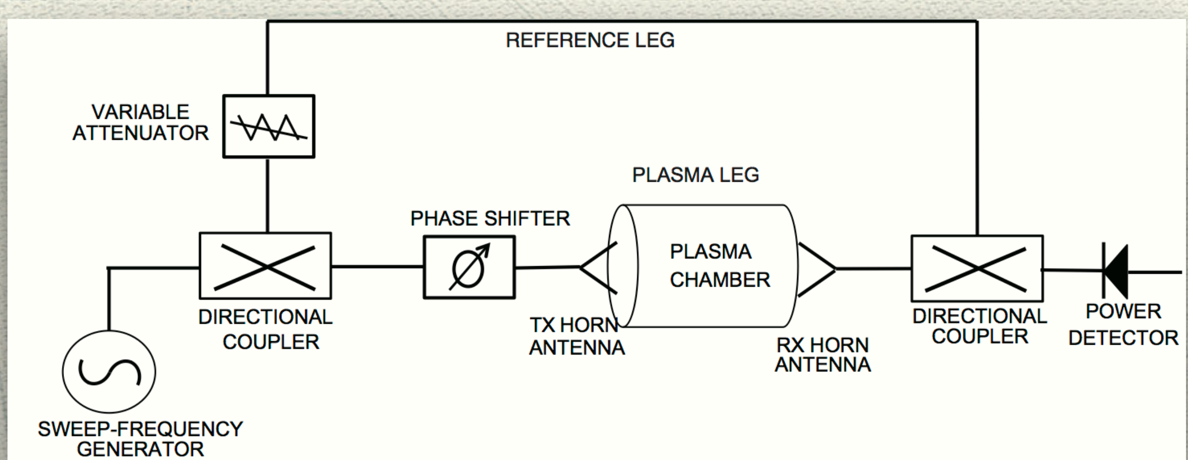

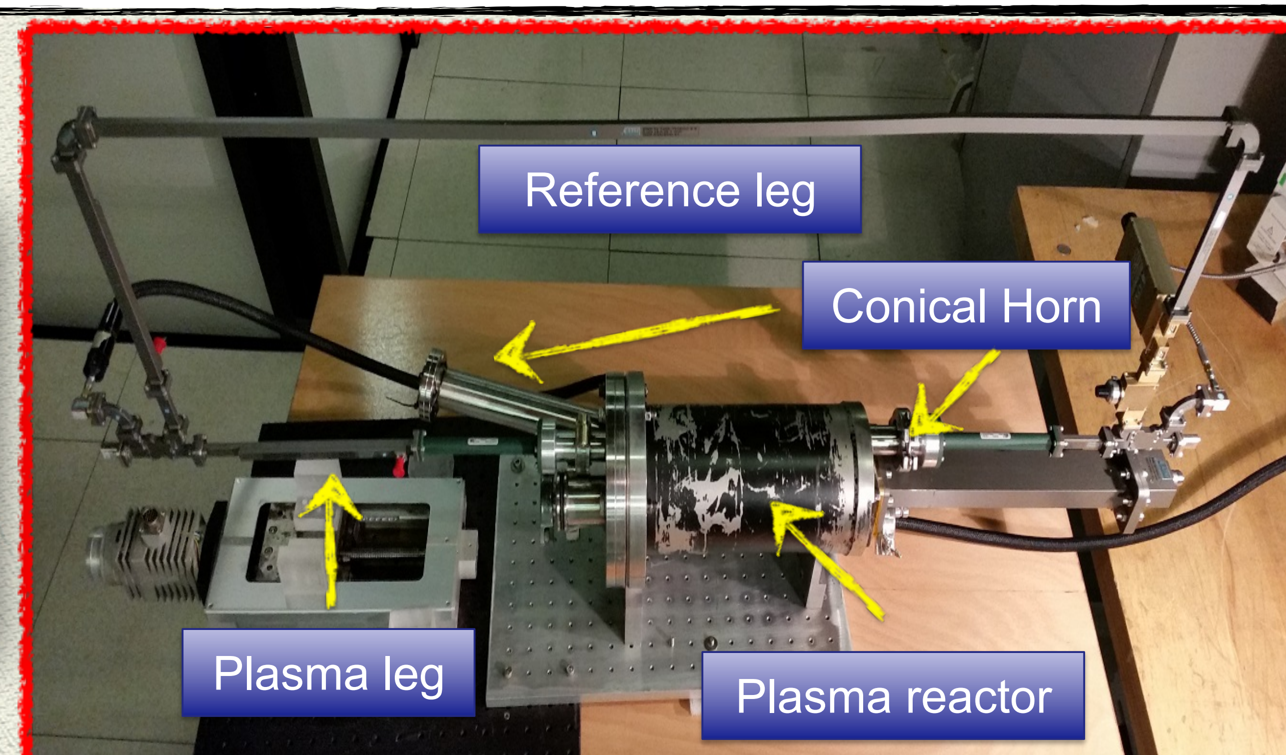

Final setup of the interferometer

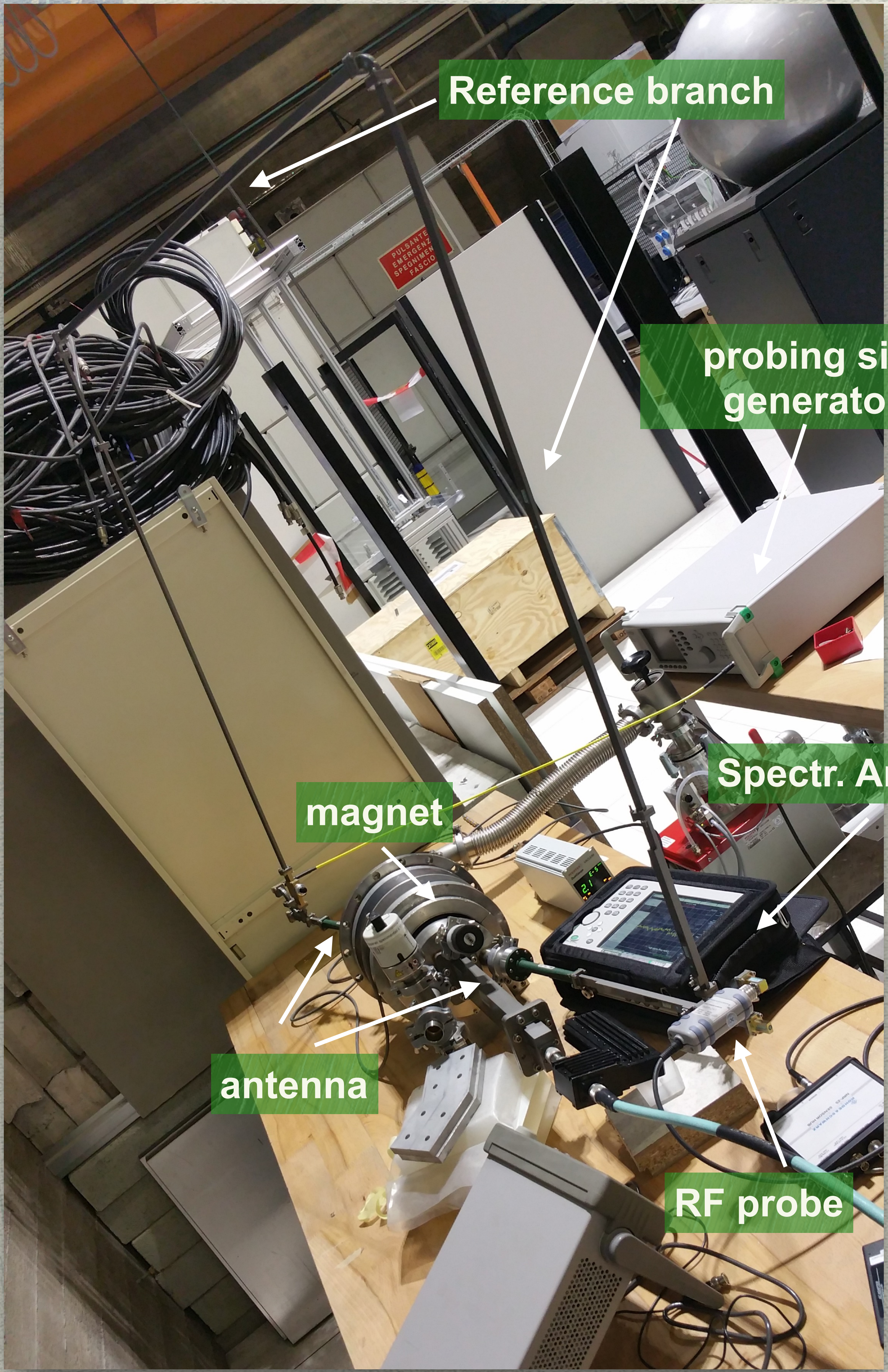

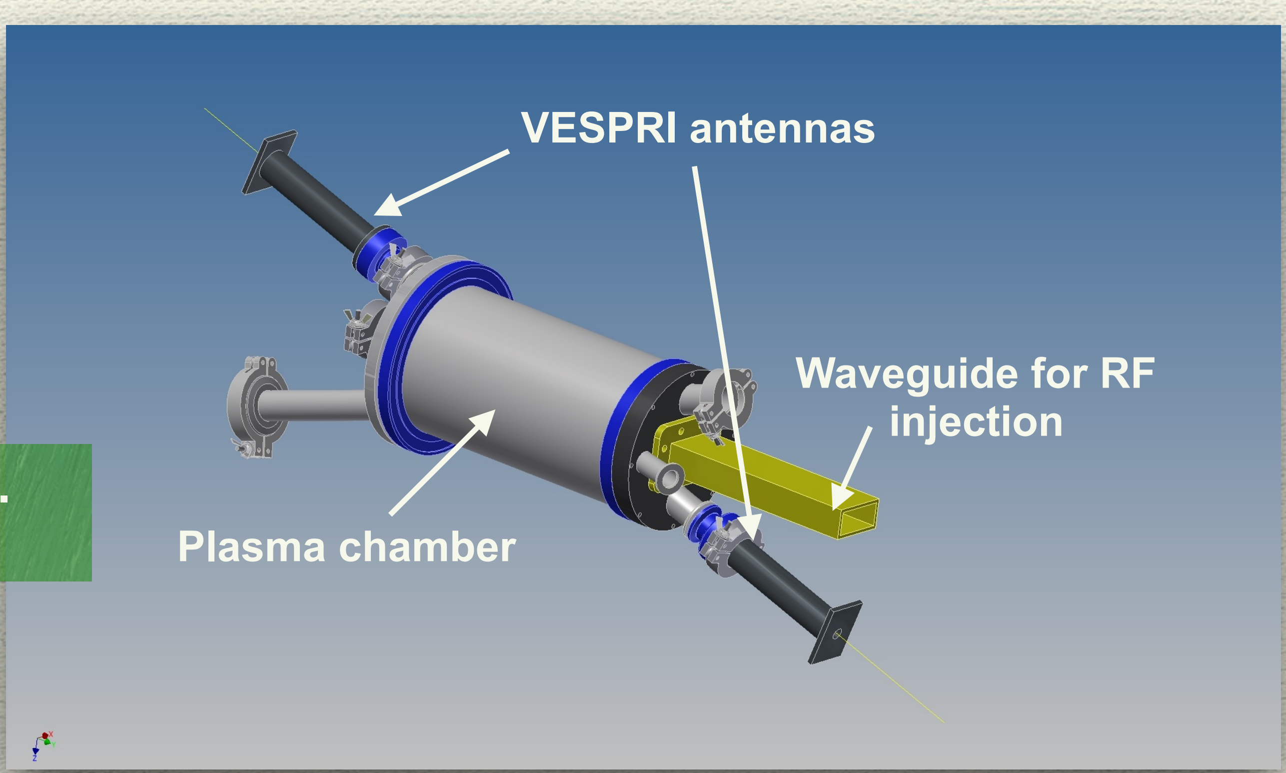

Interferometry in ECRIS:

measuring of plasma density inside the cavity of the LNS plasma reactor

Interferometry in ECRIS:

measuring of plasma density inside the cavity

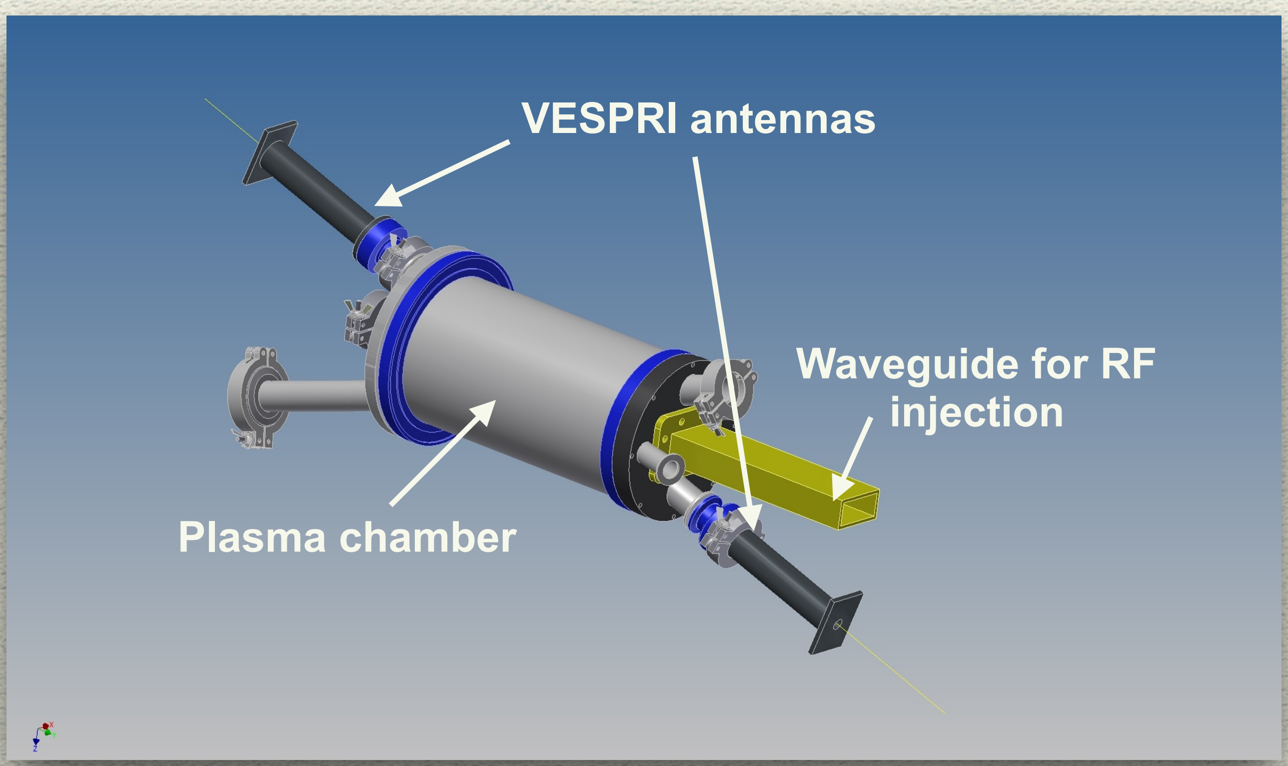

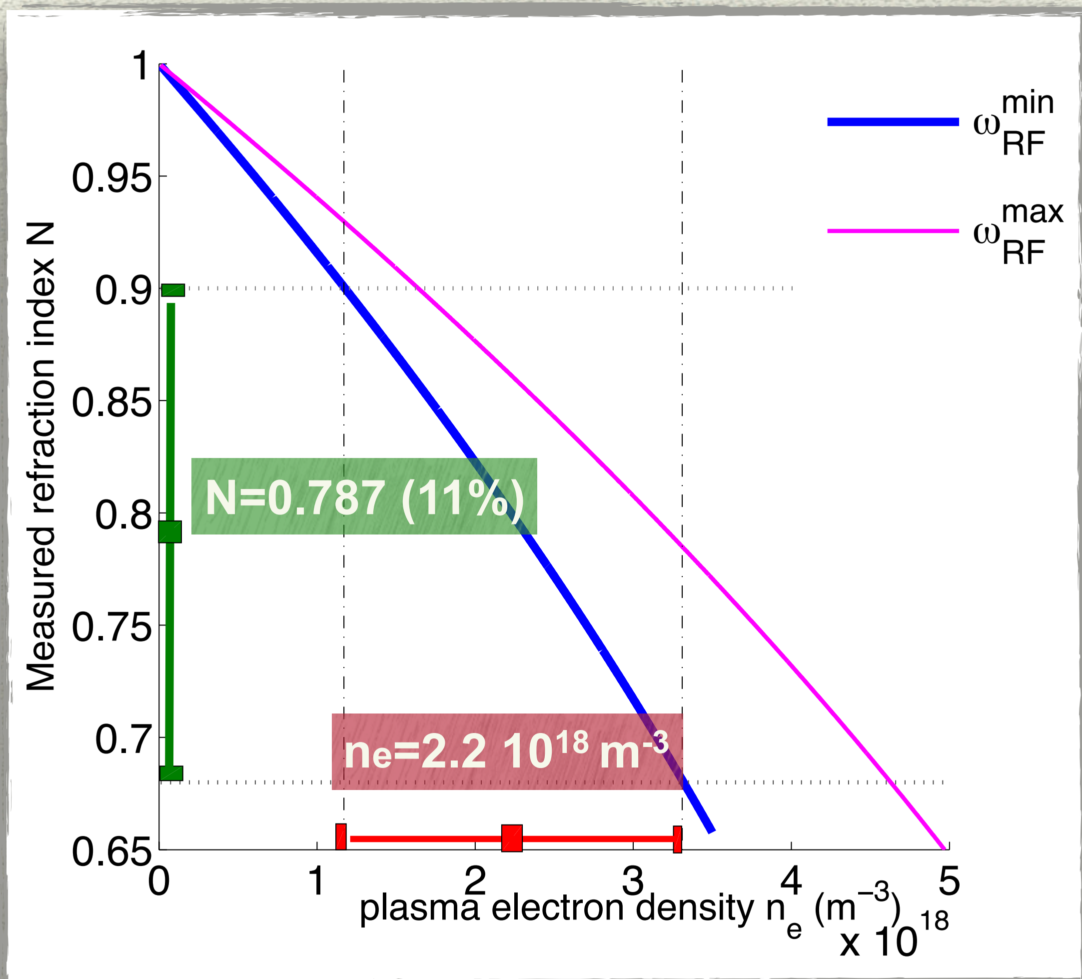

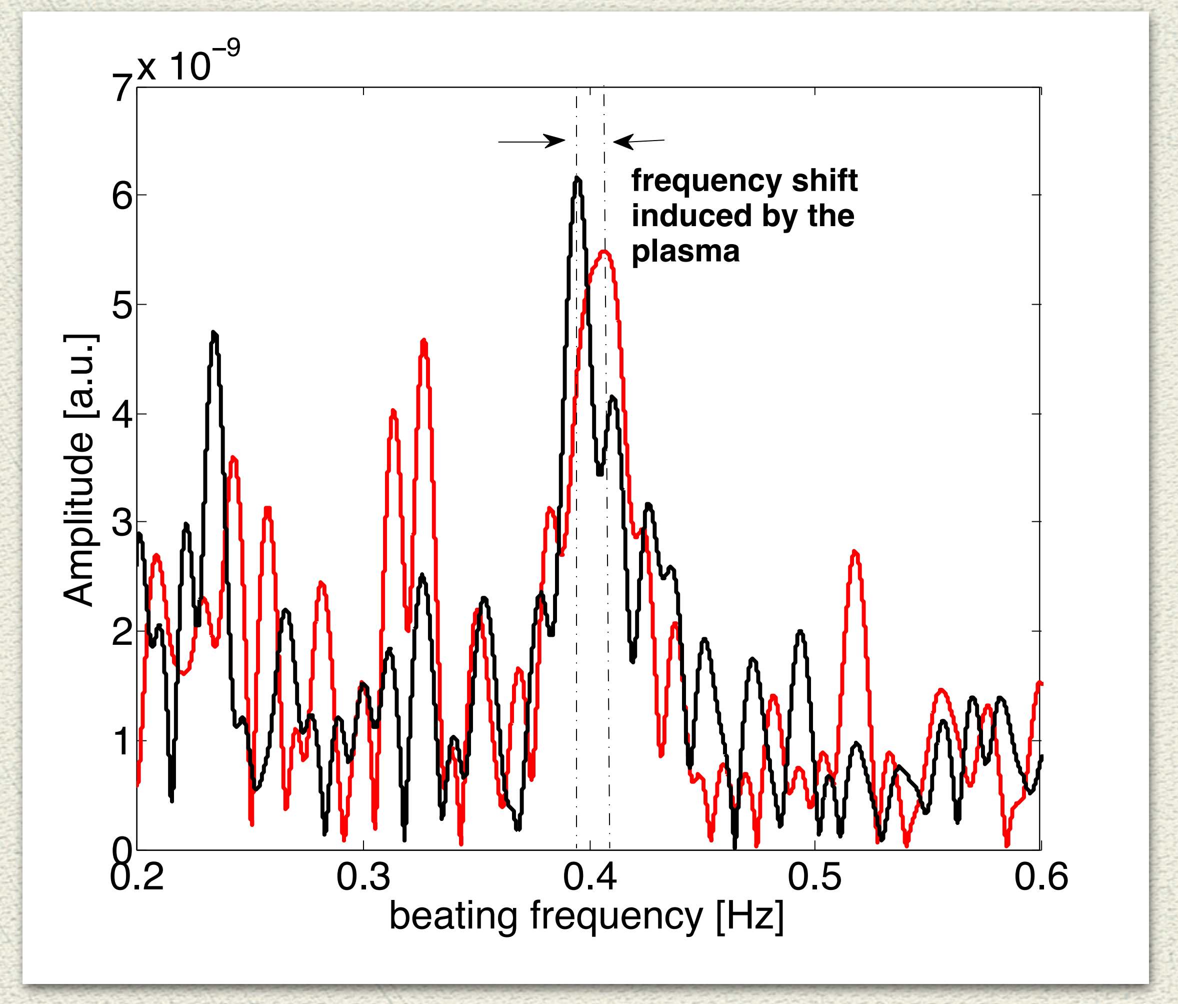

$$k_p = \frac{\omega}{c} N_p = \frac{\omega}{c}\frac{1}{2}\left(\sqrt{1-\frac{\omega_p^2}{\omega(\omega-\omega_g)}} + \sqrt{1-\frac{\omega_p^2}{\omega(\omega+\omega_g)}}\right)$$

Dispersion relation of the magnetized plasma

Numerical modelling of EBW-heating

Displacement of resonances and cutoffs

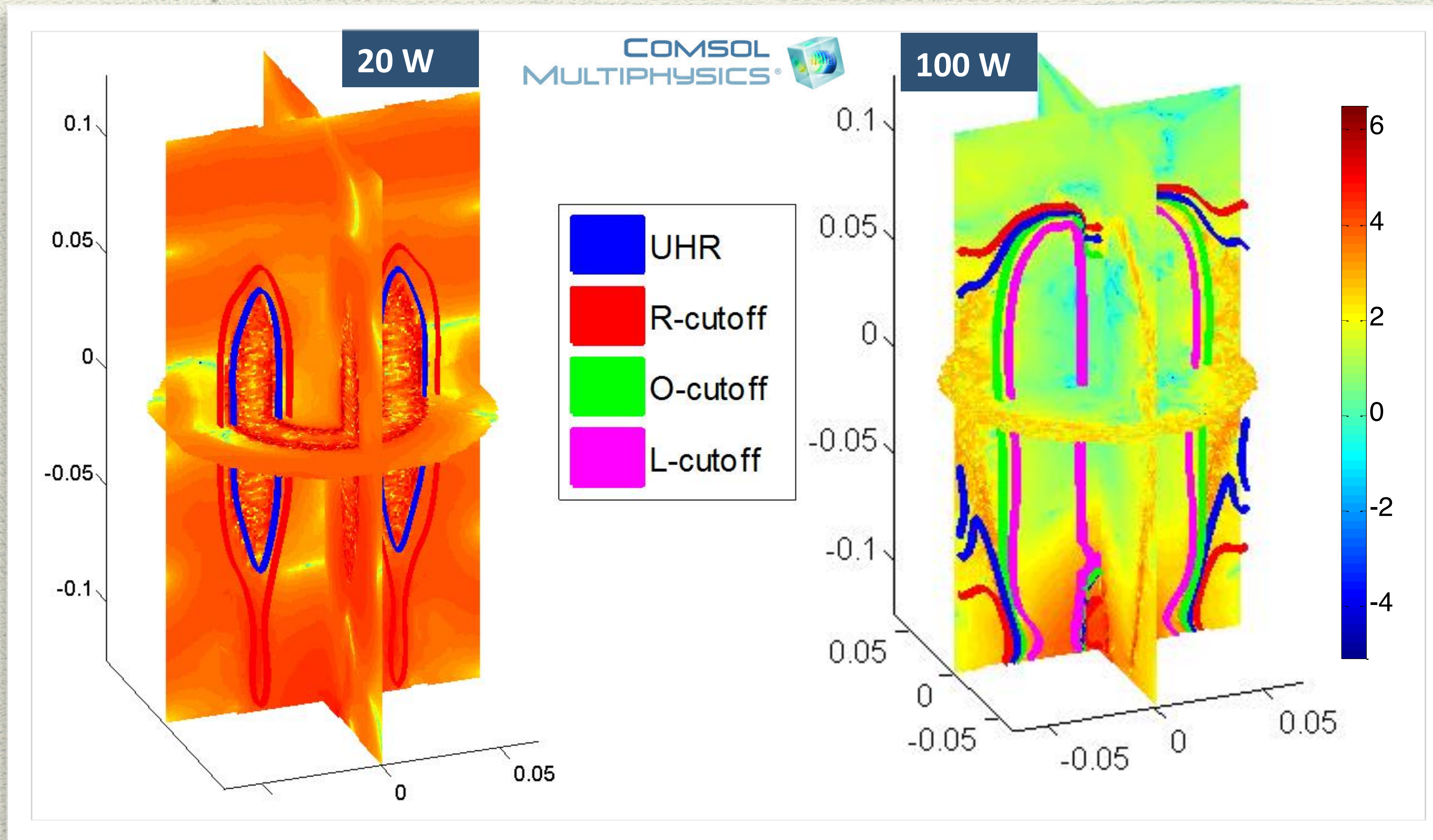

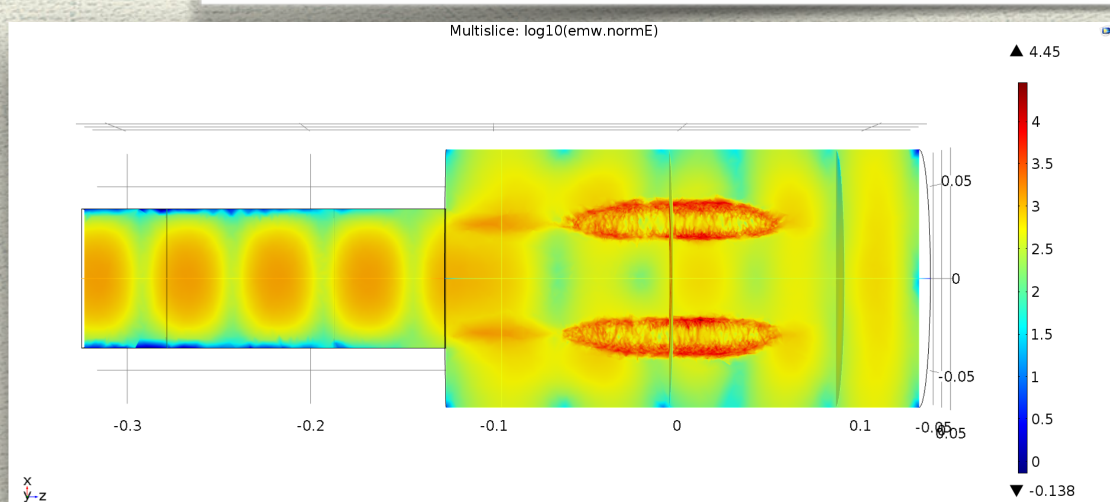

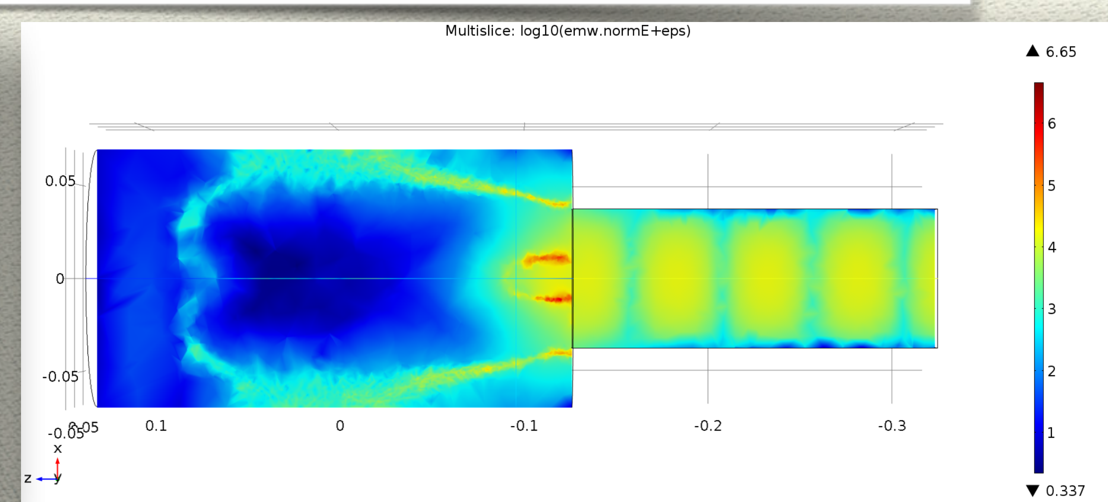

Numerical modelling of EBW-heating
Displacement of resonances and cutoffs

Results are compatible with the transition from directed FX-B absorption to the more efficient O-SX-B

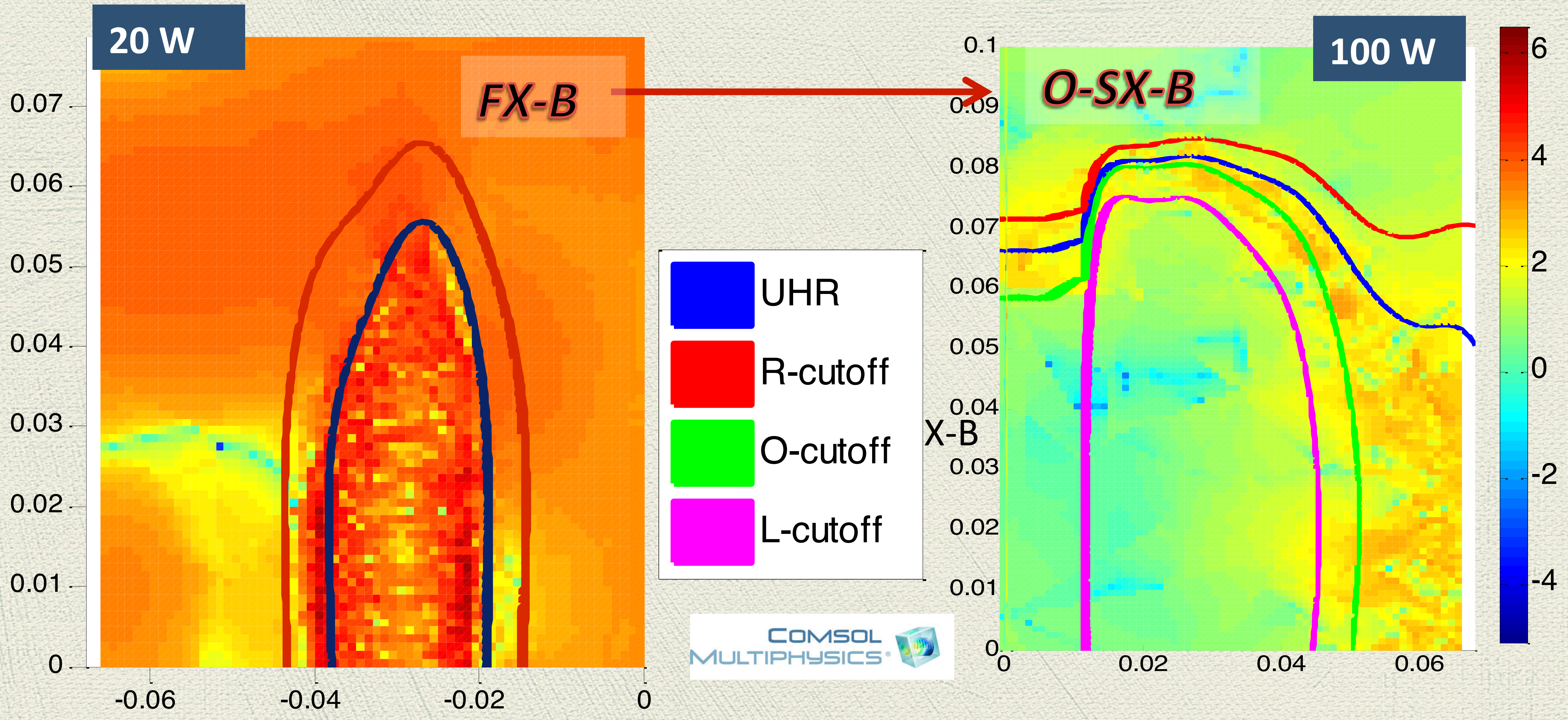

Microwave launching for EBW generation

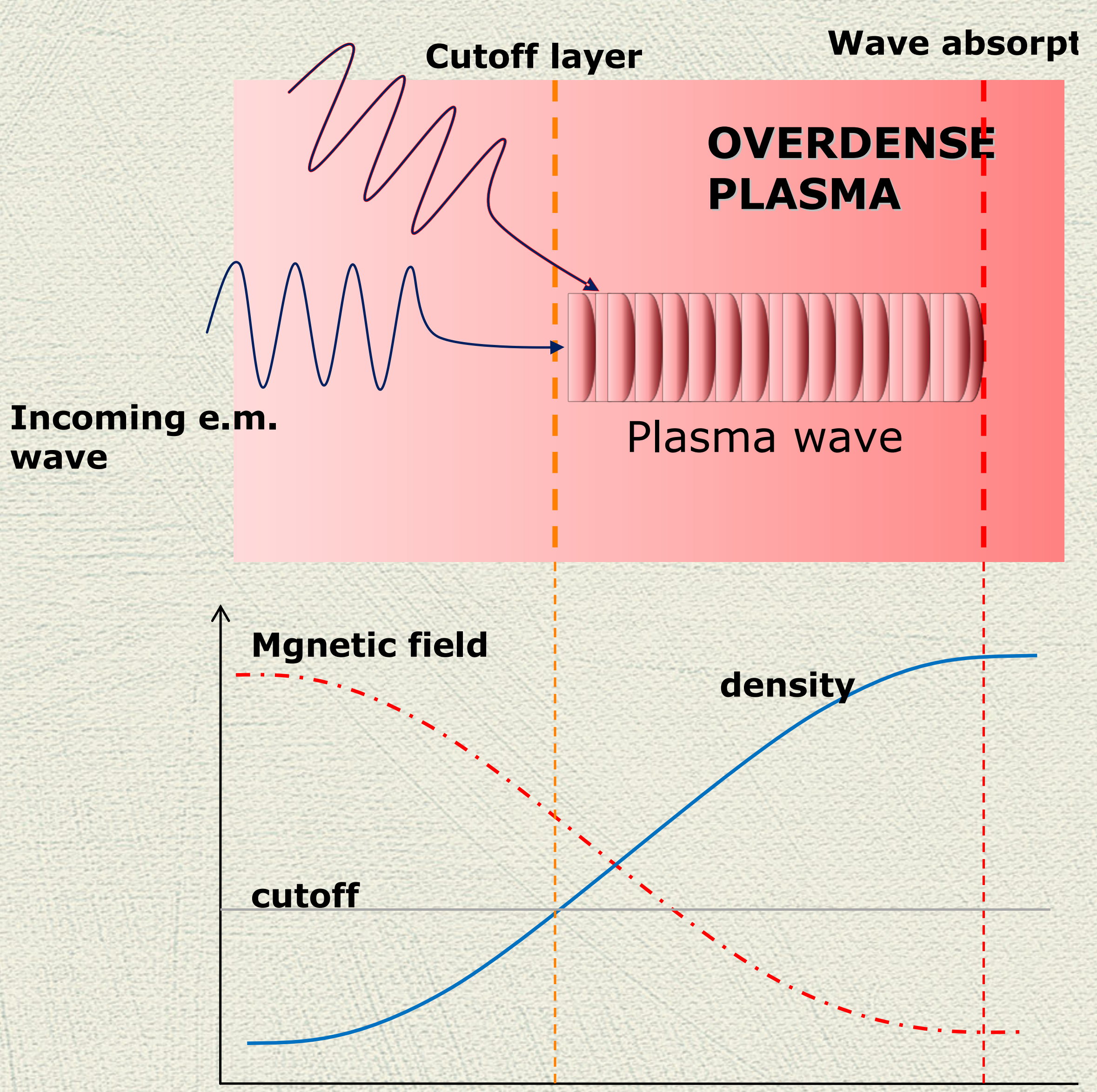

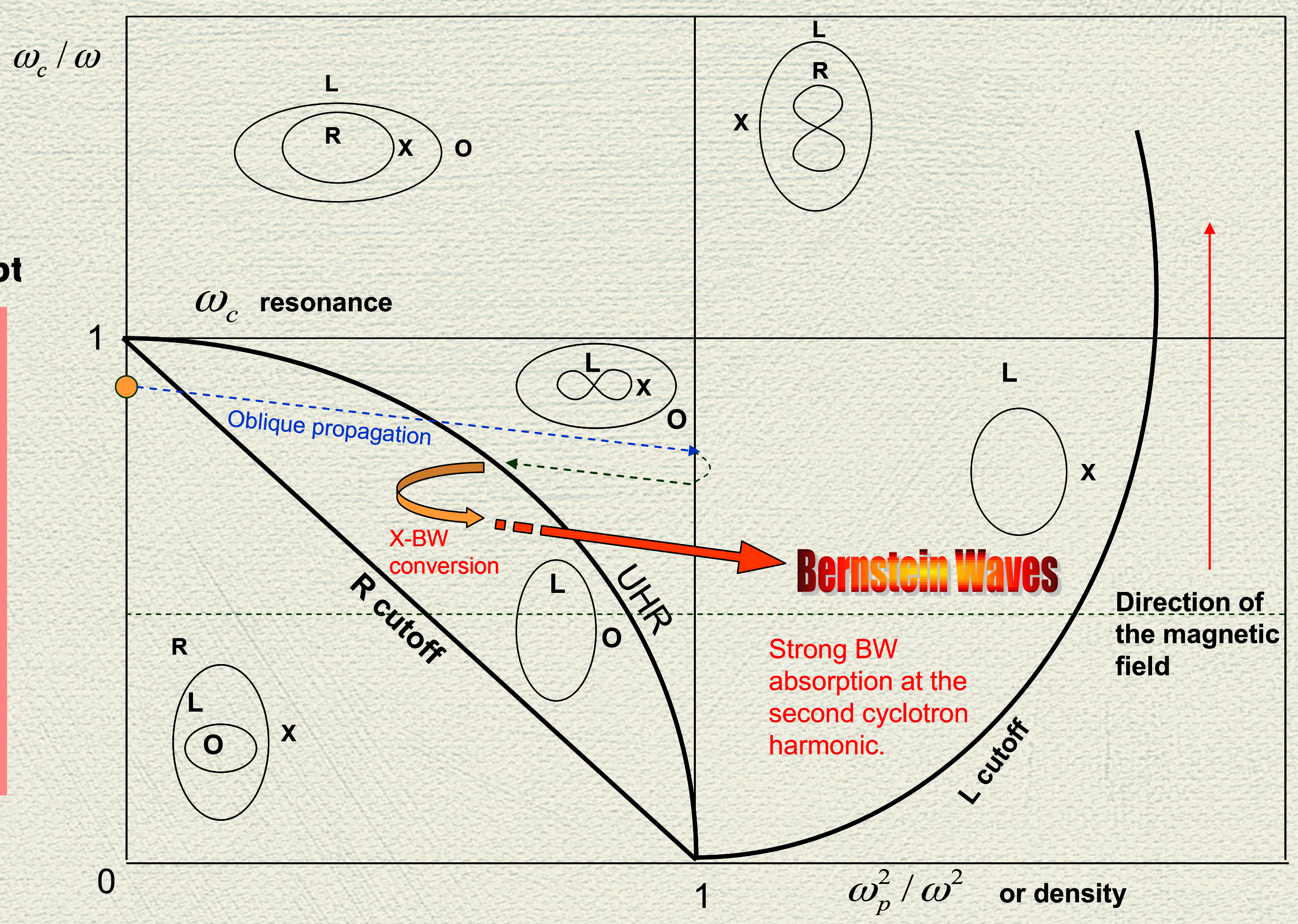

Oblique launching allow a more efficient matching of the incoming microwave radiation with the self-oscillations of the magnetized plasma

"Microwave-absorption-oriented" design

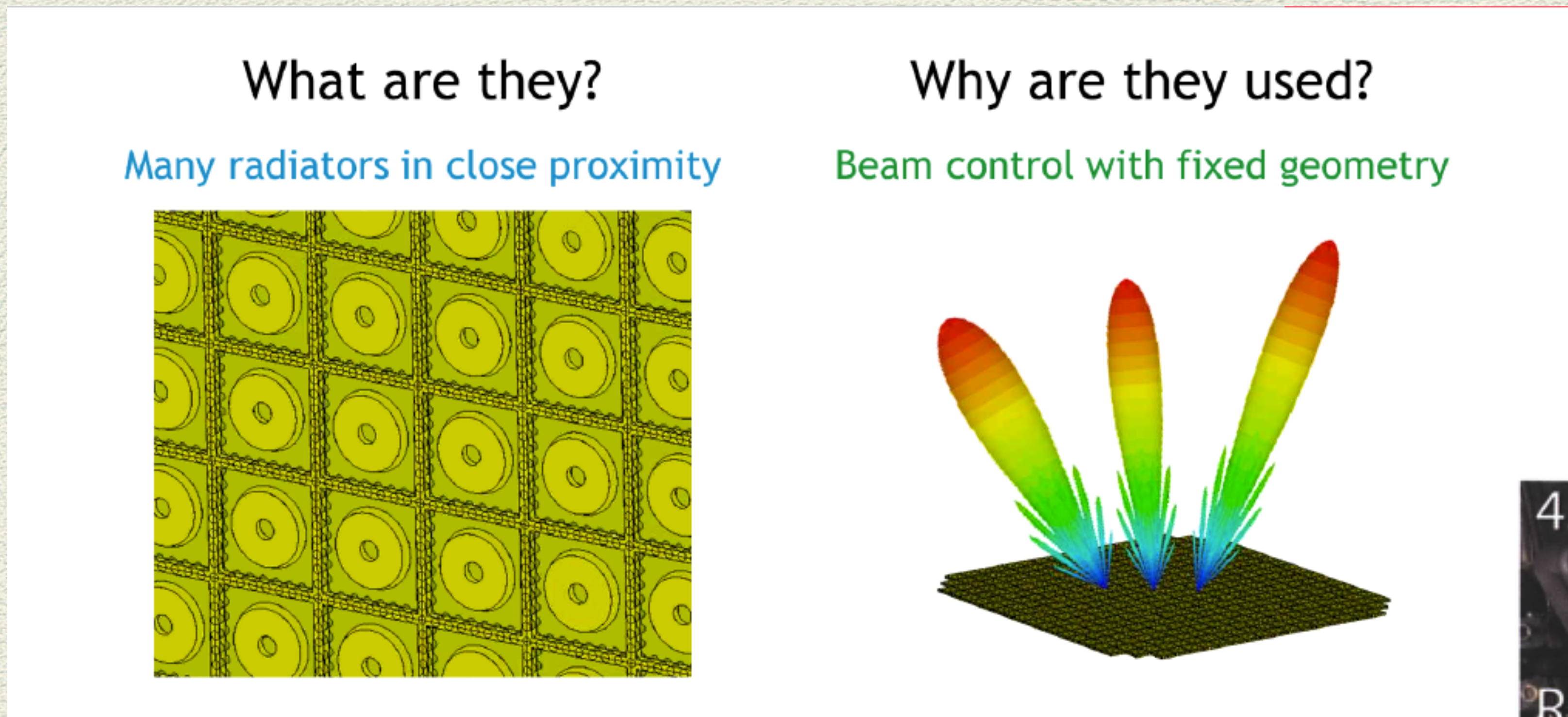

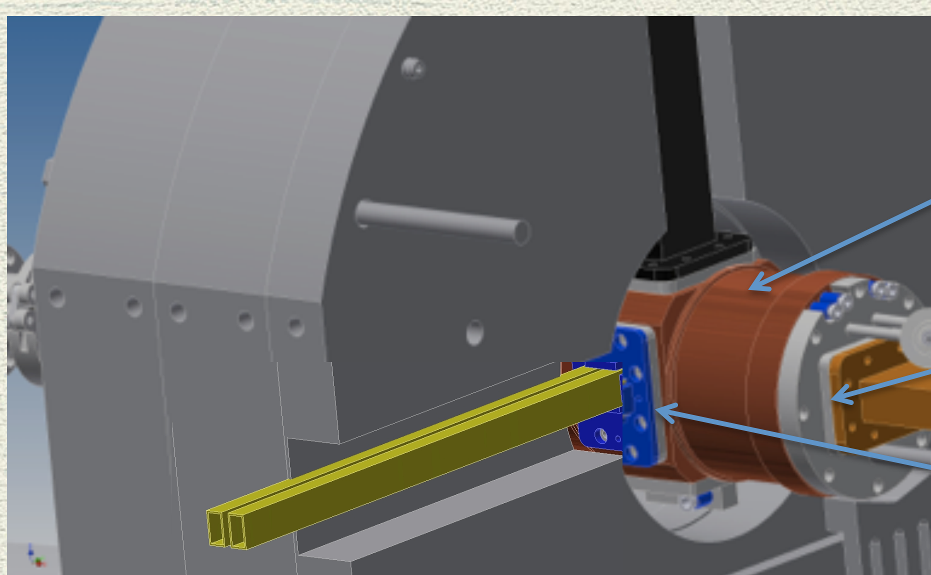

Plasma chamber

Plasma heating @ 7 GHz

Vacuum Break window

Courtesy of S. Passarello

ARRAY of two waveguides as
Alternative plasma heating @ 14 GHz

16 X 4 waveguides

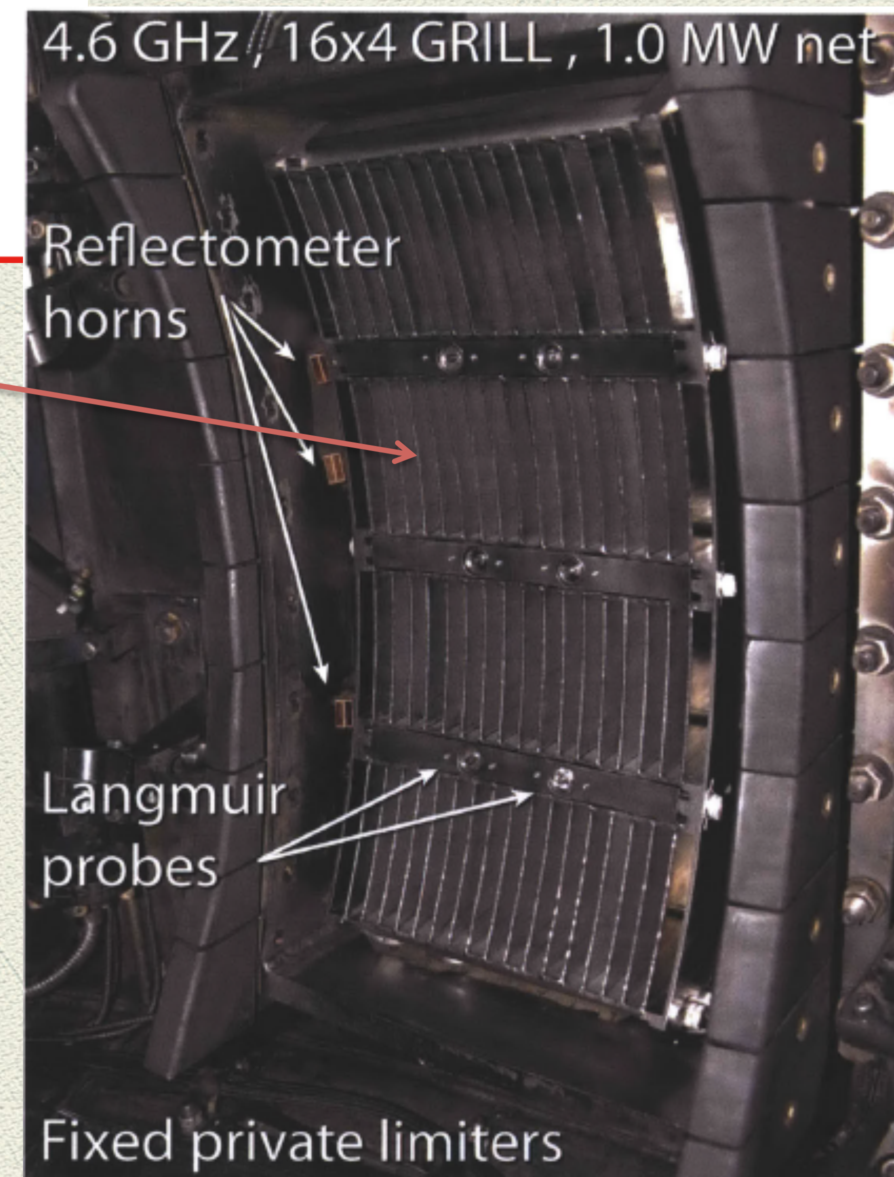

Flexible Plasma Trap for modal conversion now under assembling at LNS

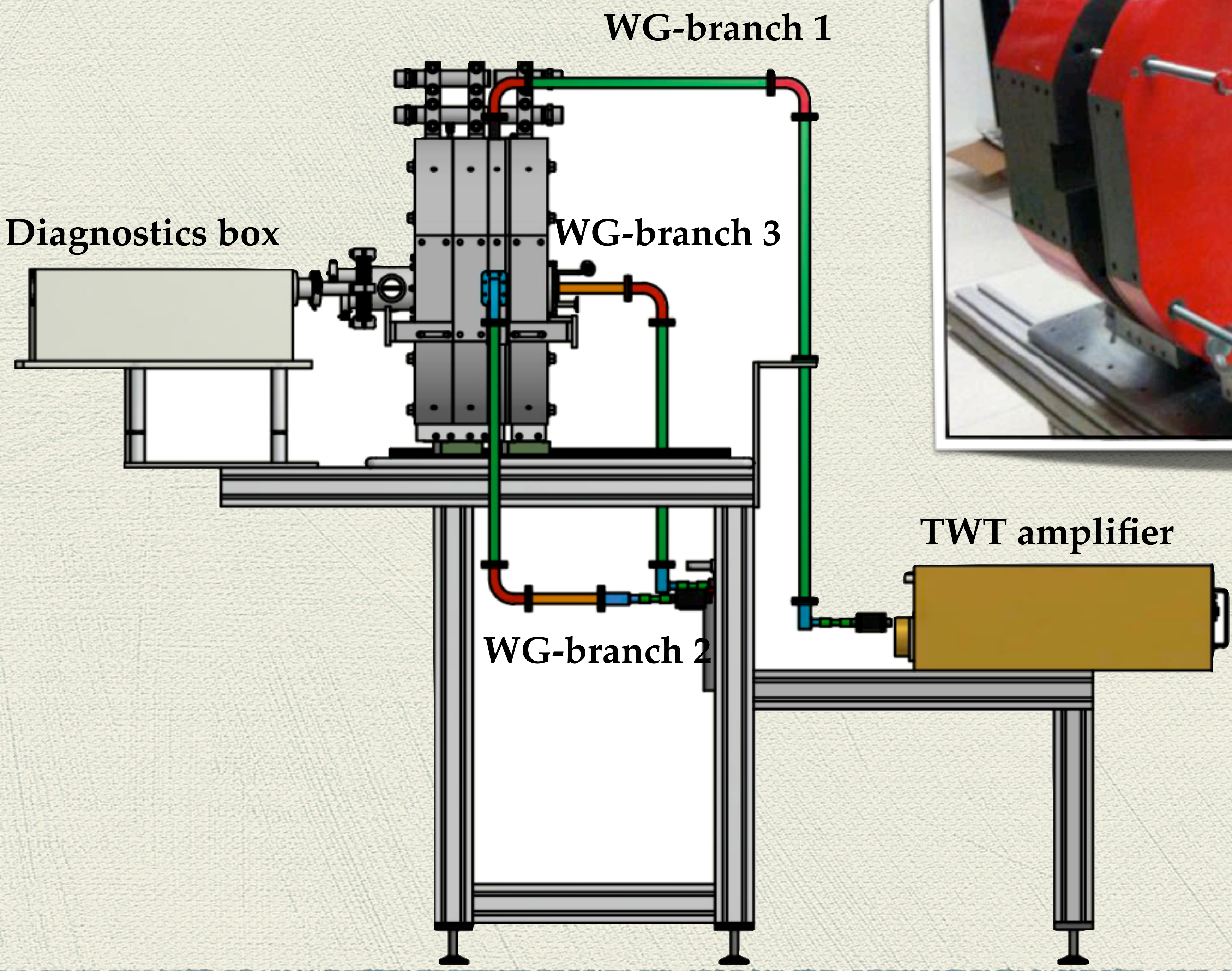

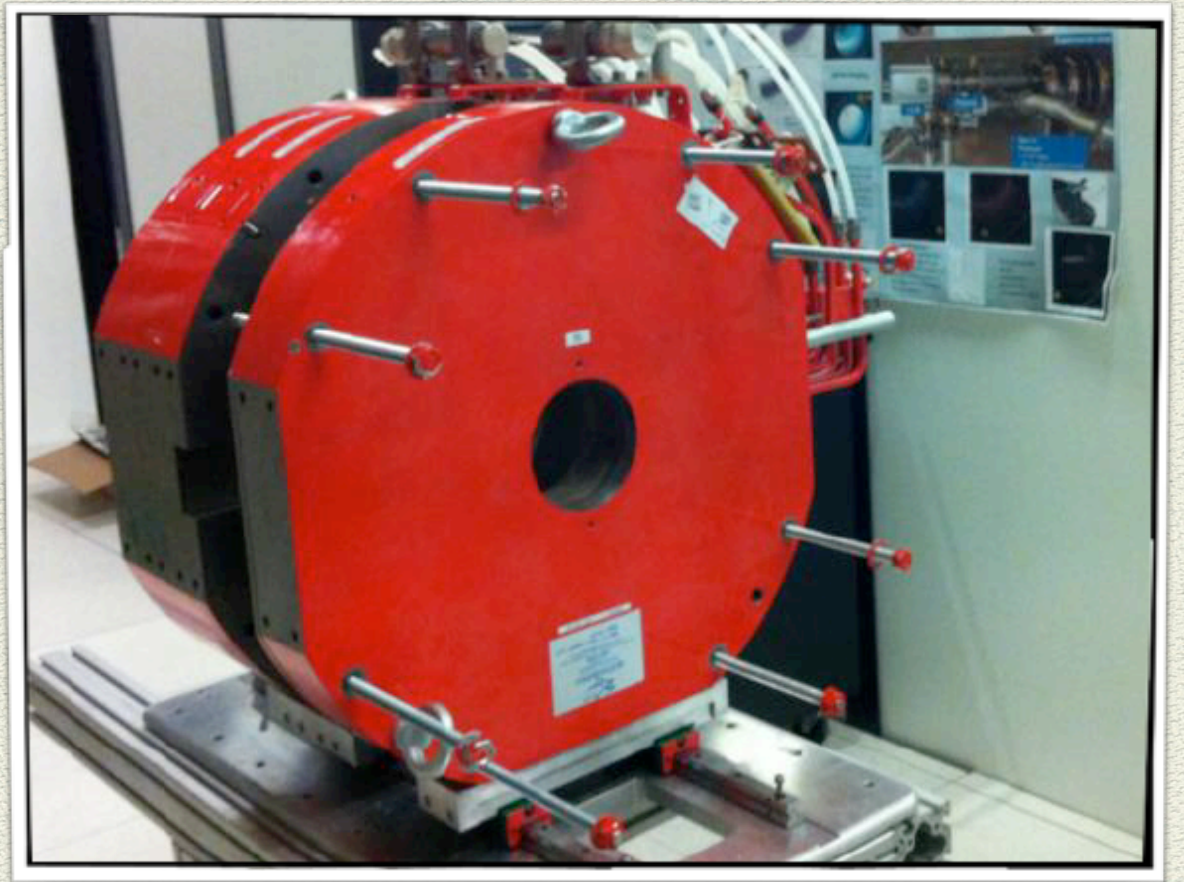

Boosting plasma density in a Two-Pumping-wave Scenario

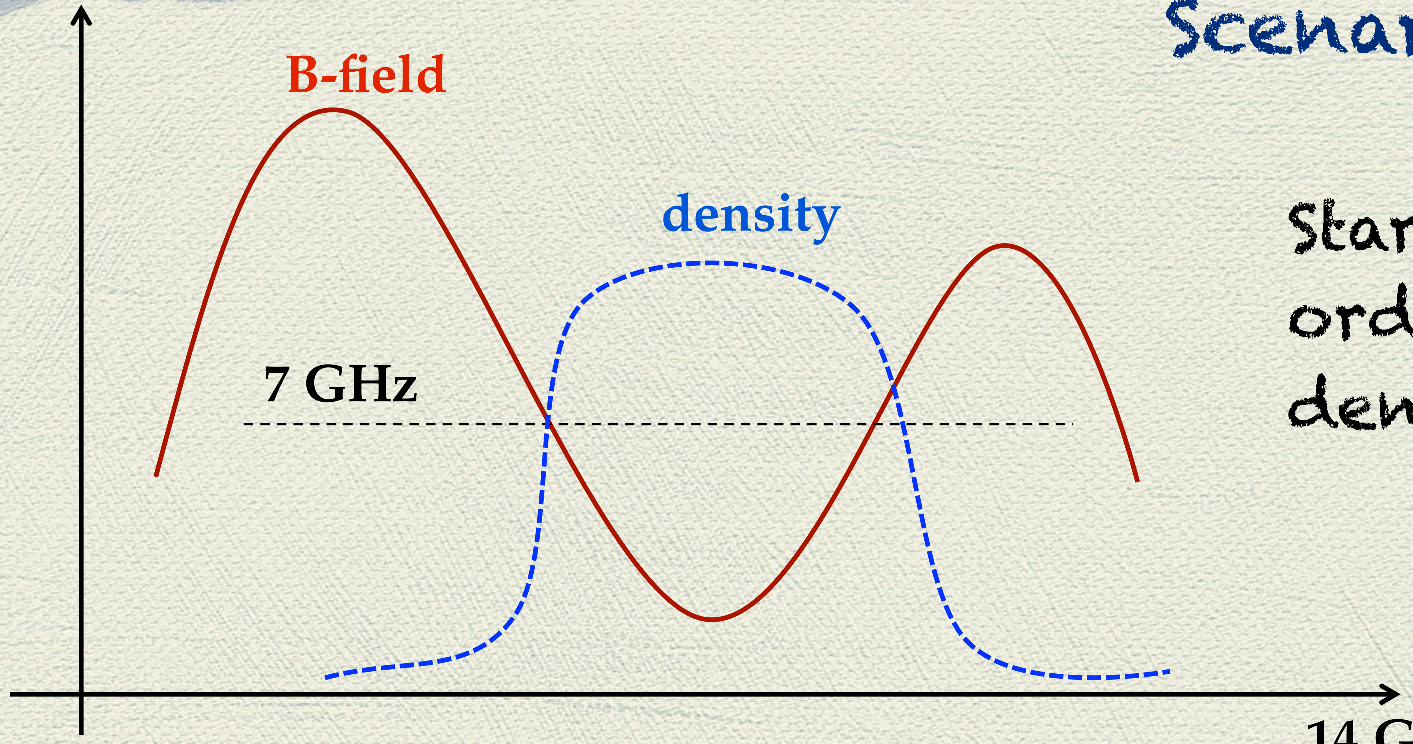

Start with one frequency in order to establish a proper density profile

Launch a second wave for modal conversion and second harmonic heating

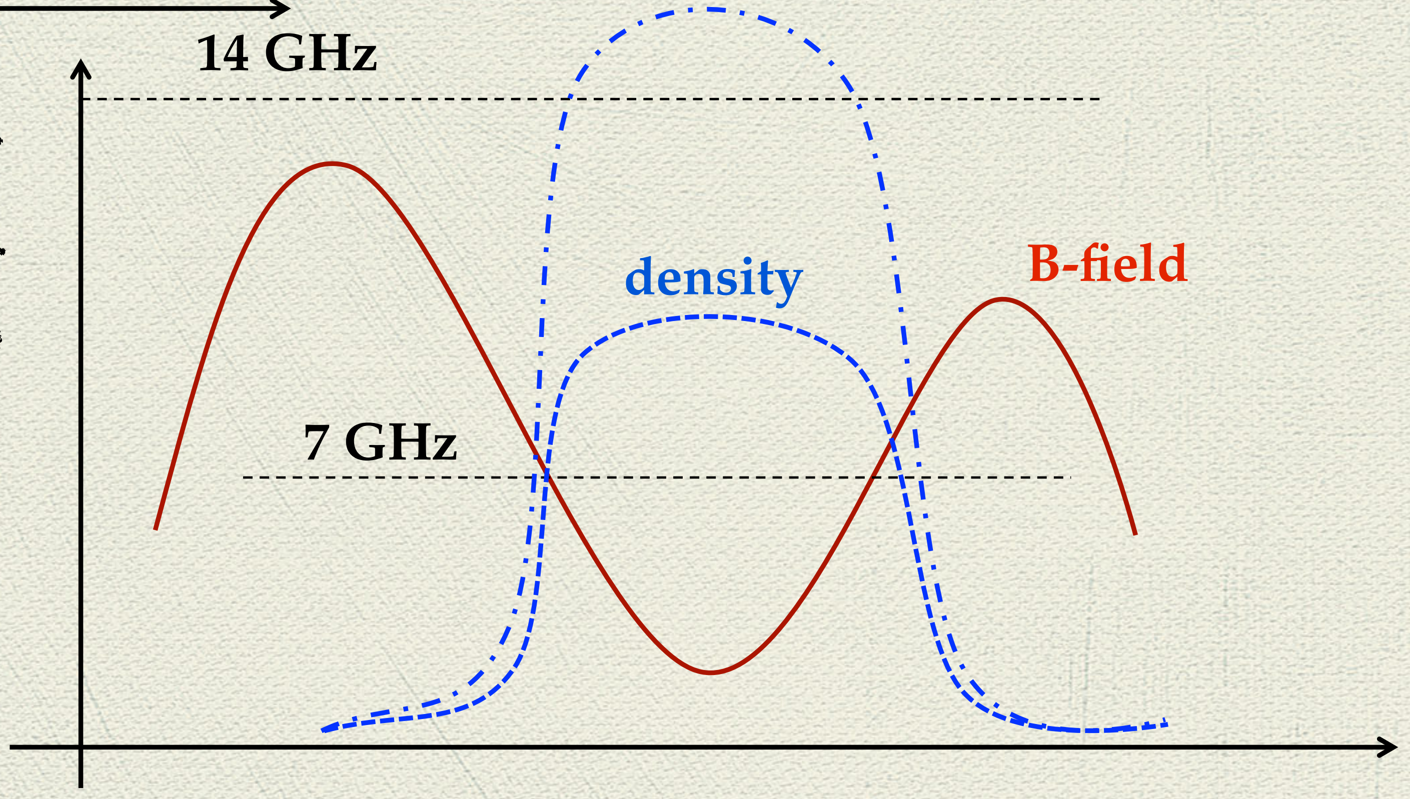

- the modal conversion is a density-magnetic field profiles dependent process
- -> mastering plasma structure is mandatory for conversion optimisation

Mastering of plasma density structure

cutoffs and res. along x

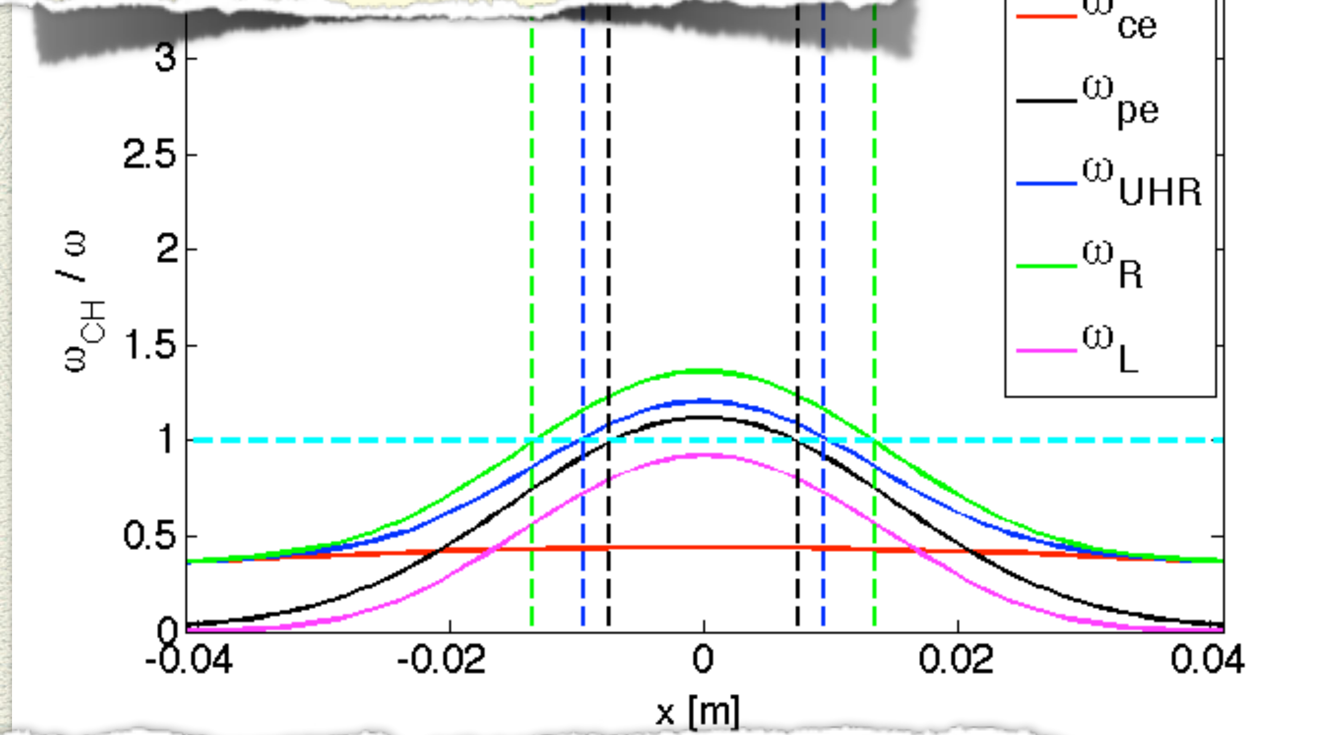

cutoffs and res. in the long. plane

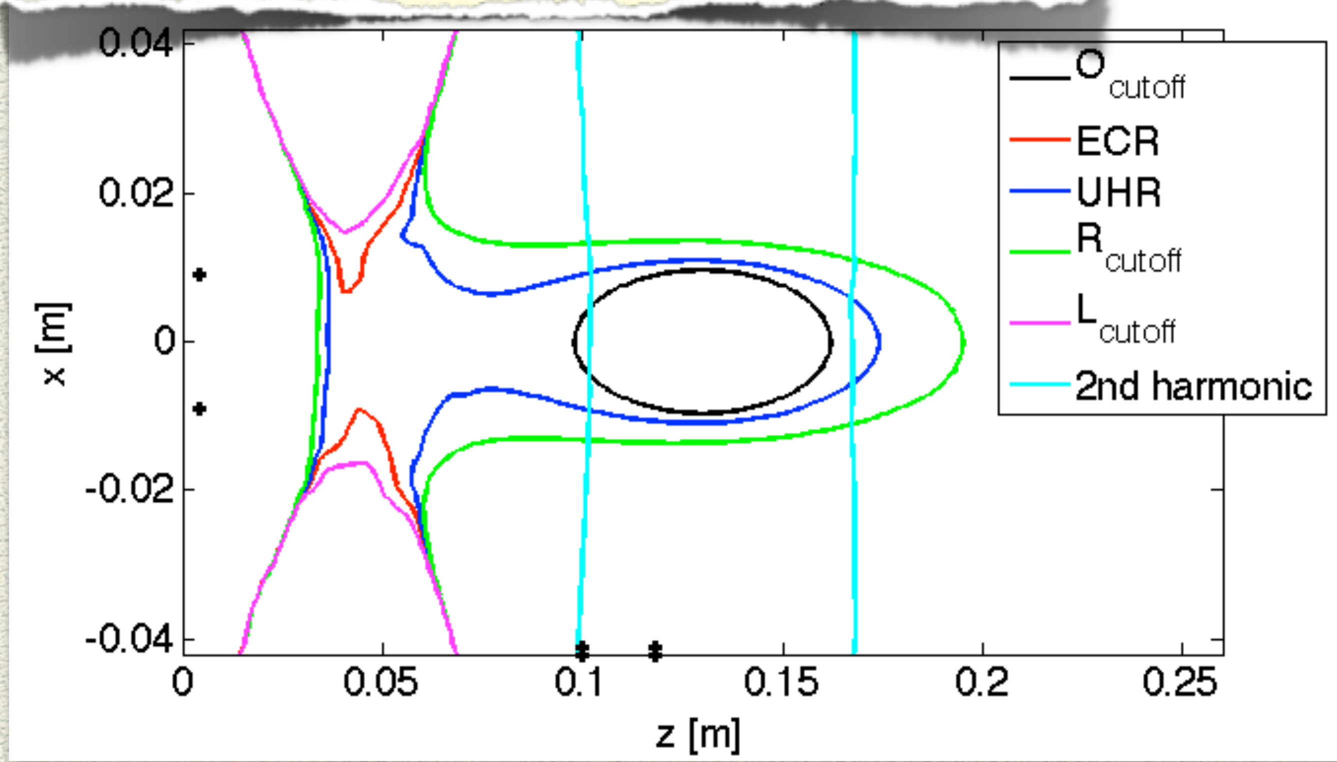

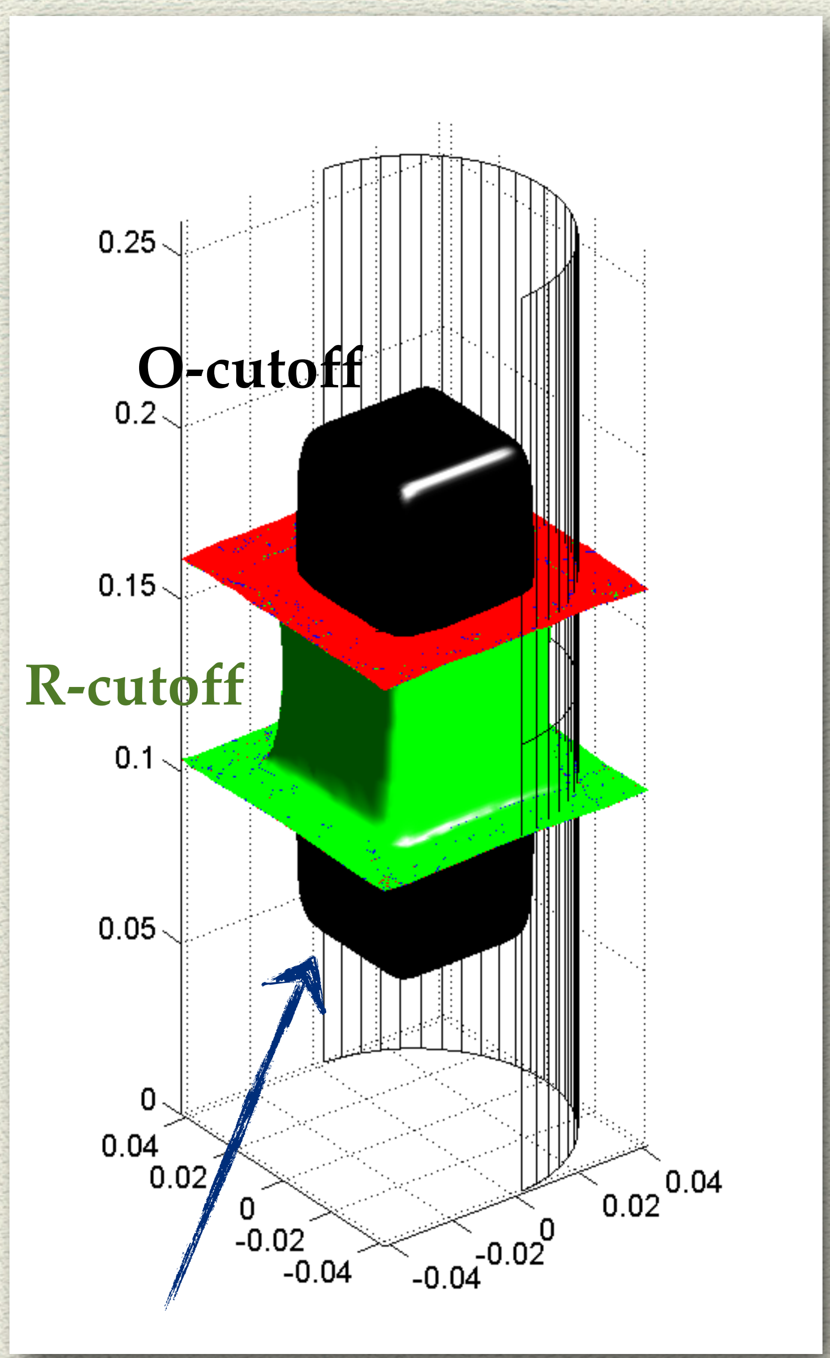

Cut-offs and resonances in 3D view

“Microwave-absorption-oriented” design

Launcher by “two-waveguides-array”: lobe tilt by phase shift for otimizing oblique coupling of O-modes --> modal conversion

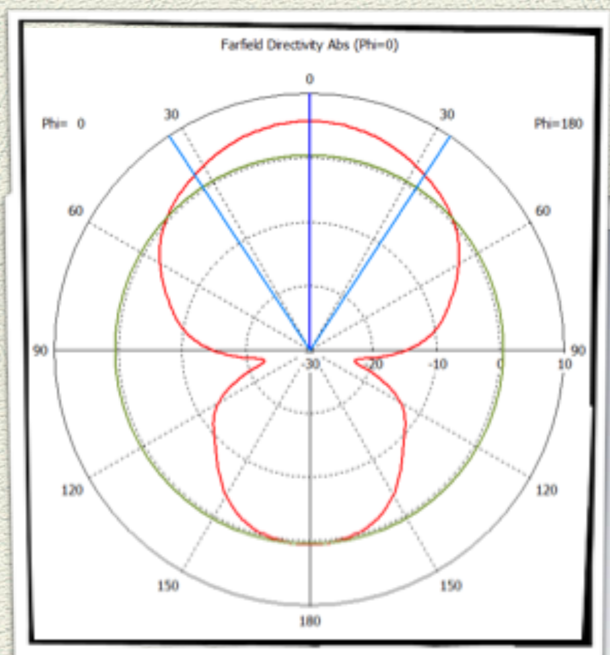

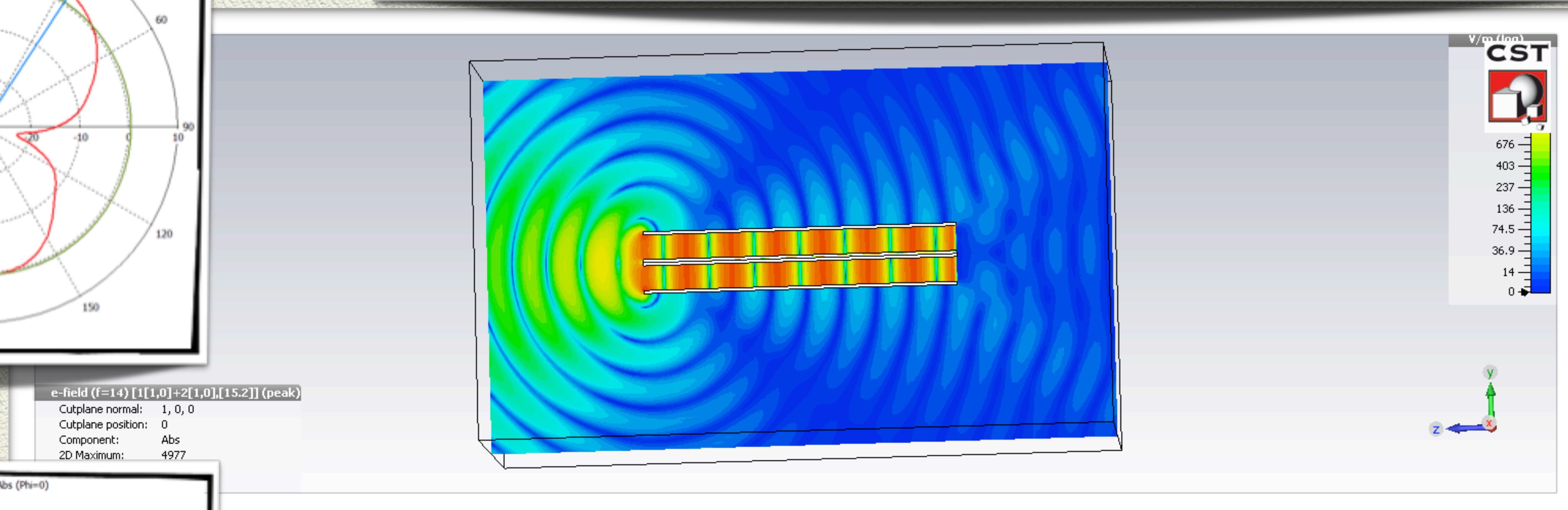

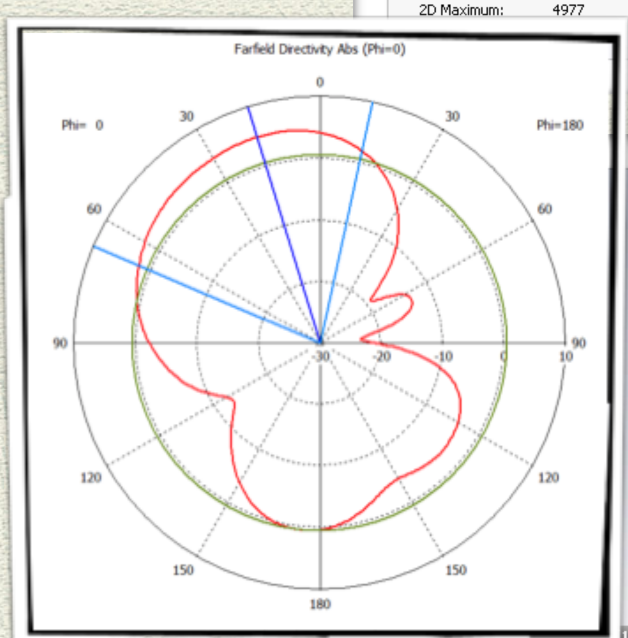

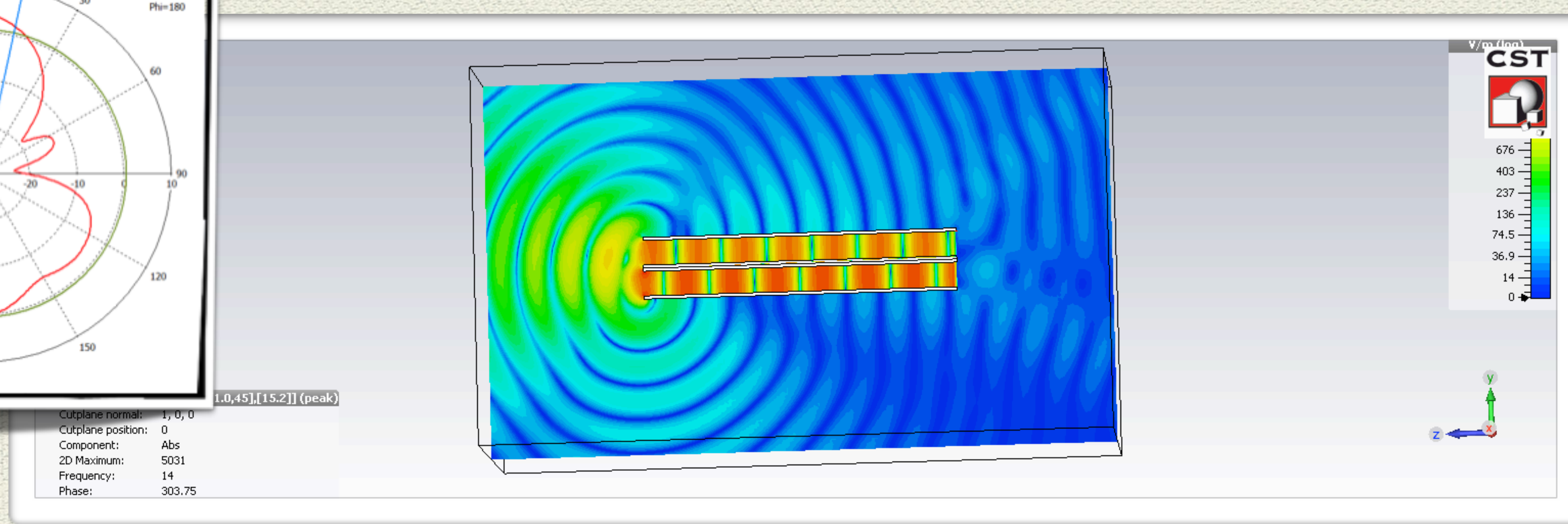

Mechanical Implementation at LNS

Phased waveguide array of two elements

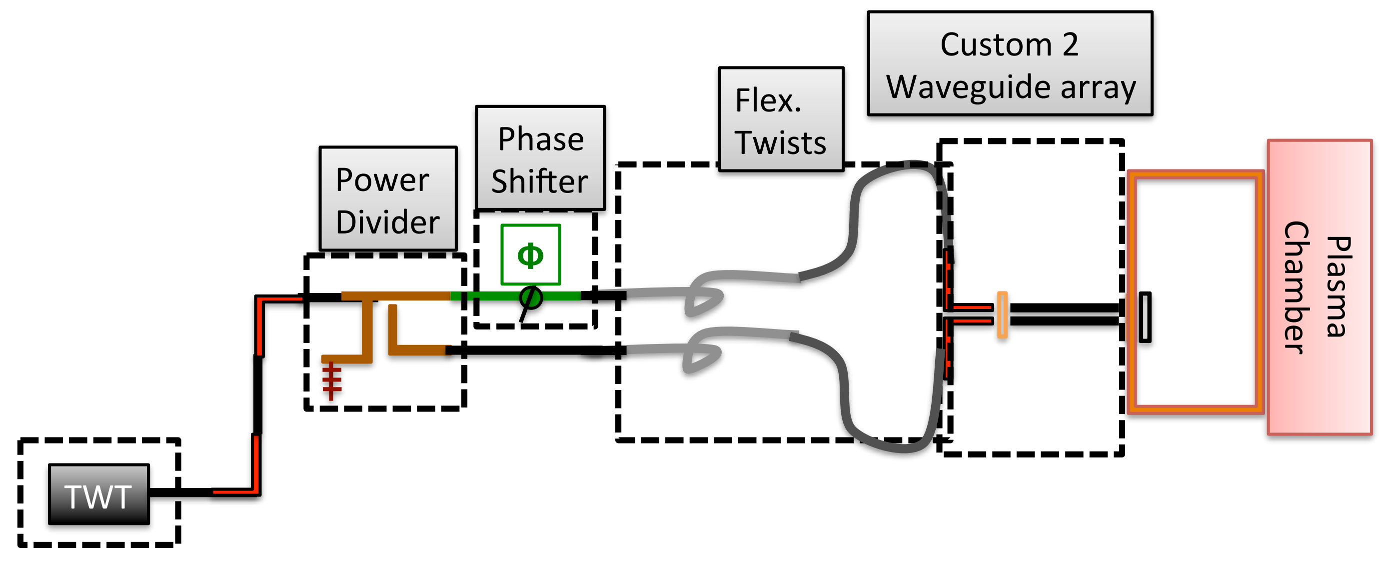

microwave launcher: proposed setup

- TWT ampl. 13.75-14.5 GHz
- Power divider
- Phase shifters
- flexible waveguides

MW component procurement completed

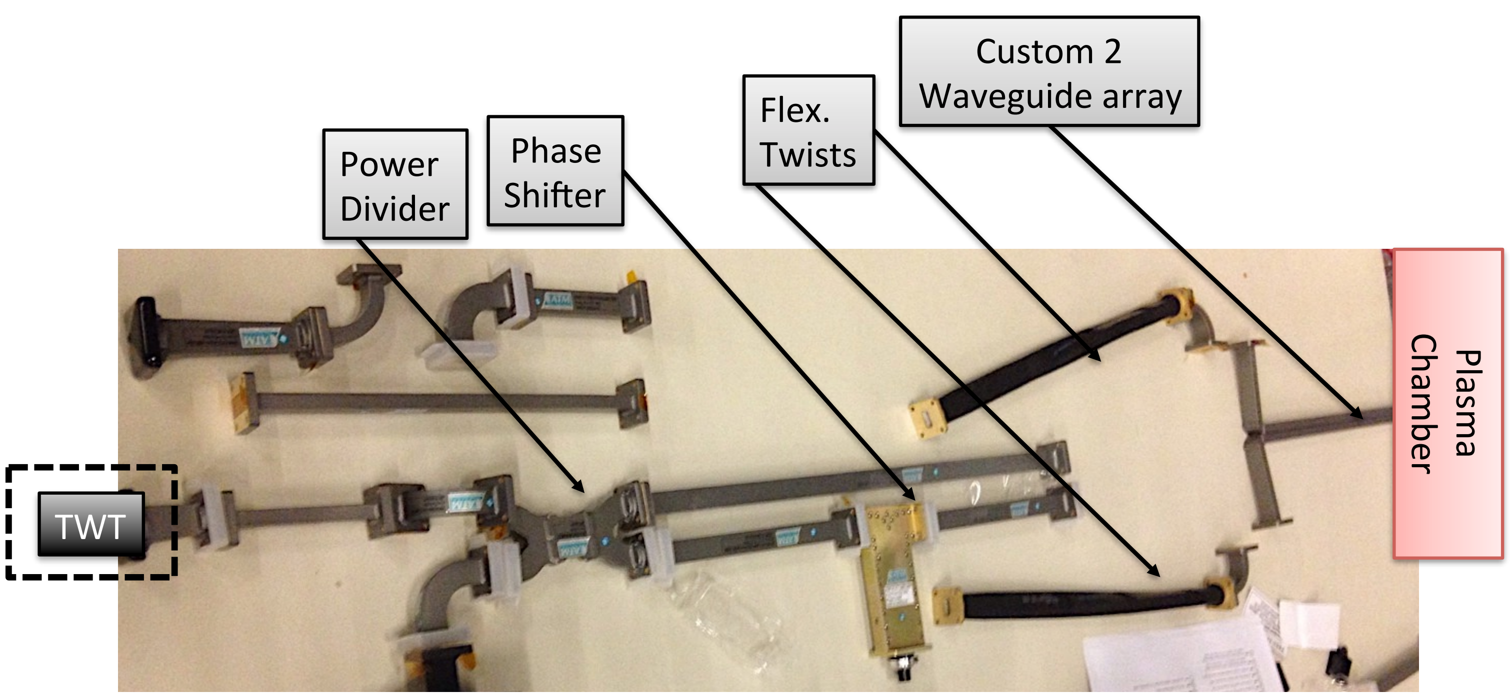

Two-waveguides array for m.w. launching

Microwave launcher Antenna assembly

Power divider

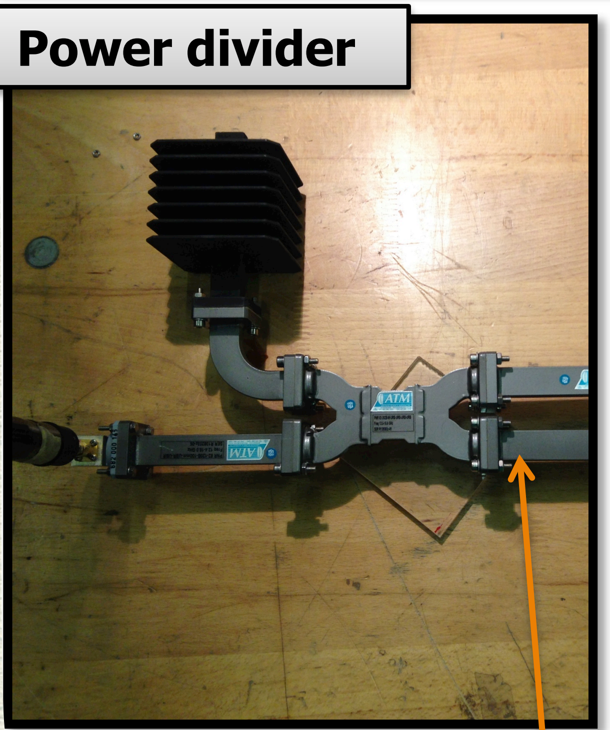

Phase shifter

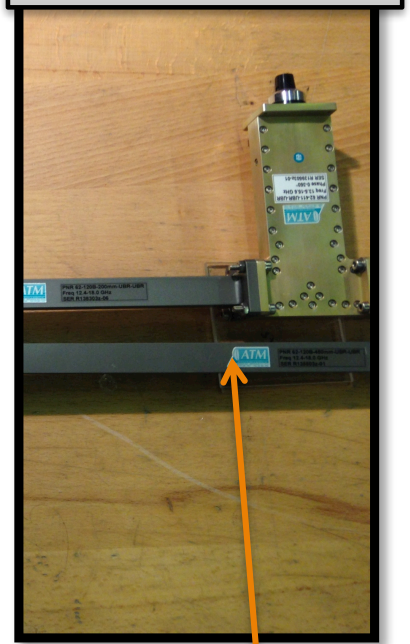

Two **Cut Waveguides Array** as **antenna**

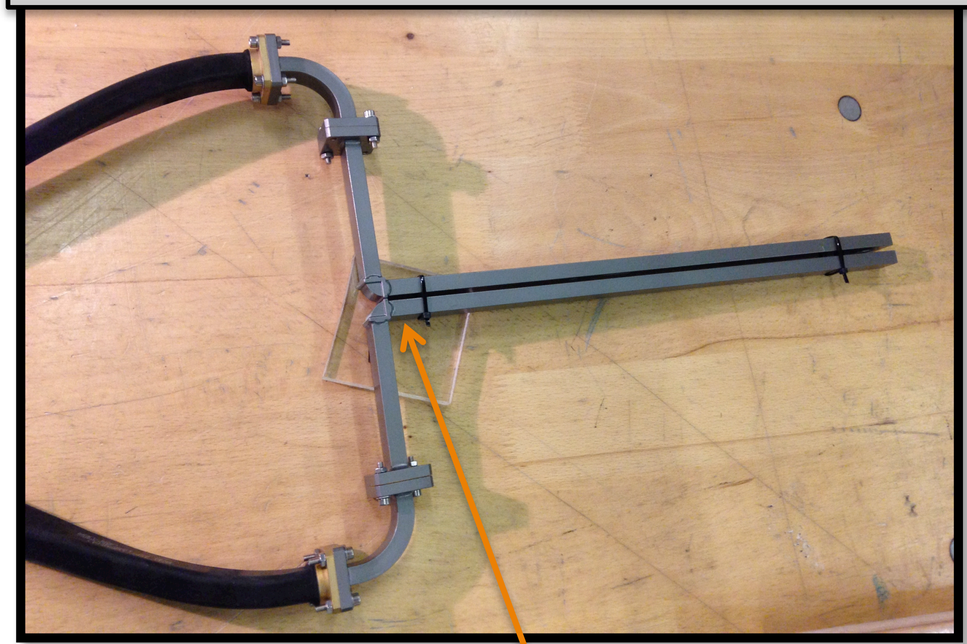

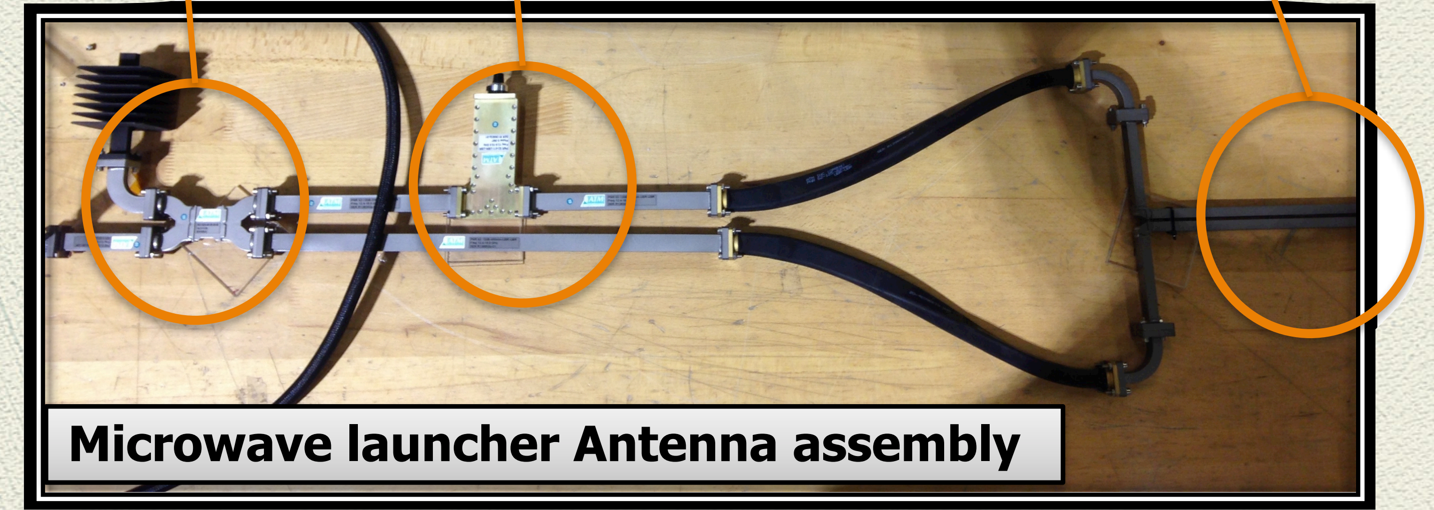

Microwave launcher Antenna assembly

Main lobe direction= 0°

$\Delta\phi = 0^{\circ}$

Measured diagram

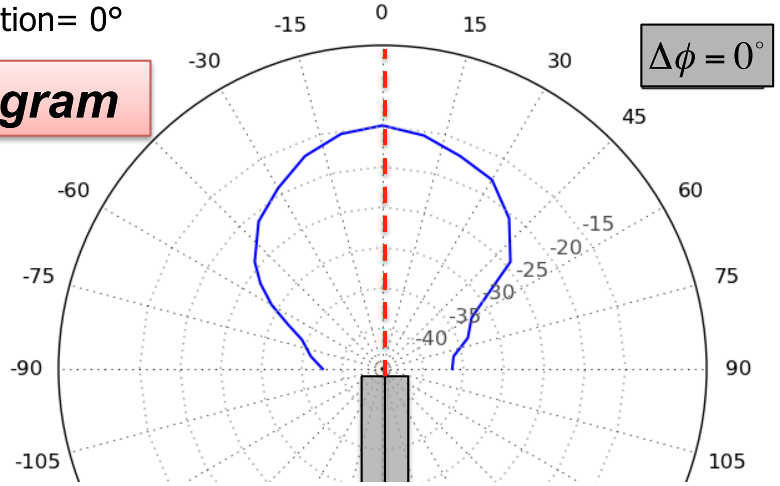

Farfield P-Field(r=0.012m) Abs (Theta=90)

Simulated diagram

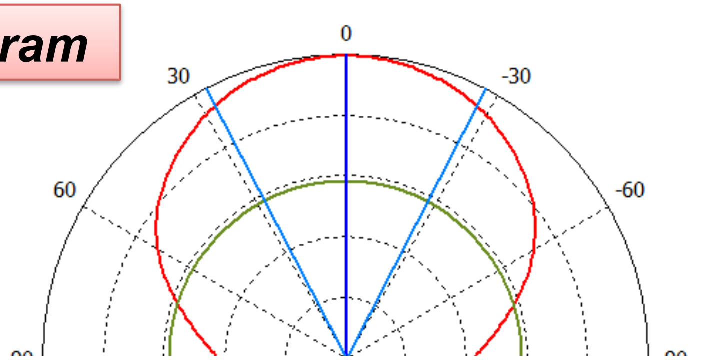

Main lobe direction= -15°

$\Delta\phi = 20^{\circ}$

Measured diagram

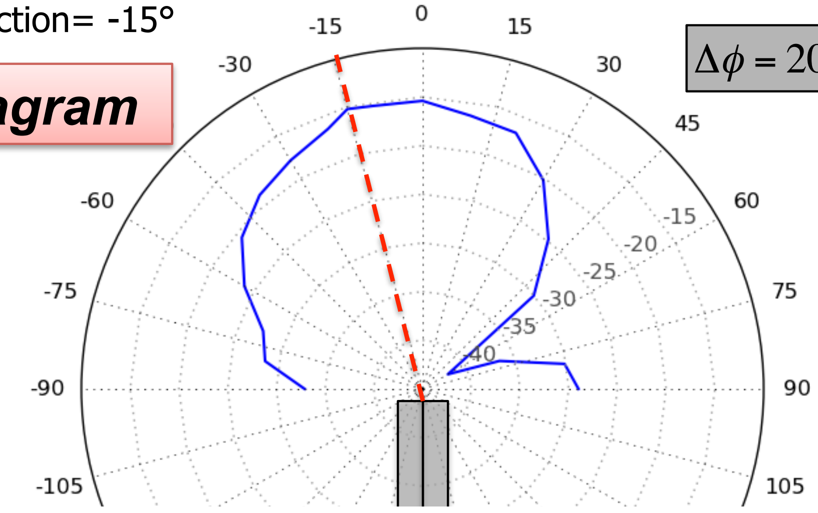

Farfield P-Field(r=0.012m) Abs (Theta=90)

Simulated diagram

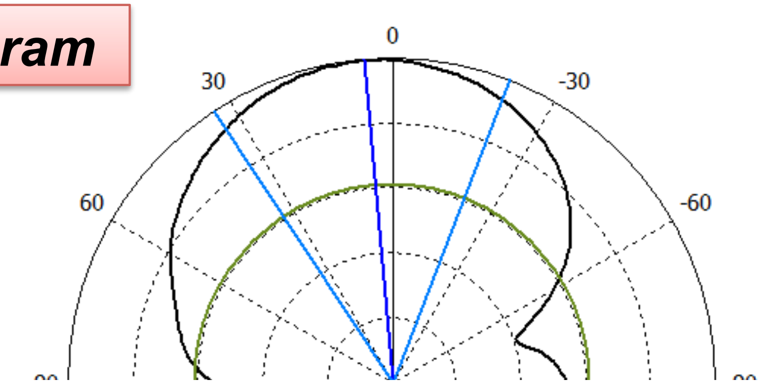

Main lobe direction= -20°

$\Delta\phi = 48^{\circ}$

Measured diagram

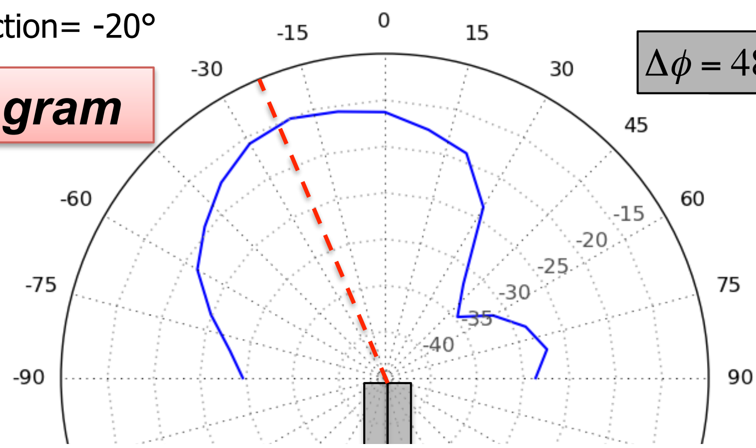

Farfield P-Field(r=0.012m) Abs (Theta=90)

Simulated diagram

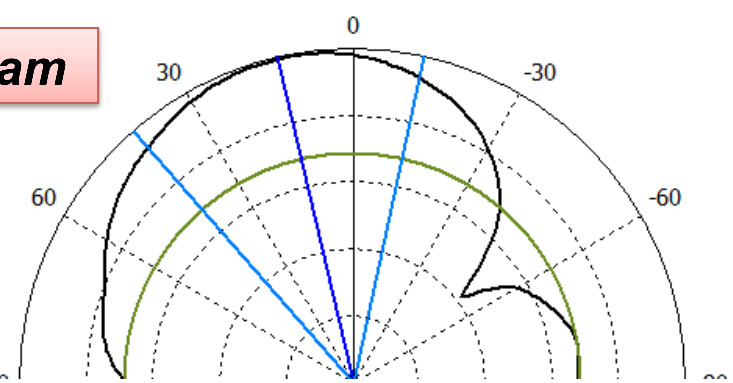

Main lobe direction= -40°

$\Delta\phi = 120^{\circ}$

Measured diagram

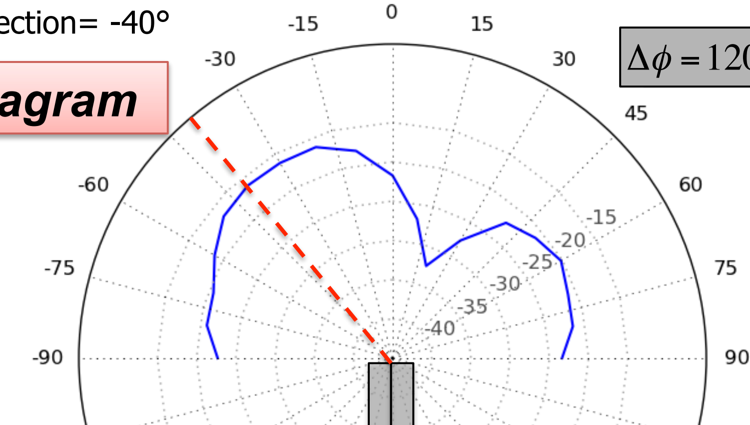

Simulated diagram

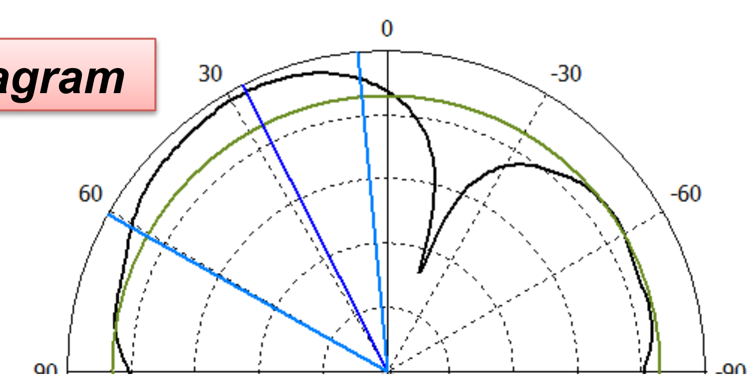

Mechanical Implementation at LNS

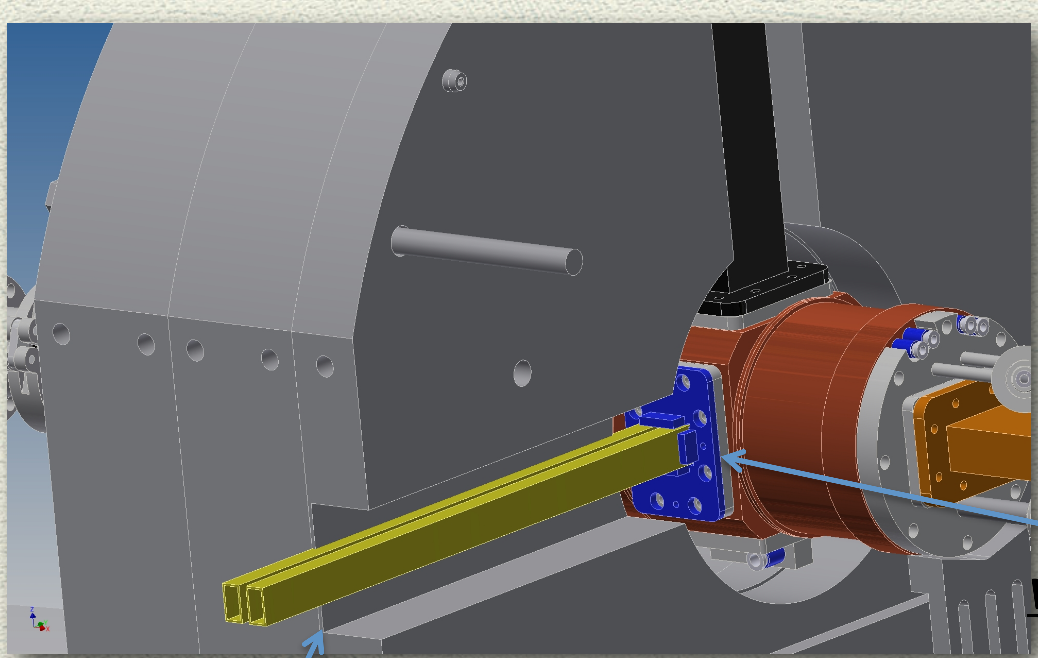

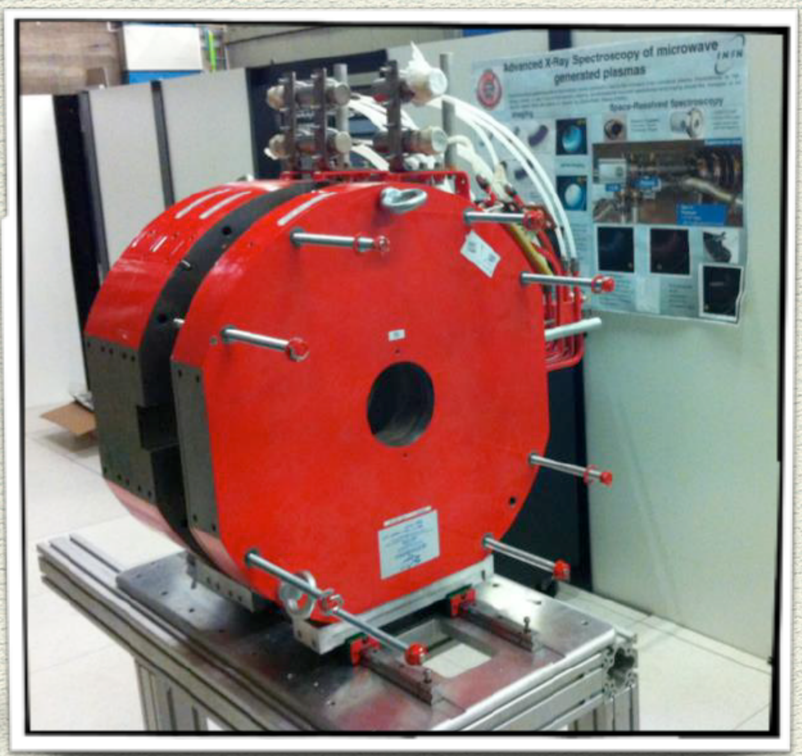

Vacuum Break window

Courtesy of S. Passarello

ARRAY of two waveguides

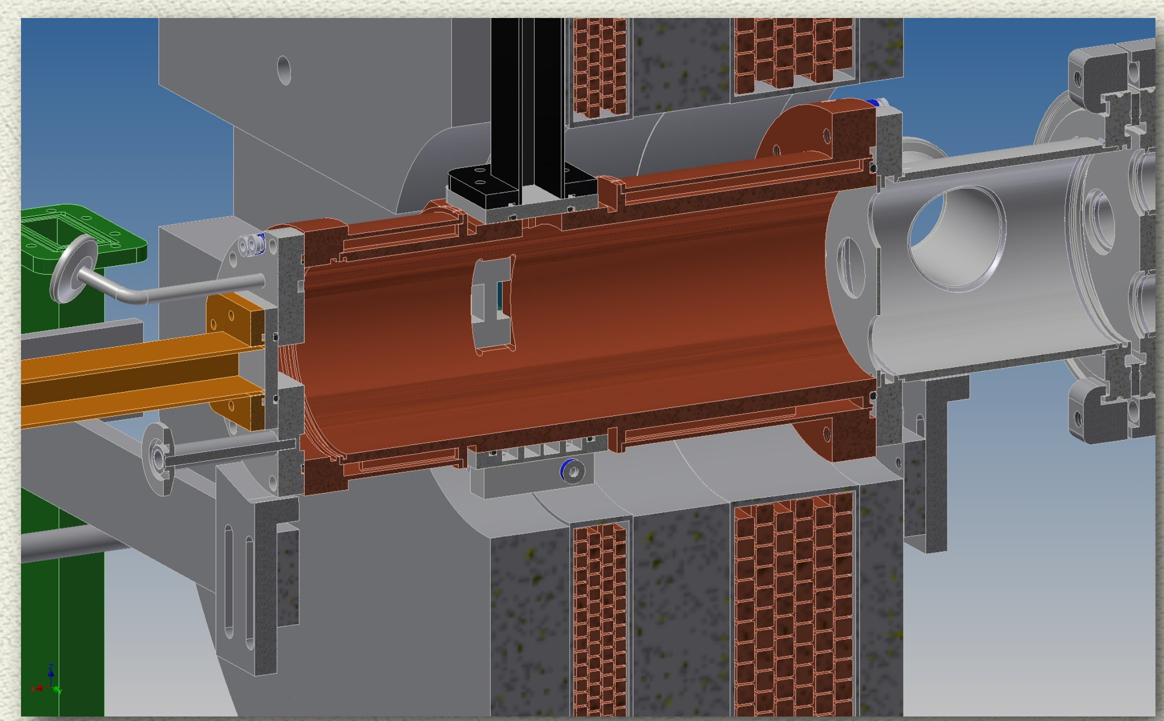

A new setup developed at LNS for fundamental studies: measurements about OXB conversion driven by the new launcher are now ongoing

Langevin formalism and charge breeding process

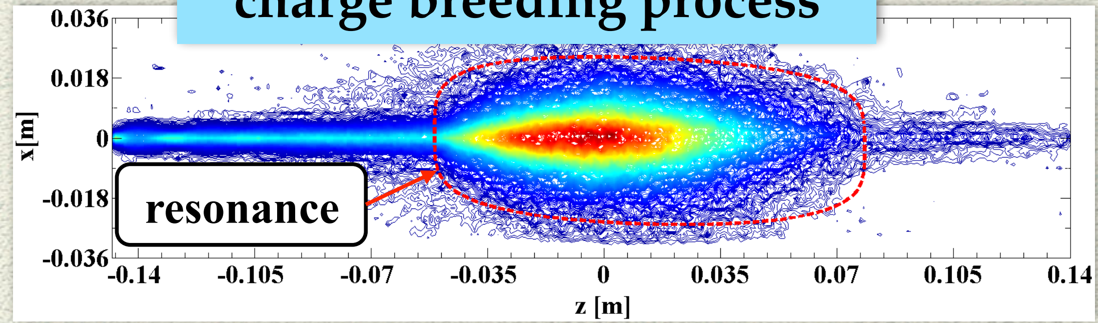

A. Galatà

Beam diagnostics

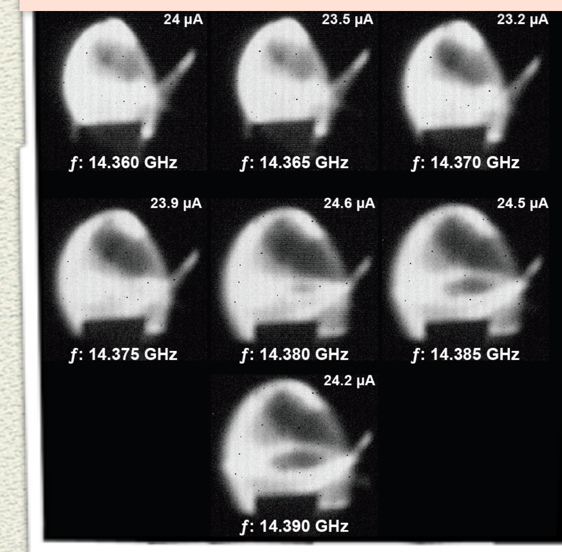

D. Nicolosi

Plasma modelling

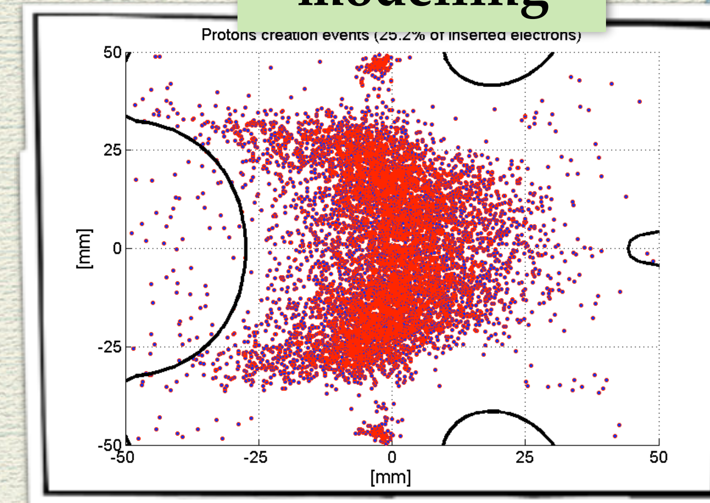

L. Neri

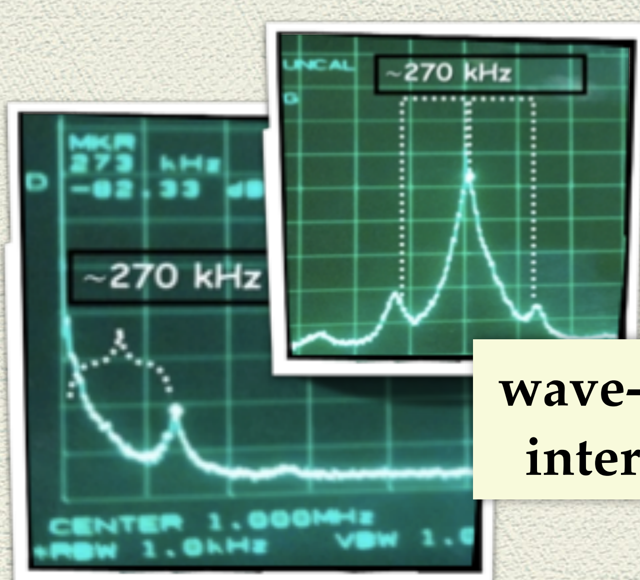

wave-plasma interaction

G. Castro

Players of an Orchestra....

pin-hole camera setup

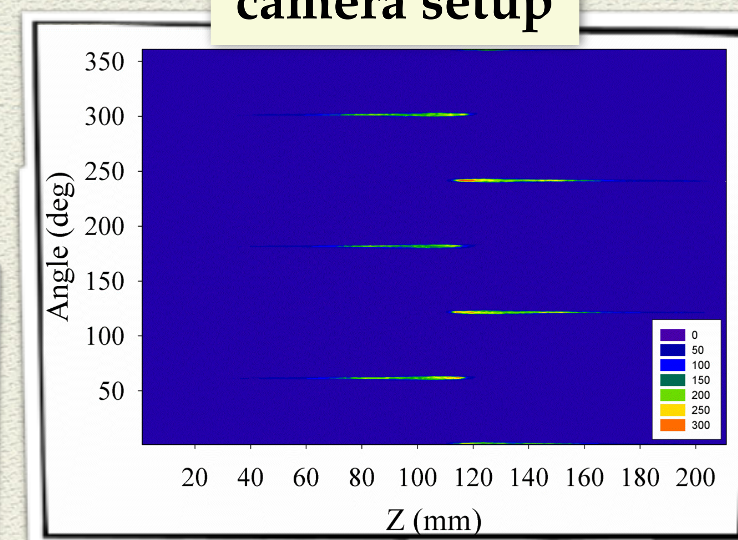

C. Altana, C. Caliri, R. Racz

interferometry

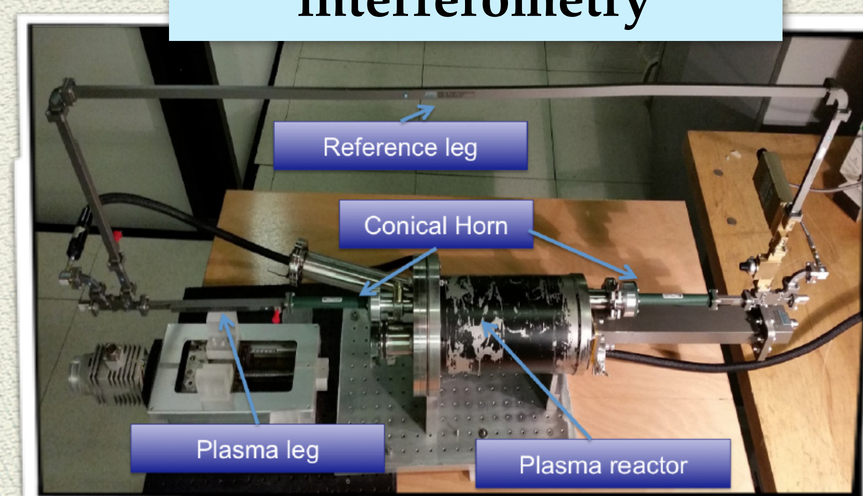

G. Torrisi

S. Gammino, L. Celona, S. Marletta, S. Passarello, F. Chines, M. Castro, S. Vinciguerra, G. Pastore, G. Gallo, L. Allegra, LNS mechanical workshop, and many others....

Thank you for you kind attention!